Preliminary Assessment of ATR-C Capabilities to Provide Integral Benchmark Data for Key Structural/Matrix Materials that May be Used for Nuclear Data Testing and Analytical Methods Validation

John D. Bess

July 2009

The INL is a U.S. Department of Energy National Laboratory operated by Battelle Energy Alliance

Preliminary Assessment of ATR-C Capabilities to Provide Integral Benchmark Data for Key Structural/Matrix Materials that May be Used for Nuclear Data Testing and Analytical Methods Validation

John D. Bess

July 2009

**Idaho National Laboratory
Idaho Falls, Idaho 83415**

http://www.inl.gov

Executive Summary

The purpose of this document is to identify some suggested types of experiments that can be performed in the Advanced Test Reactor Critical (ATR-C) facility. A fundamental computational investigation is provided to demonstrate possible integration of experimental activities in the ATR-C with the development of benchmark experiments. Criticality benchmarks performed in the ATR-C could provide integral data for key matrix and structural materials used in nuclear systems. Results would then be utilized in the improvement of nuclear data libraries and as a means for analytical methods validation.

It is proposed that experiments consisting of well-characterized quantities of materials be placed in the Northwest flux trap position of the ATR-C. The reactivity worth of the material could be determined and computationally analyzed through comprehensive benchmark activities including uncertainty analyses. Experiments were modeled in the available benchmark model of the ATR using MCNP5 with the ENDF/B-VII.0 cross section library. A single bar (9.5 cm long, 0.5 cm wide, and 121.92 cm high) of each material could provide sufficient reactivity difference in the core geometry for computational modeling and analysis. However, to provide increased opportunity for the validation of computational models, additional bars of material placed in the flux trap would increase the effective reactivity up to a limit of 1$ insertion. For simplicity in assembly manufacture, approximately four bars of material could provide a means for additional experimental benchmark configurations, except in the case of strong neutron absorbers and many materials providing positive reactivity.

Future tasks include the cost analysis and development of the experimental assemblies, including means for the characterization of the neutron flux and spectral indices. Oscillation techniques may also serve to provide additional means for experimentation and validation of computational methods and acquisition of integral data for improving neutron cross sections. Further assessment of oscillation techniques for implementation in the ATR-C may be of additional benefit. The establishment of benchmark experiment capabilities in the ATR-C would allow for the further development of techniques and facility enhancements involving neutronics experimentation in the ATR-C.

1. Introduction

The scope of this document is to suggest potential research experiments using the Advanced Test Reactor Critical (ATR-C) facility at the Idaho National Laboratory (INL). A preliminary computational investigation is provided to develop the possibility of performing benchmark experiments in the ATR-C to provide integral data for key structural and matrix materials that would be utilized in nuclear systems. Results could be used for improvement of nuclear data libraries and means for analytical methods validation.

The proposed research would be in accordance with activities supported by the Advanced Test Reactor National Scientific User Facility (ATR NSUF) and use available critical facilities. The ATR-C design is very similar to the core geometry of the Advanced Test Reactor but operates at a thermal power of less than 5 kW. The proposed experiments would involve placement of known quantities of well-characterized materials into the ATR-C to determine reactivity worth of the material for subsequent computational analysis. An investigation into a possible experimental approach and estimation of results is provided in this report. The establishment of benchmark experiment capabilities in the ATR-C would provide means for further development of techniques and facility enhancements involving neutronics experimentation in the ATR-C.

2. Investigational Approach

The ATR-C facility is typically used with prototype experiments to characterize in advance, with precision and accuracy, the expected changes in core reactivity of the ATR. This pool-type reactor usually operates at a power level of about 100 W and can provide physics data useful for evaluating the following:

- worth and calibration of control elements,
- excess reactivities and charge lifetimes,
- thermal and fast neutron distributions,
- gamma heat generation rates,
- fuel loading requirements,
- effects of inserting and removing experiments and experiment void reactivities, and
- temperature and void reactivity coefficients.[a]

A diagram of ATR core is provided in Figure 2.1; the ATR-C core is similar in design. The primary difference between the ATR-C and ATR is that the highly-enriched uranium fuel in the ATR-C is uniformly loaded with boron while the ATR fuel is not. A second difference of note is that the ATR-C uses five cadmium-plated safety rods while the ATR uses six hafnium-plated safety rods. During operation, this difference is insignificant. Available positions within the ATR-C that are accessible for experiment movement are the Northwest (NW), Center (C), and Southeast (SE) flux trap positions. The NW position is the largest, with an internal diameter of 5.25 in (13.335 cm).[b]

---

[a] INL – ATR National Scientific User Facility, http://nuclear.inl.gov/atr/overview/index.shtml, last updated December 11, 2007.

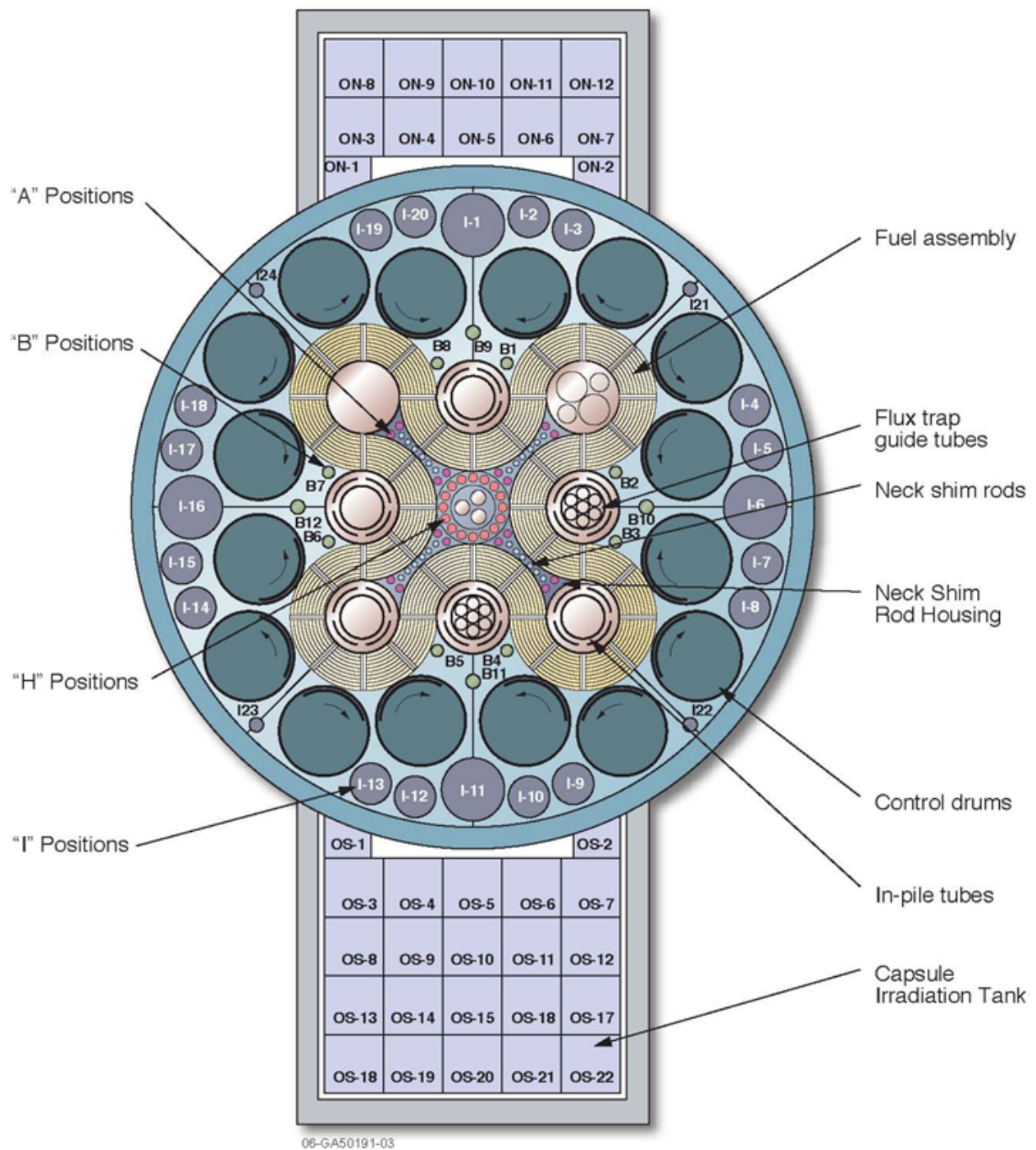[b] Personal communication with ATR-C personnel on September 22, 2008.

Figure 2.1: ATR Core Cross Section [1].

At the time of this study, a benchmark model of the ATR-C was not available. As the ATR-C is very similar to the ATR, the benchmark model of the ATR [2] was selected for use in these computational analyses. This benchmark model has been through minor revisions, and will be updated in the 2009 release of the benchmark handbooks [3-4]. The revisions include a correction in the diameter of the A-13 through A-16 positions in the core, and then a correction to the calculated density of the water throughout the reactor system. No changes were effected to account for differences between the ATR-C and ATR. Analysis of the benchmark model was performed using Monte Carlo N-Particle (MCNP) version 5.1.4 [5] with the evaluated nuclear data file library, ENDF/B-VII.0 [6]. The ATR model, as analyzed using MCNP, is shown in Figure 2.2, where the NW flux trap is located in the top-most position of the figure.

A summary of the structural and matrix materials of interest are shown in Table 2.1. These materials are often used in nuclear reactor systems, transportation and/or storage of nuclear fuels, and have been proposed for use in possible space nuclear reactor systems. Aluminum is included in the list as also a reference material to evaluate voiding effects in the ATR-C as water is replaced in the NW flux trap with experimental material. The densities, molecular weights, and isotopic abundances shown in Table 1 have been collected from the 16th edition of the Chart of the Nuclides [7]. The one exception is the density of SiO_2 (glass), which was obtained from the internet.[a] The mean free path of thermal neutrons through the selected materials has been compiled in Table 2.2, where the absorption cross sections are obtained from the Chart of the Nuclides [7], and the scattering cross sections, where available, are obtained from a nuclear engineering textbook [8].

The benchmark model on the ATR has an aluminum filler, pressure tube, and insulation tube in the NW flux trap (Figure 2.3). Criticality in the ATR-C is obtained by rotating the control drums to approximately 70.35º and then rotating them out more, as necessary, in the lobe surrounding the flux trap position being used for the experiment. Typically a limit of 1$ in reactivity insertion is imposed, where β=0.0075. Repeatability of an experiment can be performed within about 0.05$.[b] Removal of the aluminum filler in the NW flux trap (Figure 2.4) equates to a negative reactivity insertion of approximately 1$.

The computational analysis consisted of two phases. Each material was analyzed in both phases, as well as configurations with voided material, for comparative purposes. The first phase involved the modeling of blocks of the materials in Table 2.1 in the NW flux trap after the aluminum filler and tubes have been removed. The initial block had dimensions of 9.5 cm in length, 0.5 cm in width, and 121.92 cm in height (Figure 2.5), where 121.92 cm (48 in) is the active fueled length of the ATR and ATR-C cores. The thickness of the block was increased by increments of 0.5 cm until a square block of 9.5 cm × 9.5 cm × 121.92 cm was achieved (Figure 2.6). The effective eigenvalues were computed in MCNP and then compared against benchmark eigenvalues to calculate the approximate change in reactivity for the experimental configuration.

The second phase of the analysis involved modeling of multiple bars of material (9.5 cm × 0.5 cm × 121.92 cm) such that self-shielding effects would be minimized. The initial configuration matched that of the smallest block configuration. Additional bars were included in the model and equidistantly placed until a total of 19 bars were analyzed, which is equivalent to the largest block configuration. Figure 2.7 shows the various configurations in the second phase of the analysis. The eigenvalues were computed and used to calculate effective reactivities for the proposed experiments. A bar thickness of 0.5 cm was selected as the minimum thickness for ease of manufacturability while maintaining rigidity.

---

[a] WebElements Periodic Table of the Elements, http://www.webelements.com/compounds/silicon/silicon_dioxide.html, last accessed March 16, 2009.

[b] Personal communication with ATR-C personnel on September 22, 2008.

Table 2.1: Structural/Matrix Materials of Interest.

Material	Density (g/cm³)	Molecular Weight	Atom Density (a/b-cm)	Isotope	Abundance (%)	MCNP5/ ENDF/B-VII.0
Aluminum	2.6989	26.9815384	6.0238×10^{-2}	^{27}Al	100	13027.00c + Al.00t
Beryllium	1.848	9.0121821	1.2349×10^{-1}	^{9}Be	100	4009.00c + Be.00t
Chromium	7.19	51.9961	8.3273×10^{-2}	^{50}Cr	4.345	24050.00c
				^{52}Cr	83.789	24052.00c
				^{53}Cr	9.501	24053.00c
				^{54}Cr	2.365	24054.00c
Manganese	7.3	54.938049	8.0020×10^{-2}	^{55}Mn	100	25055.00c
Molybdenum	10.22	95.94	6.4150×10^{-2}	^{92}Mo	14.84	42092.00c
				^{94}Mo	9.25	42094.00c
				^{95}Mo	15.92	42095.00c
				^{96}Mo	16.68	42096.00c
				^{97}Mo	9.55	42097.00c
				^{98}Mo	24.13	42098.00c
				^{100}Mo	9.63	42100.00c
Nickel	8.902	58.6934	9.1337×10^{-2}	^{58}Ni	68.0769	28058.00c
				^{60}Ni	26.2231	28060.00c
				^{61}Ni	1.1399	28061.00c
				^{62}Ni	3.6345	28062.00c
				^{64}Ni	0.9256	28064.00c
Niobium	8.57	92.906378	5.5550×10^{-2}	^{93}Nb	100	41093.00c
Rhenium	21.02	186.207	6.7981×10^{-2}	^{185}Re	37.4	75185.00c
				^{187}Re	62.6	75187.00c
Titanium	4.54	47.867	5.7117×10^{-2}	^{46}Ti	8.25	22046.00c
				^{47}TI	7.44	22047.00c
				^{48}Ti	73.72	22048.00c
				^{49}Ti	5.41	22049.00c
				^{50}Ti	5.18	22050.00c
Tungsten	19.3	183.84	6.3222×10^{-2}	^{180}W	0.12	--
				^{182}W	26.5	74182.00c
				^{183}W	14.31	74183.00c
				^{184}W	30.64	74184.00c
				^{186}W	28.43	74186.00c
Vanadium	6.11	50.9415	7.2230×10^{-2}	^{50}V	0.25	23000.00c
				^{51}V	99.75	
Zirconium	6.506	91.224	4.2949×10^{-2}	^{90}Zr	51.45	40090.00c
				^{91}Zr	11.22	40091.00c
				^{92}Zr	17.15	40092.00c
				^{94}Zr	17.38	40094.00c
				^{96}Zr	2.8	40096.00c
SiO₂ (Glass)	2.533	60.084	2.5388×10^{-2}	^{16}O	99.757	8016.00c
				^{17}O	0.038	8017.00c
				^{18}O	0.205	--
				^{28}Si	92.2297	14028.00c
				^{29}Si	4.6832	14029.00c
				^{30}Si	3.0872	14030.00c

Table 2.2: Thermal Mean Free Paths for Selected Materials.

Material	Isotope	σ_γ (b)	σ_s (b)	Σ_t (cm^{-1})	λ (cm)
Aluminum	^{27}Al	0.23	1.49	1.0361×10^{-1}	9.65
Beryllium	^{9}Be	0.008	6.14	7.5920×10^{-1}	1.32
Chromium	^{50}Cr	15.5	3.8	5.7146×10^{-1}	1.75
	^{52}Cr	0.8			
	^{53}Cr	18			
	^{54}Cr	0.36			
Manganese	^{55}Mn	13.3	2.1	1.2323×10^{0}	0.81
Molybdenum	^{92}Mo	0.06	5.8	5.3412×10^{-1}	1.87
	^{94}Mo	--			
	^{95}Mo	14			
	^{96}Mo	--			
	^{97}Mo	2.5			
	^{98}Mo	0.13			
	^{100}Mo	0.19			
Nickel	^{58}Ni	4.6	17.3	1.9877×10^{0}	0.50
	^{60}Ni	2.9			
	^{61}Ni	2.5			
	^{62}Ni	14.5			
	^{64}Ni	1.6			
Niobium	^{93}Nb	1.1	--	6.1105×10^{-2}	16.37
Rhenium	^{185}Re	112.3	11.3	6.8491×10^{0}	0.15
	^{187}Re	75.8			
Titanium	^{46}Ti	0.6	4	5.7849×10^{-1}	1.73
	^{47}TI	1.7			
	^{48}Ti	7.9			
	^{49}Ti	2.2			
	^{50}Ti	0.177			
Tungsten	^{180}W	30	--	1.1484×10^{0}	0.87
	^{182}W	20			
	^{183}W	10.3			
	^{184}W	1.802			
	^{186}W	38			
Vanadium	^{50}V	21	4.93	7.1293×10^{-1}	1.40
	^{51}V	4.9			
Zirconium	^{90}Zr	0.01	6.4	2.8275×10^{-1}	3.54
	^{91}Zr	1.2			
	^{92}Zr	0.2			
	^{94}Zr	0.05			
	^{96}Zr	0.022			
SiO$_2$ (Glass)	^{16}O	0.00019	3.76	7.8904×10^{-2}	12.67
	^{17}O	0.0004			
	^{18}O	0.00016			
	^{28}Si	0.169			
	^{29}Si	0.12	2.2		
	^{30}Si	0.107			
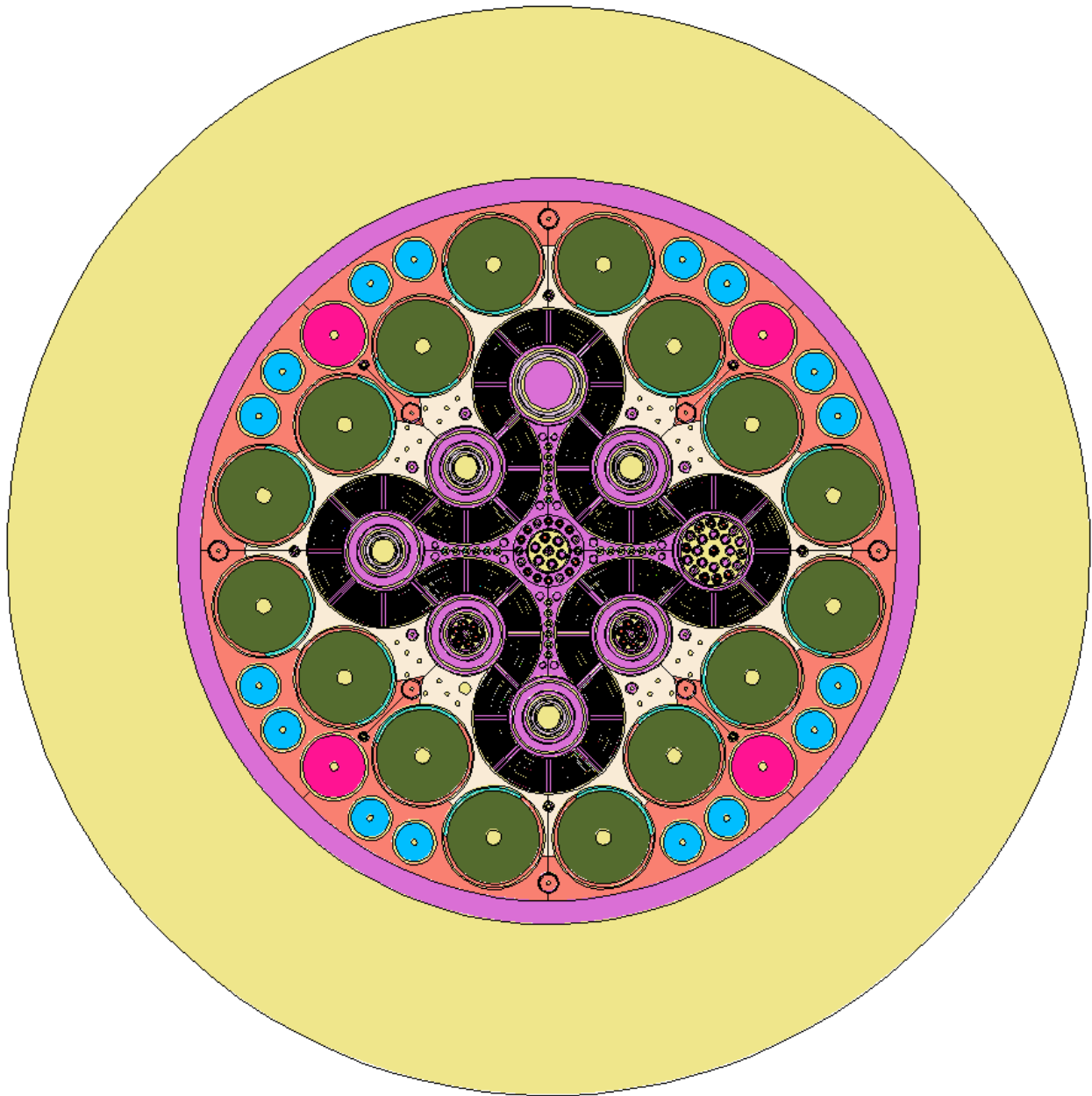
Figure 2.2: ATR Core Cross Section as Shown in the MCNP Visual Editor.
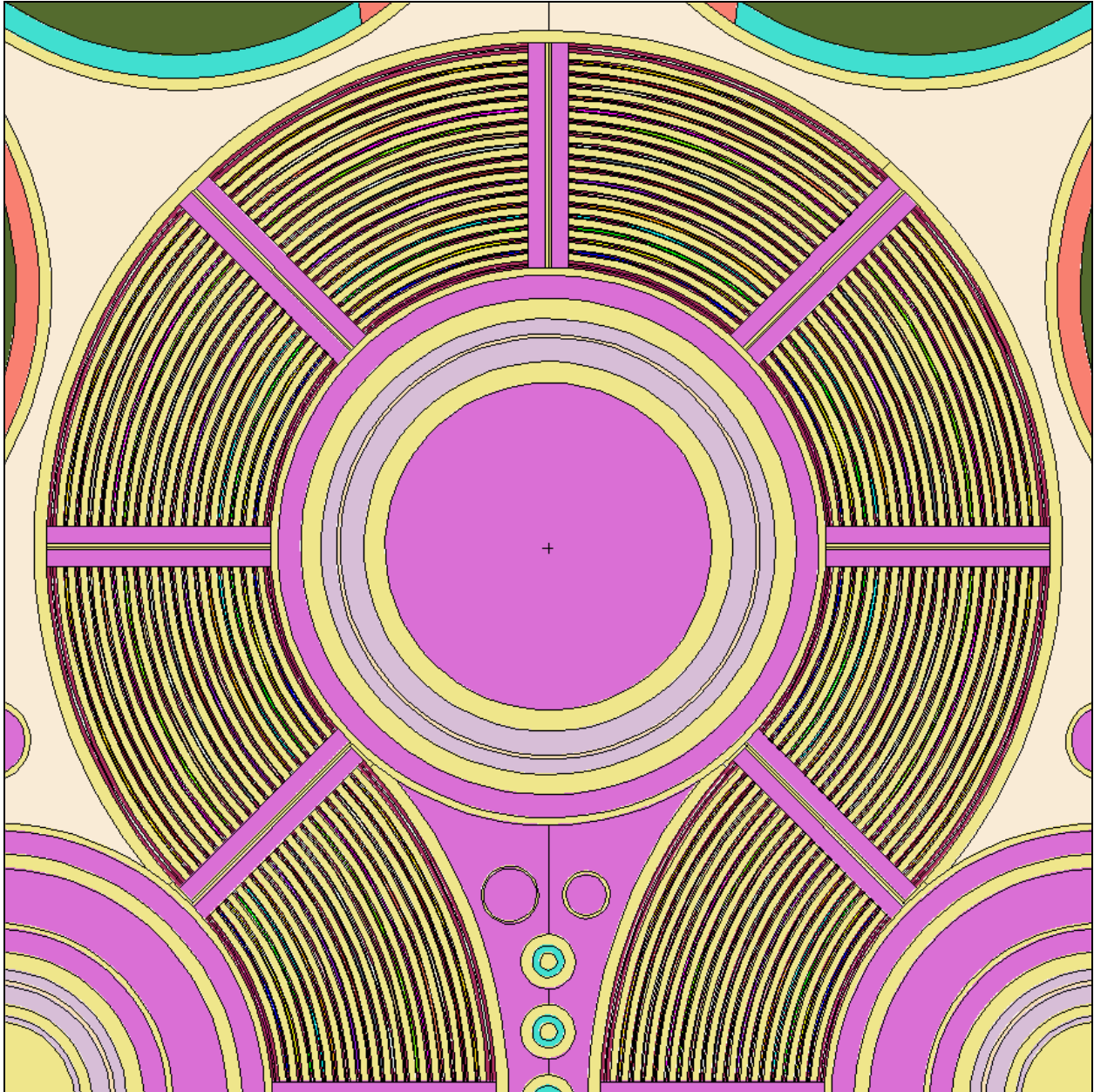
Figure 2.3: Northwest Flux Trap (Benchmark Model) containing an Aluminum Filler, Pressure Tube, and Insulation Tube.
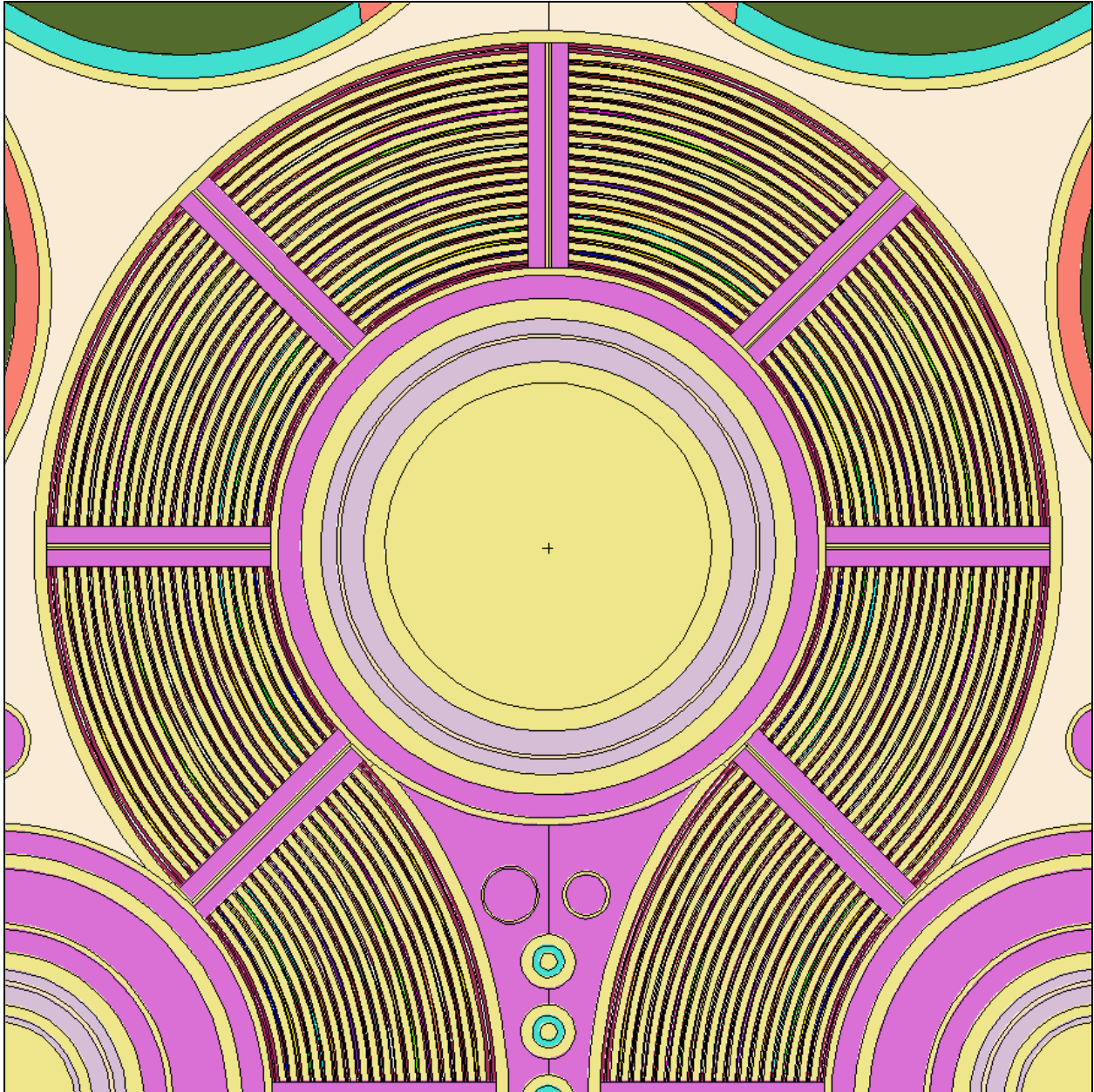
Figure 2.4: Northwest Flux Trap containing a Water-Filled Pressure Tube and Insulation Tube.
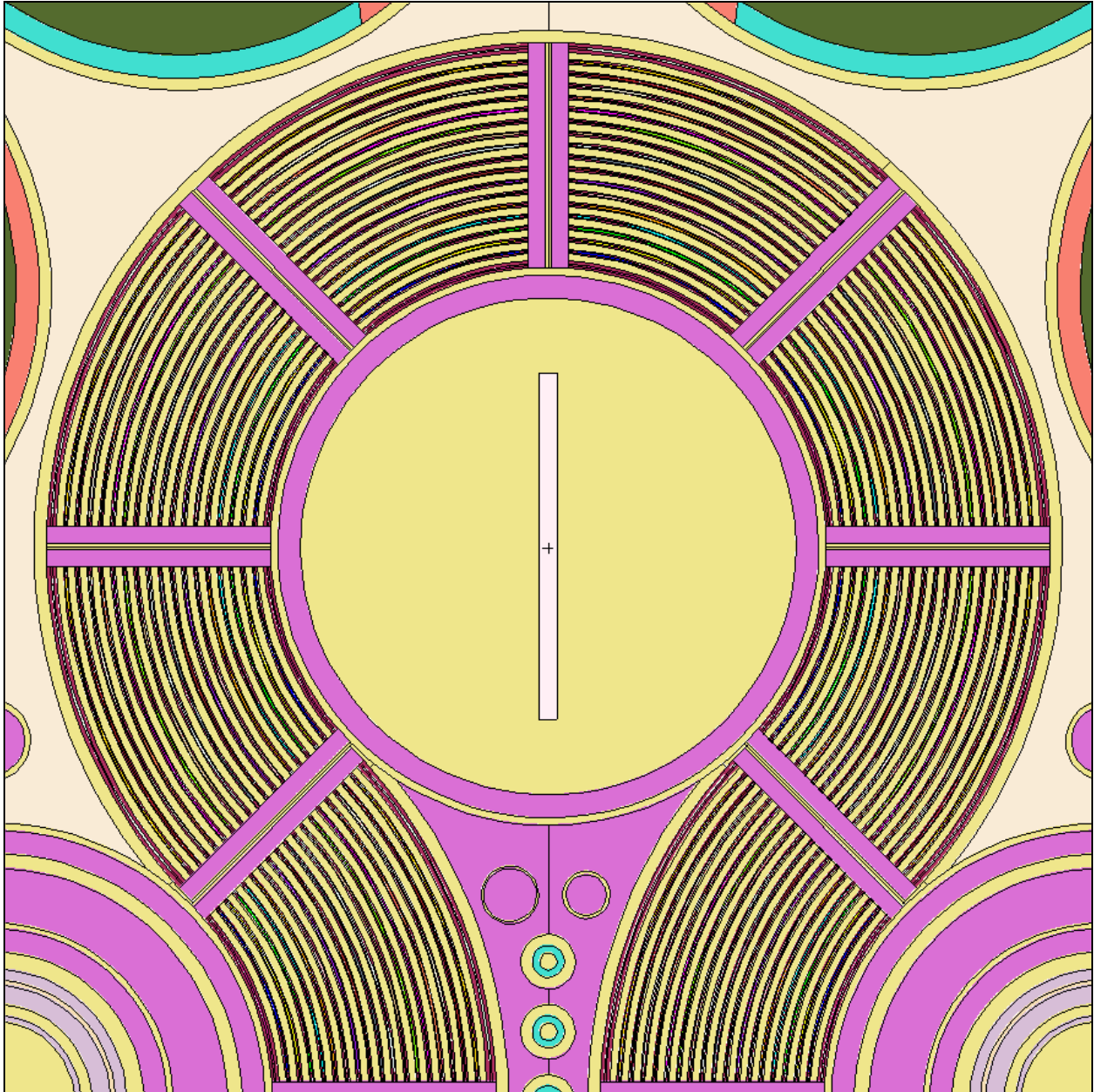
Figure 2.5: Northwest Flux Trap containing a Single Bar of Material: 9.5 cm long, 0.5 cm wide, and 121.92 cm high (height not shown).
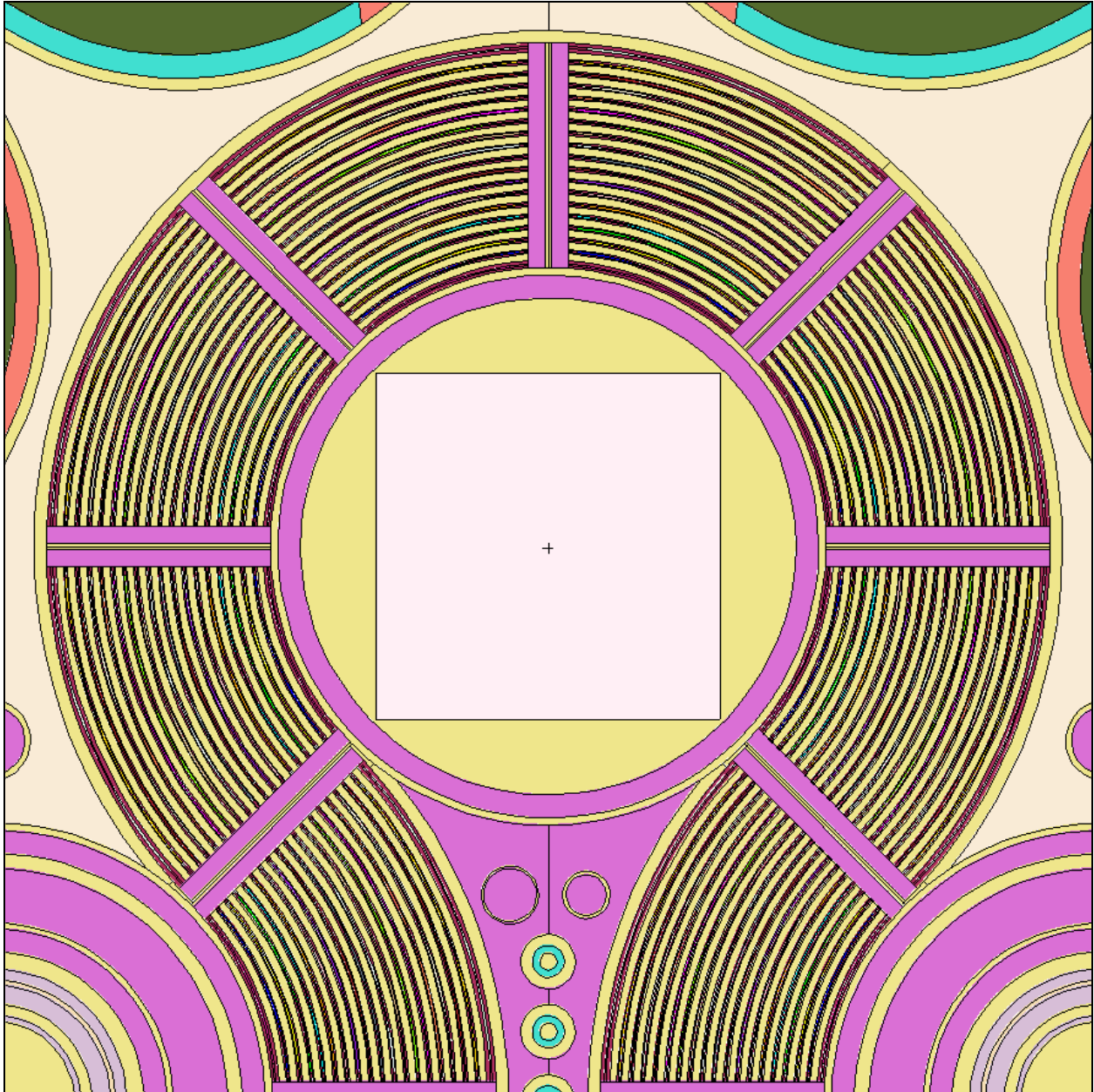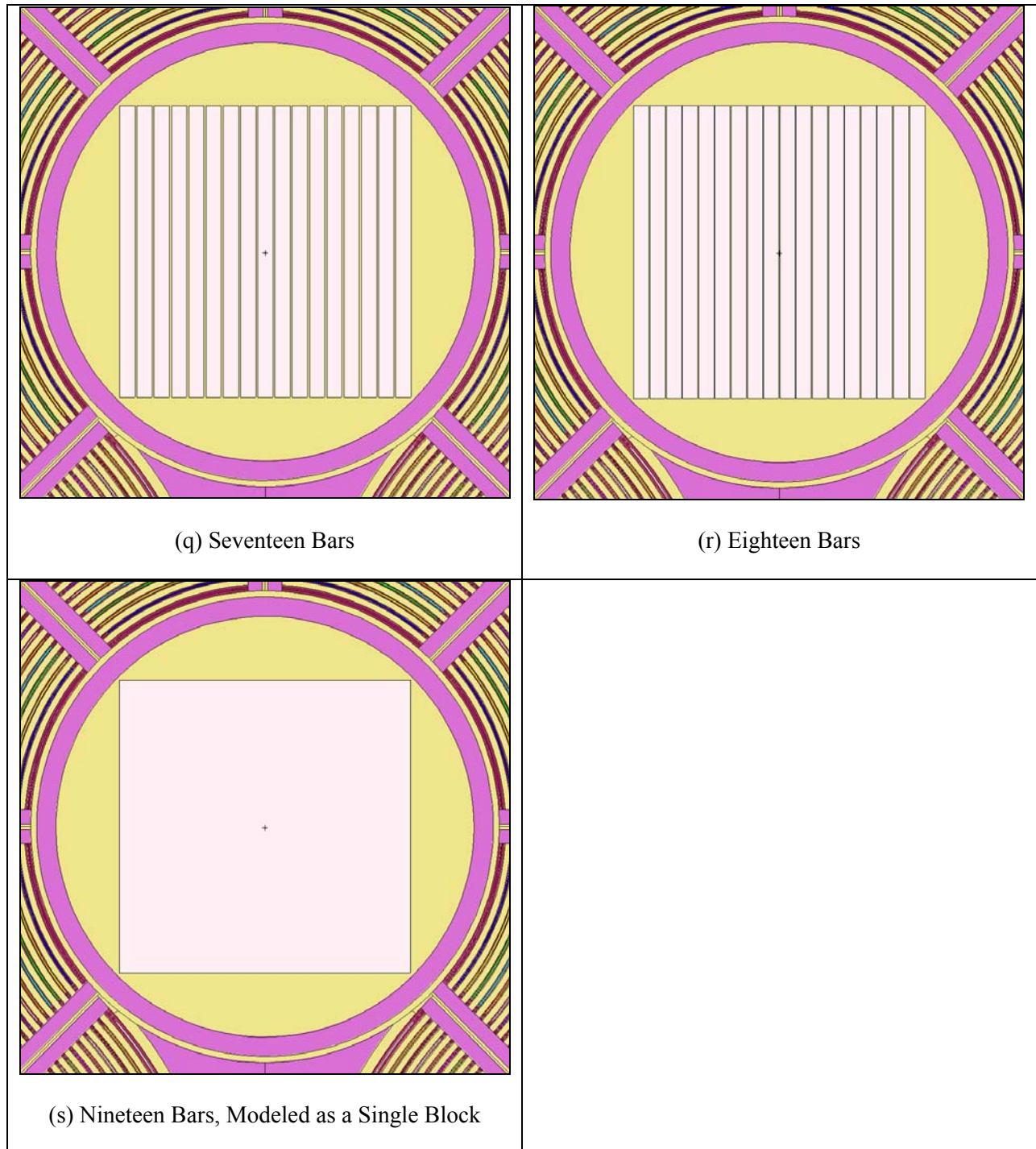
Figure 2.6: Northwest Flux Trap containing a Large Block of Material: 9.5 cm long, 9.5 cm wide, and 121.92 cm high (height not shown).

(a) Single Bar

(b) Two Bars

(c) Three Bars

(d) Four Bars
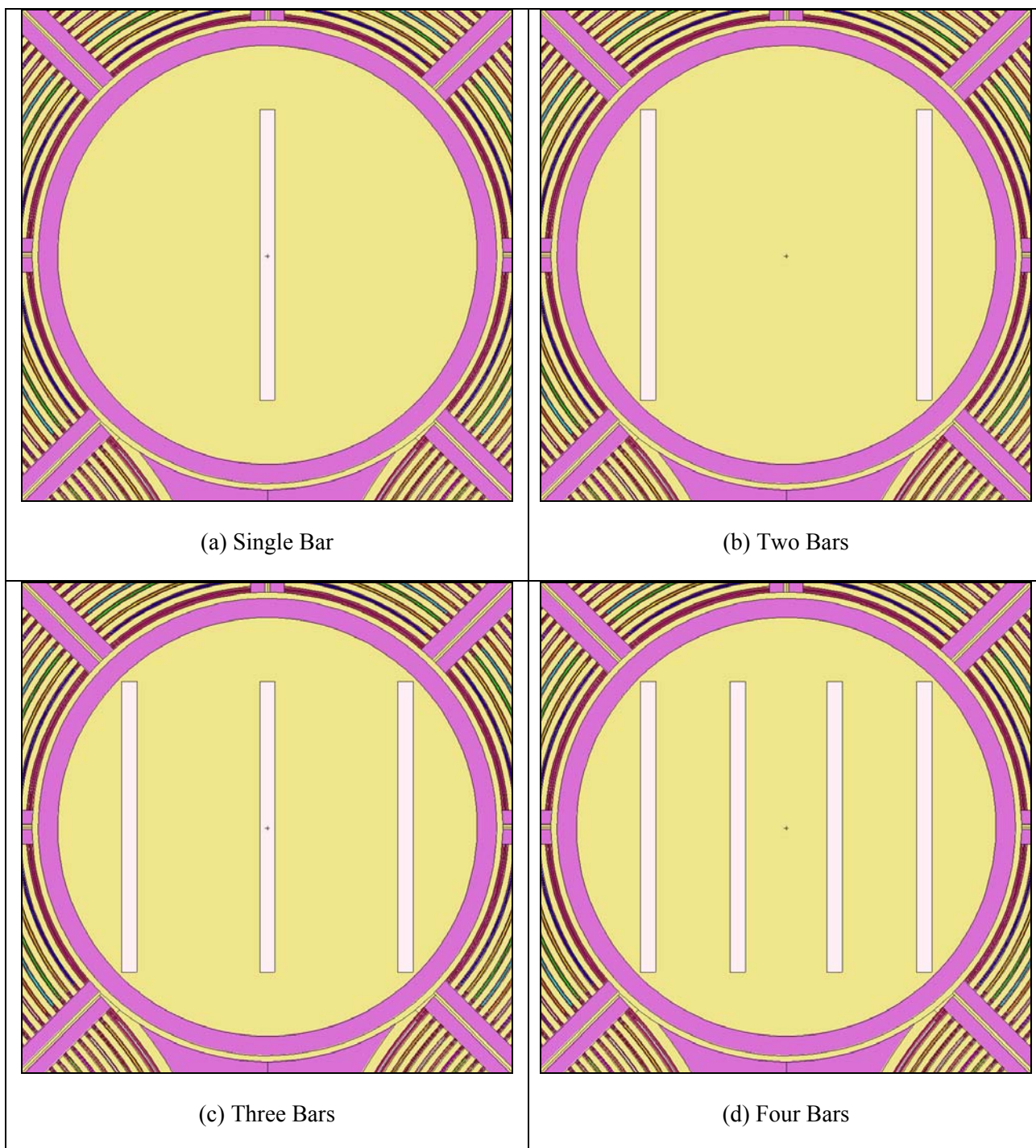
Figure 2.7: Northwest Flux Trap containing a Bars of Material: 9.5 cm long, 0.5 cm wide, and 121.92 cm high (height not shown).

(e) Five Bars

(f) Six Bars

(g) Seven Bars

(h) Eight Bars

Figure 2.7 (cont.): Northwest Flux Trap containing a Bars of Material: 9.5 cm long, 0.5 cm wide, and 121.92 cm high (height not shown).

(i) Nine Bars

(j) Ten Bars

(k) Eleven Bars

(l) Twelve Bars

Figure 2.7 (cont.): Northwest Flux Trap containing a Bars of Material: 9.5 cm long, 0.5 cm wide, and 121.92 cm high (height not shown).

(m) Thirteen Bars

(n) Fourteen Bars

(o) Fifteen Bars

(p) Sixteen Bars

Figure 2.7 (cont.): Northwest Flux Trap containing a Bars of Material: 9.5 cm long, 0.5 cm wide, and 121.92 cm high (height not shown).

(q) Seventeen Bars

(r) Eighteen Bars

(s) Nineteen Bars, Modeled as a Single Block

Figure 2.7 (cont.): Northwest Flux Trap containing a Bars of Material: 9.5 cm long, 0.5 cm wide, and 121.92 cm high (height not shown).

3.   Results and Discussion

The MCNP calculations were performed such that the statistical uncertainty in the eigenvalues is approximately ±0.00014; therefore, the uncertainty in Δk_{eff} is ±0.00020. Propagation of the uncertainty through the calculations of the reactivity ($\rho\$$) is negligible compared to the values reported here. The benchmark model k_{eff}, using MCNP5 and ENDF/B-VII.0 is 1.00082 with a benchmark model uncertainty of ±0.00350 (1σ). The uncertainty in the benchmark model is not necessary in the results because most of this uncertainty is eliminated when comparing eigenvalue results from very similar configurations. However, it should be noted that the uncertainty in the benchmark eigenvalue roughly equates to a reactivity uncertainty of approximately 0.47$. The calculated k_{eff} value for the model with the aluminum filler removed from the NW flux trap is 0.99322, which equates to an effective negative reactivity insertion of 1.02$.

Calculated eigenvalues for the experiments in phase one are shown in Figure 3.1, with the calculated reactivities, compared against the benchmark eigenvalue, shown in Figure 3.2. Similar results from the experiments modeled in phase two are shown in Figures 3.3 and 3.4, respectively. Materials with positive reactivity effects cumulative with the positive effect of voiding water in the flux trap include aluminum, beryllium, zirconium, and silicon dioxide. Many of the other materials demonstrated a negative insertion of reactivity that was partially compensated for by the positive effects of voiding. It becomes apparent from a comparison of Figures 3.2 and 3.4, that geometry and self-shielding effects influence the expected reactivities. A good example is that of titanium (Figure 3.5), where for a total thickness of 3.0 cm, the difference between a single block of material and six 0.5-cm-thick bars is approximately 0.45$. Appendix A contains comparison charts for all materials listed in Table 2.1. Materials with positive reactivity effects do not demonstrate this same pattern between the different experiment types. As expected, tungsten and rhenium demonstrated the largest negative reactivity effects. The mean free path of neutrons through rhenium was smaller than the thickness of the experiment materials. Manufacture of very thin rhenium plates to eliminate any self-shielding effects might prove impractical, and a well-characterized rhenium alloy might be analyzed instead.

Comparison of the eigenvalues against the water-filled flux trap configuration essentially shifts the results shown in Figures 3.2 and 3.4 ~1$ in the positive direction. Appendix B shows individual results for the various materials. This shift in reactivity would be more useful in comparing positive reactivity experiments using aluminum, beryllium, zirconium, and silicon dioxide, in which a more significant difference between configurations is apparent.

Calculated reactivities for modeling "voided" material in the core are shown in Figure 3.6, which compares effects from both phases of the experimental modeling. Comparison of the actual materials against the voided configurations is shown in Appendix C, where the reactivity effects from voiding can be approximated and true reactivity effects of the materials can be estimated. This comparison does not provide acceptable results for some of the materials with positive reactivity effects, as the effective difference in eigenvlaues of the two configurations is very small.

A similar comparison of material reactivity against the equivalent aluminum experiment is found in Appendix D. This provides an experimental configurations of positive reactivity upon which the materials providing negative reactivity can be compared against for a larger difference in reactivity between configurations. Results are similar to the "voided" material comparison but can be experimentally performed and then validated. As the water-filled configuration increases the reactivity difference for positive reactivity experiments, the aluminum material configurations increase the comparison difference for negative reactivity experiments.
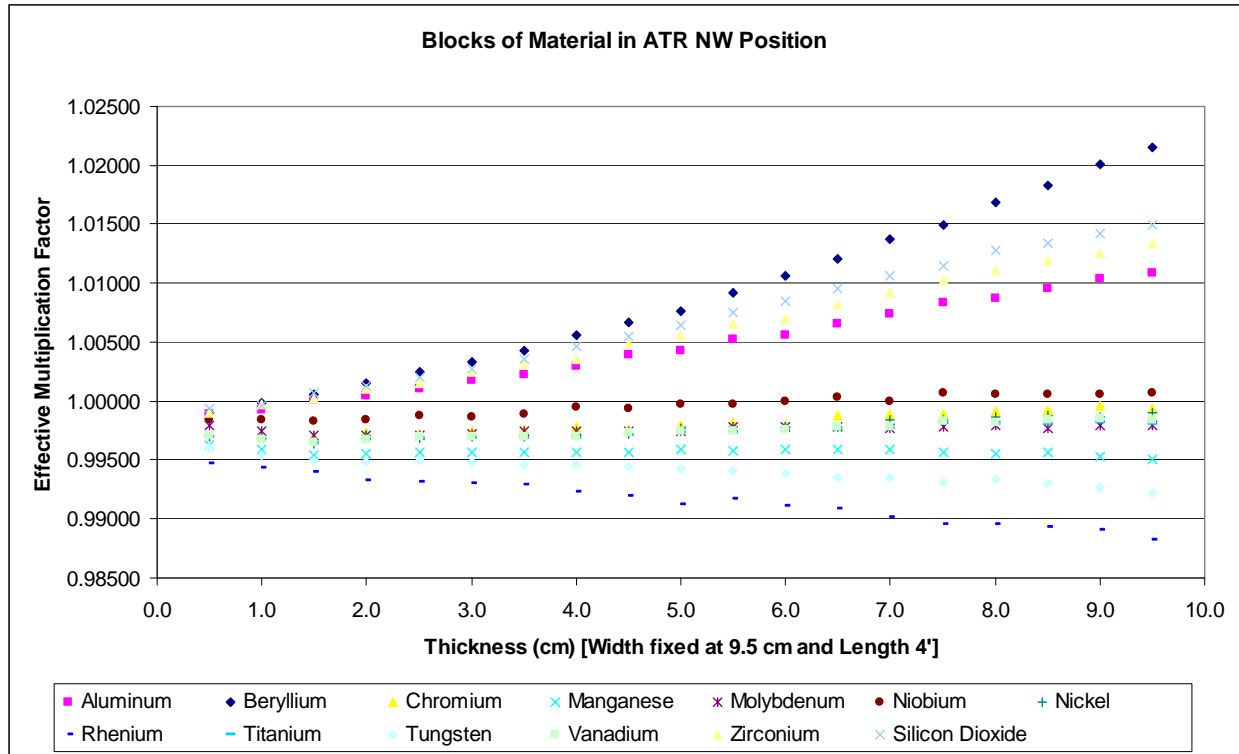
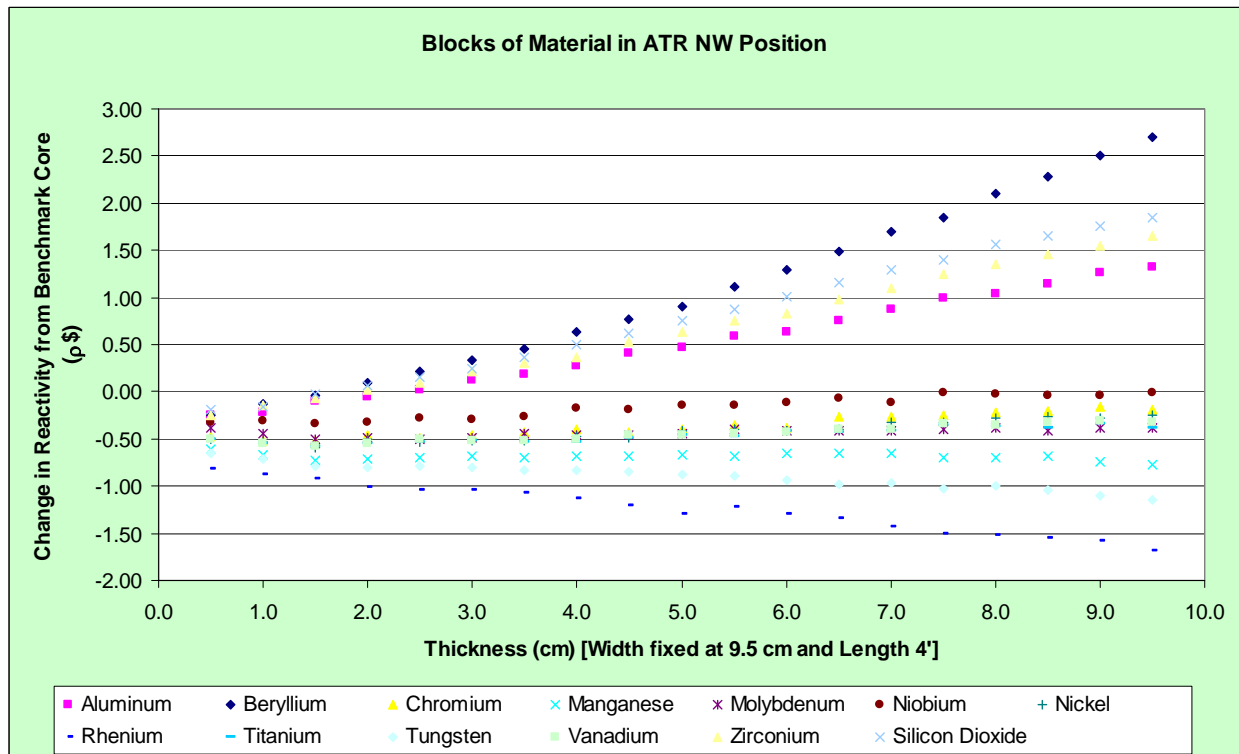Figure 3.1: Calculated Eigenvalues for Experiments in Phase One.

Figure 3.2: Calculated Reactivities for Experiments in Phase One.
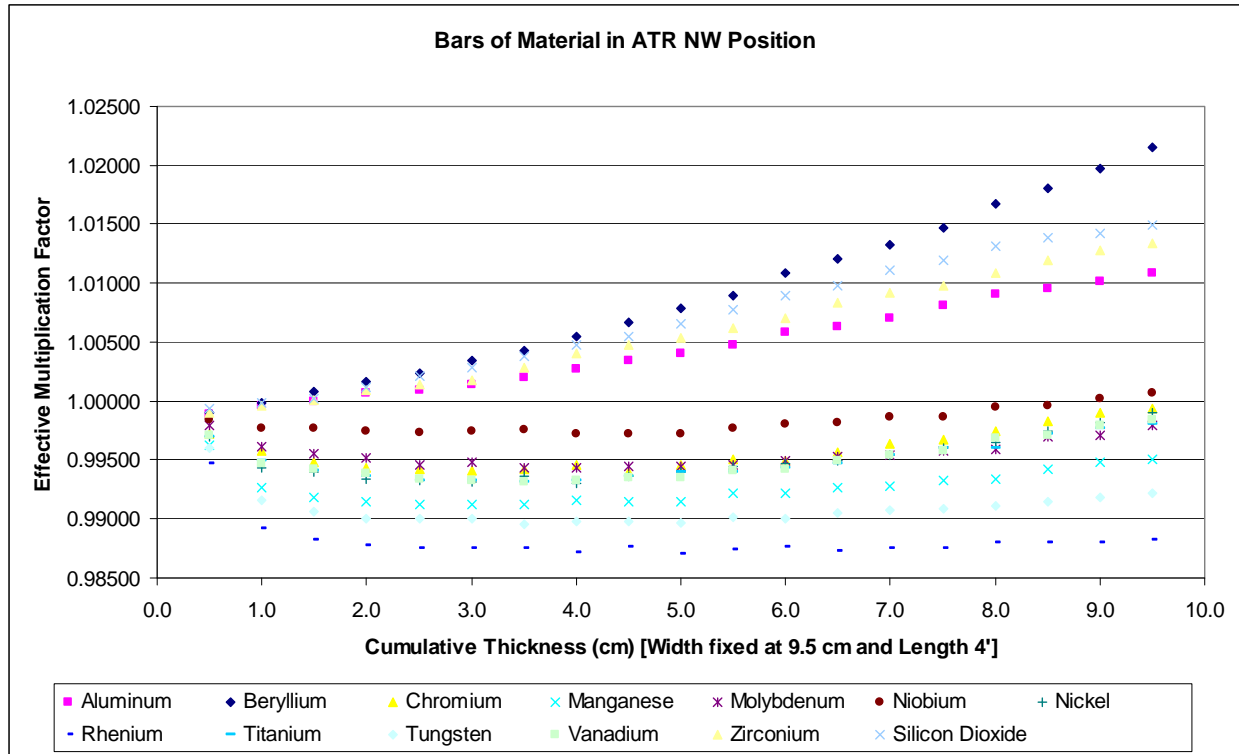
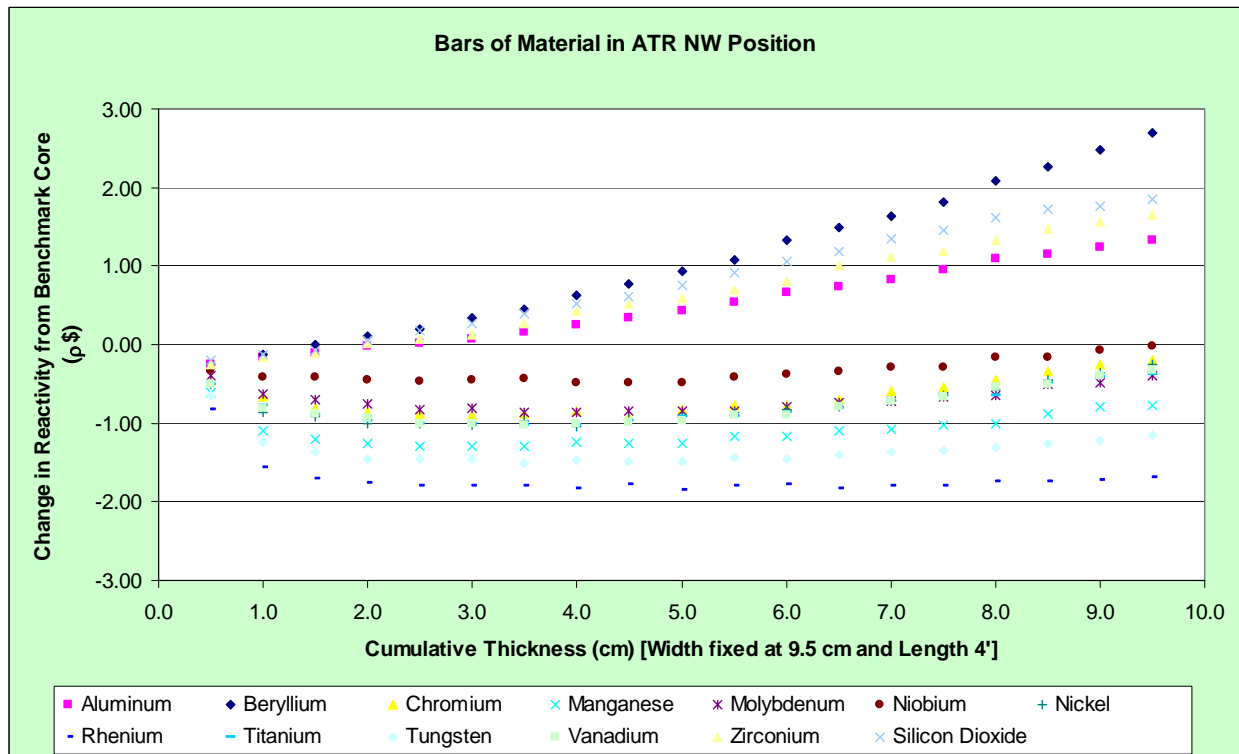Figure 3.3: Calculated Eigenvalues for Experiments in Phase Two.

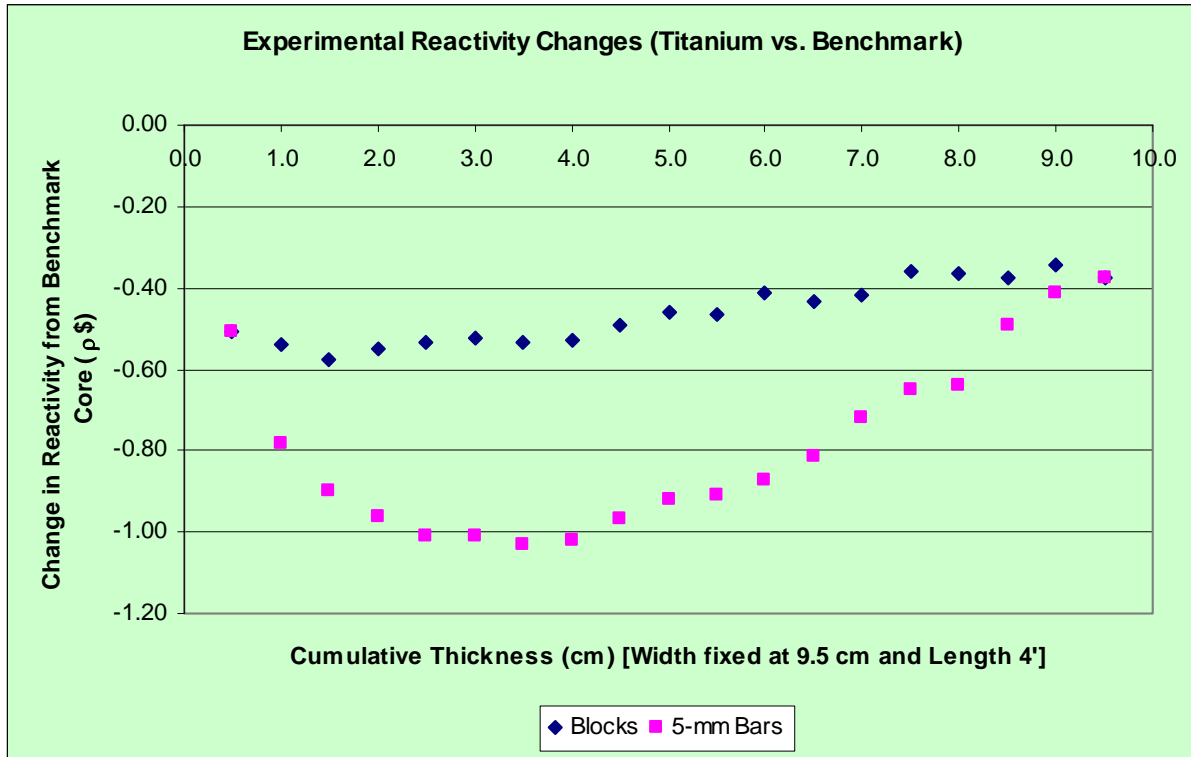Figure 3.4: Calculated Reactivities for Experiments in Phase Two.

Figure 3.5: Effective Reactivity of Titanium for Varying Material Quantities.
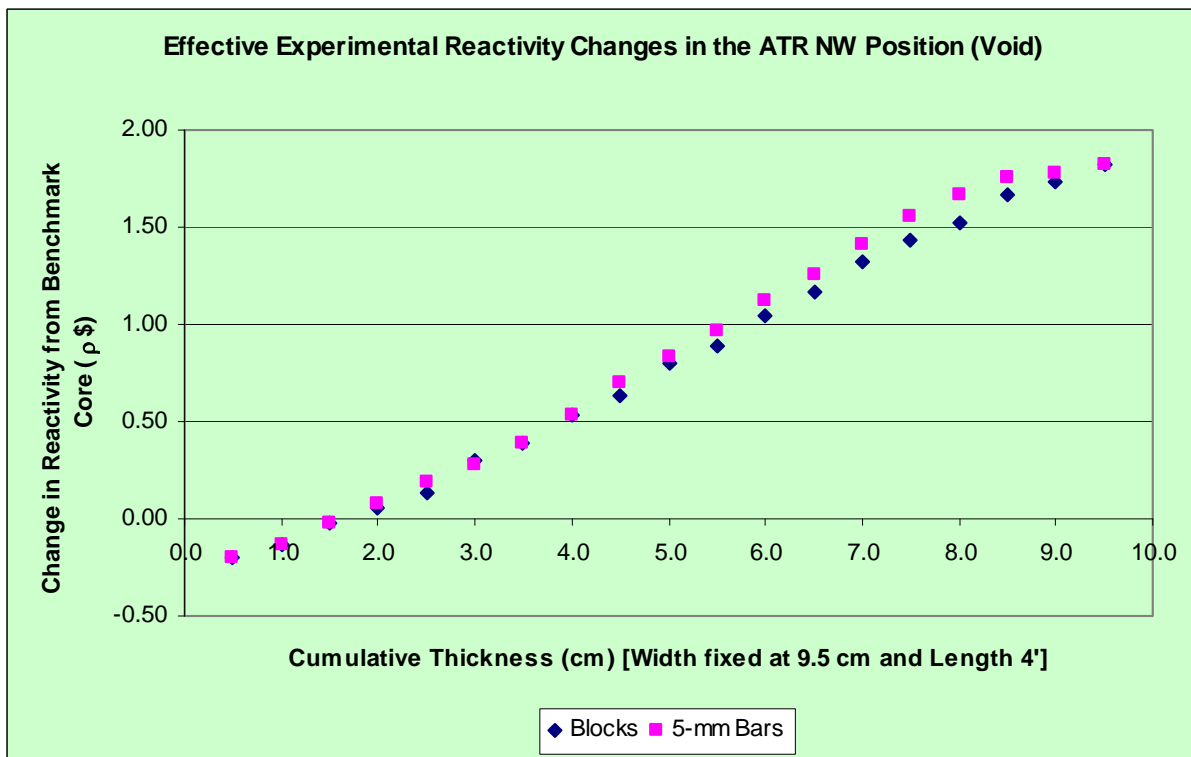

Figure 3.6: Voiding Effects on Core Reactivity.

The proposed experimental approach is to evaluate material configurations in the core that provide measurable reactivity effects within the operational limits of the reactor facility. A single bar of material would provide a means to determine the effective worth of a given sample of material. Utility of additional material would provide valuable means for computationally evaluating material and geometric effects in the experimental facility. Table 3.1 contains a summary of the estimated worth of a single bar of material (9.5 cm long, 0.5 cm wide, and 121.92 cm high) and multiple bars arranged such that their effective reactivity insertion is less than 1$. To simplify manufacture of the experimental assemblies, use of configurations with the equivalent number of bars would be necessary. Except for experiments where the worth of more than one bar would be greater than 1$, the nominal number of bars for maintaining geometric similarity between all experiments is four; however, selection of multi-bar geometry may be different depending on the desired increase in reactivity insertion (such as for beryllium, zirconium, and silicon dioxide). Together these experiments would provide valuable integral data for improving the cross sections of neutron data libraries and offer additional means of validating computational models of the experimental benchmarks.

Table 3.1: Estimated Experimental Reactivities for Integral Benchmarks in the ATR-C.

Material	Worth of One Bar (ρ\$)	Max Number of Multiple Bars	Worth of Multiple Bars (ρ\$)	Equal Number of Multiple Bars	Worth of Multiple Bars (ρ\$)
Aluminum	-0.25	4	1.00	4	1.00
Beryllium	-0.24	10	0.93	4	0.10
Chromium	-0.48	6	-0.90	4	-0.86
Manganese	-0.60	--	--	1	-0.60
Molybdenum	-0.39	7	-0.87	4	-0.76
Nickel	-0.51	4	-1.00	4	-1.00
Niobium	-0.32	9	-0.49	4	-0.46
Rhenium	-0.82	--	--	1	-0.82
Titanium	-0.51	4	-0.96	4	-0.96
Tungsten	-0.65	--	--	1	-0.65
Vanadium	-0.50	5	-1.00	4	-0.94
Zirconium	-0.24	13	1.00	4	0.01
SiO$_2$ Glass	-0.19	11	0.91	4	0.05

4. Future Efforts

Of primary importance is the development and characterization of a benchmark model of the ATR-C in compliance with guidelines described in the *International Handbook of Evaluated Criticality Safety Benchmark Experiments* [3]. Further characterization of the reactor in accordance with guidelines in the *International Handbook of Evaluated Reactor Physics Benchmark Experiments* [4] would further provide benefit for these, and future, experimental applications with the ATR-C facility. With the development of a more descriptive model, comprehensive modeling of the experiments with appropriate movement of control drums can be performed. Reactivity effects measurements can then be compared against qualified reactivity data obtained for the ATR-C control drum positions [9].

Development of the experiment assemblies is also necessary. Cylindrical end caps comprised of aluminum material can be used to aid in the placement of the experiment material within the flux trap. The bottom end cap would assist in maintaining nearly linear alignment through the length of the active core. The top end cap would provide structural support from which the bars of material are suspended. The means of attachment has yet to be investigated. Alignment guides and handling attachments on the top of the experiment assembly would provide means for proper emplacement within the flux trap position. Complete assessment of the materials and manufacturing costs is necessary. As currently evaluated, two assembly types would be necessary: a single-bar geometry and a multi-bar geometry capable of holding four bars. However, some materials with positive reactivity effects might require the addition of more bars to reduce the ratio of modeling uncertainty to the computed reactivity values.

Characterization of the flux and spectral indices is also of importance. Pacific Northwest National Laboratory (PNNL) provides neutron dosimetry capsules for experiments performed in the ATR. These capsules can be placed throughout the experiment assembly and analyzed to determine activation rates from various wires placed in these capsules. Capsules are custom designed to specific irradiation conditions of the experiment. Further questions regarding their application, cost, and development can be provided as necessary.[a] The spectral indices can be evaluated using thin foils of fissionable material attached to the sides of the bar material.

The ATR-C also has the capabilities of performing oscillation experiments. Typically only three to four standard experiments can be performed in the ATR-C per day. However, three to four oscillation experiments can be performed within an hour. This is because complete startups of the ATR-C are unnecessary when performing oscillation experiments. The facility has a digital reactivity measurement system with a manual reactivity insertion limit of 0.22$ and an uncertainty of ±0.05$.[b]

Oscillation techniques utilize small sample reactivity insertion for deriving information about the mechanism of neutron interaction with materials introduced into a nuclear reactor, for the determination of material properties such as cross sections, and for determining the characteristics of the reactor itself. Typically reactivity oscillation measurements involve the insertion and withdrawal of a well-calibrated fine-control element to maintain a constant critical configuration in a reactor while simultaneously withdrawing and inserting a well-characterized material sample. Multiple measurements and application of perturbation theory allow for precise and accurate determination of small reactivities with very low uncertainty [10]. The use of small samples does not significantly perturb the flux and spectra in the location of the experiment.

---

[a] Personal communication with Larry Greenwood from PNNL on February 25, 2009.

[b] Personal communication with ATR-C personnel on September 22, 2008.

Further assessment of the capabilities and limitations of oscillation techniques in the ATR-C is necessary, as it could further enhance capabilities for developing integral data and validating computational methods. Additional information regarding the application in historic nuclear reactors can be found listed elsewhere [10]. More recent activities include the OSMOSE program with France's MINERVE reactor [11, 12] and the ongoing installation of an oscillator experiment on the AGN reactor at Idaho State University.[a] Validation of computational codes will be different than for the previously proposed experiments. As the oscillation methods are not geometry-dependent, validation of diffusion-theory or discrete-ordinate methods might be more applicable than models using Monte Carlo methods.

5.   Conclusions

It is proposed that experiments consisting of well-characterized quantities of materials placed in the ATR-C facility could provide integral data for key matrix and structural materials used in nuclear systems. Results would then be utilized to improve nuclear data libraries and provide additional benchmarks for the validation of analytical and computational methods.

Calculations using MCNP and the benchmark model of the ATR were used to estimate the effective reactivity insertion of the materials into the Northwest flux trap of the ATR-C. A total of thirteen materials were studied and compared against the benchmark configuration with an aluminum plug in the Northwest flux trap, the benchmark configuration with the plug removed and the flux trap filled with water, and configurations involving aluminum and "void" material to view the effects from removing water from the flux trap position. Materials with positive reactivity effects cumulative with the positive effect from voiding water include aluminum, beryllium, zirconium, and silicon dioxide. A comparison of blocks of material and multiple bars of identical amounts of material were analyzed to determine the effect of geometric placement and self-shielding. For materials causing negative reactivity insertion, typically multiple bars would represent a more significant effect than a single block of the same total mass. A single bar measuring 9.5 cm in length, 0.5 cm in width, and 121.92 cm in height could provide between -0.19$ and -0.82$ compared to the benchmark model configuration. The use of multiple bars (a total of four bars for most materials, if a standard design is implemented for the experimental assemblies) could provide additional means of computational validation and provide up to the maximum reactivity insertion limit of 1$ for many of the materials.

Future tasks include the cost analysis and development of the experimental assemblies, including means for the characterization of the neutron flux and spectral indices. Oscillation techniques may also serve to provide additional means for experimentation and validation of computational methods and acquisition of integral data for improving neutron cross sections. Further assessment of oscillation techniques for implementation in the ATR-C should be of additional benefit. The establishment of benchmark experiment capabilities in the ATR-C will allow for the further development of techniques and facility enhancements involving neutronics experimentation in the ATR-C.

6.   Acknowledgments

---

[a] Personal communication with George Imal at ISU from March 3, 2009.

7. References

[1]   "FY 2009 Advanced Test Reactor National Scientific User Facility Users' Guide," INL/EXT-08-14709, Idaho National Laboratory, 2008.

[2]   S. S. KIM and B. G. SCHNITZLER, "Advanced Test Reactor: Serpentine Arrangement of Highly Enriched Water-Moderated Uranium-Aluminide Fuel Plates Reflected by Beryllium," HEU-SOL-THERM-022, *International Handbook of Evaluated Criticality Safety Benchmark Experiments*, NEA/NSC/DOC(95)03, OECD-NEA (2008).

[3]   *International Handbook of Evaluated Reactor Physics Benchmark Experiments*, NEA/NSC/DOC(2006)1, OECD-NEA, March (2008).

[4]   *International Handbook of Evaluated Criticality Safety Benchmark Experiments*, NEA/NSC/DOC(95)03, OECD-NEA, September (2008).

[5]   F. B. BROWN, R. F. BERRETT, T. E. BOOTH, J. S. BULL, L. J. COX, R. A. FORSTER, T. J. GOORLEY, R. D. MOSTELLER, S. E. POST, R. E. PRAEL, E. C. SELCOW, A. SOOD, and J. SWEEZY, "MCNP Version 5," LA-UR-02-3935, Los Alamos National Laboratory (2002).

[6]   J. K. TULI, "Special Issue on Evaluated Nuclear Data File ENDF/B-VII.0," *Nucl. Data Sheets*, **107**, (2006).

[7]   E. M. BAUM, H. D. KNOX, and T. R. MILLER, *Nuclides and Isotopes: Chart of the Nuclides*, 16th ed., Knolls Atomic Power Laboratory, (2002).

[8]   J. R. LAMARSH and A. J. BARATTA, *Introduction to Nuclear Engineering*, 3rd ed., Prentice-Hall, Upper Saddle River, NJ (2001).

[9]   R. T. MCCRACKEN and L. S. LORET, "Results of ATR Critical Facility Core Reconfiguration and Requalification Testing for Post-Core Internals Changeout Operations," PG-T-94-006, EG&G Idaho (1994).

[10]   W. K. FOELL, *Small-Sample Reactivity Measurements in Nuclear Reactors*, American Nuclear Society (1972).

[11]   J-P. HUDELOT, C. CHABERT, J-P. CHAUVIN, P. FOUGERAS, G. PERRET, X. GENIN, C. LEORIER, J-M. MOULINIER, "The OSMOSE Experimental Program in MINERVE for the Qualification of the Integral Cross Sections of Actinides," *Nucl. Sci. Tech.*, Supplement 2, 1077-1080 (2002).

[12]   R. T. KLANN, J-P. HUDELOT, G. PERRET, N. DRIN, J. LEE, and Y. CAO, "Final Report on the International Nuclear Energy Research Initiative OSMOSE (FY01-FY04)," ANL-04-25, Argonne National Laboratory (2004).

APPENDIX A – Reactivity Effects Compared to Benchmark Model

Experimental reactivity changes due to the insertion of materials into the ATR benchmark model.
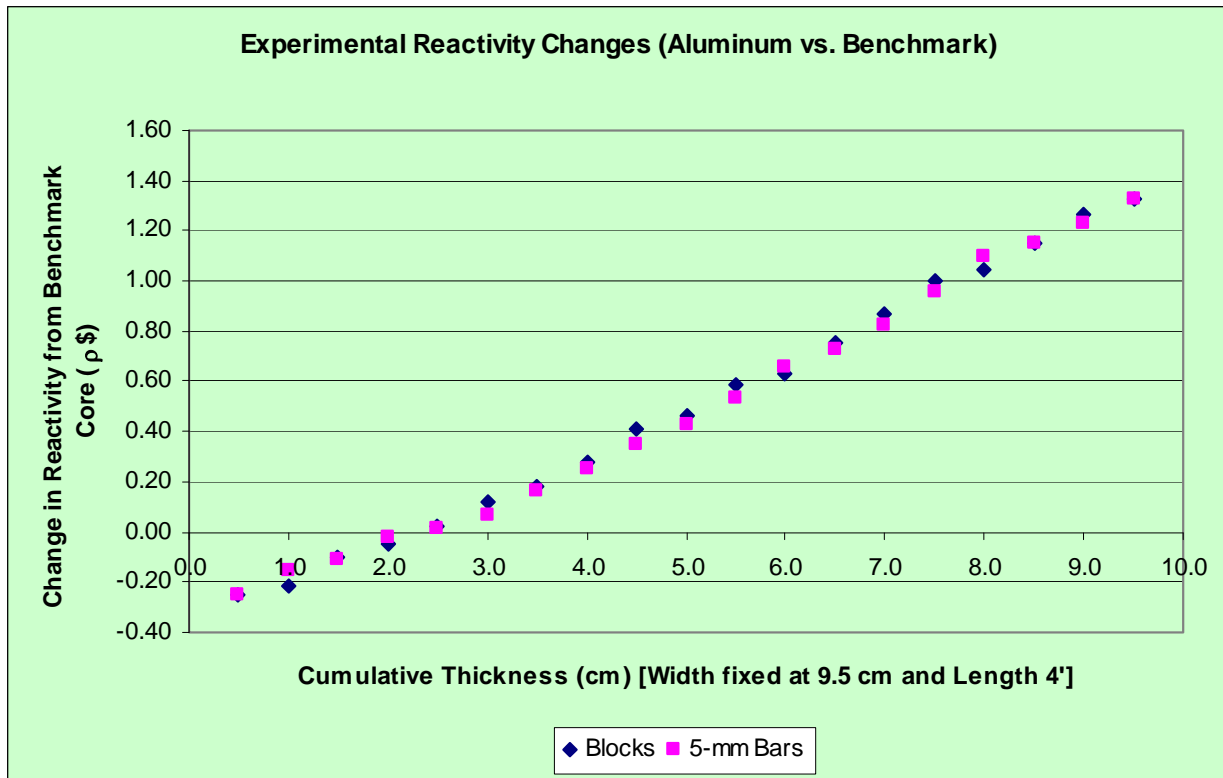
Figure A.1: Effective Reactivity of Aluminum for Varying Material Quantities.
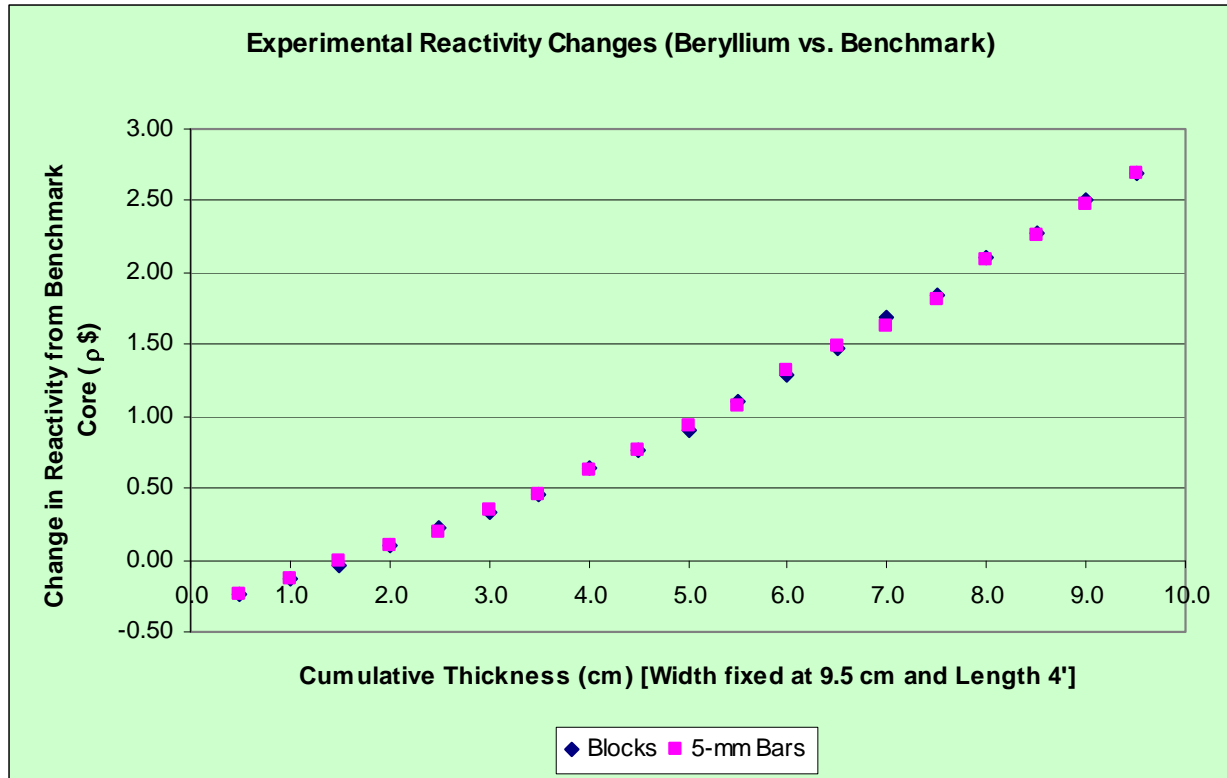
Figure A.2: Effective Reactivity of Beryllium for Varying Material Quantities.
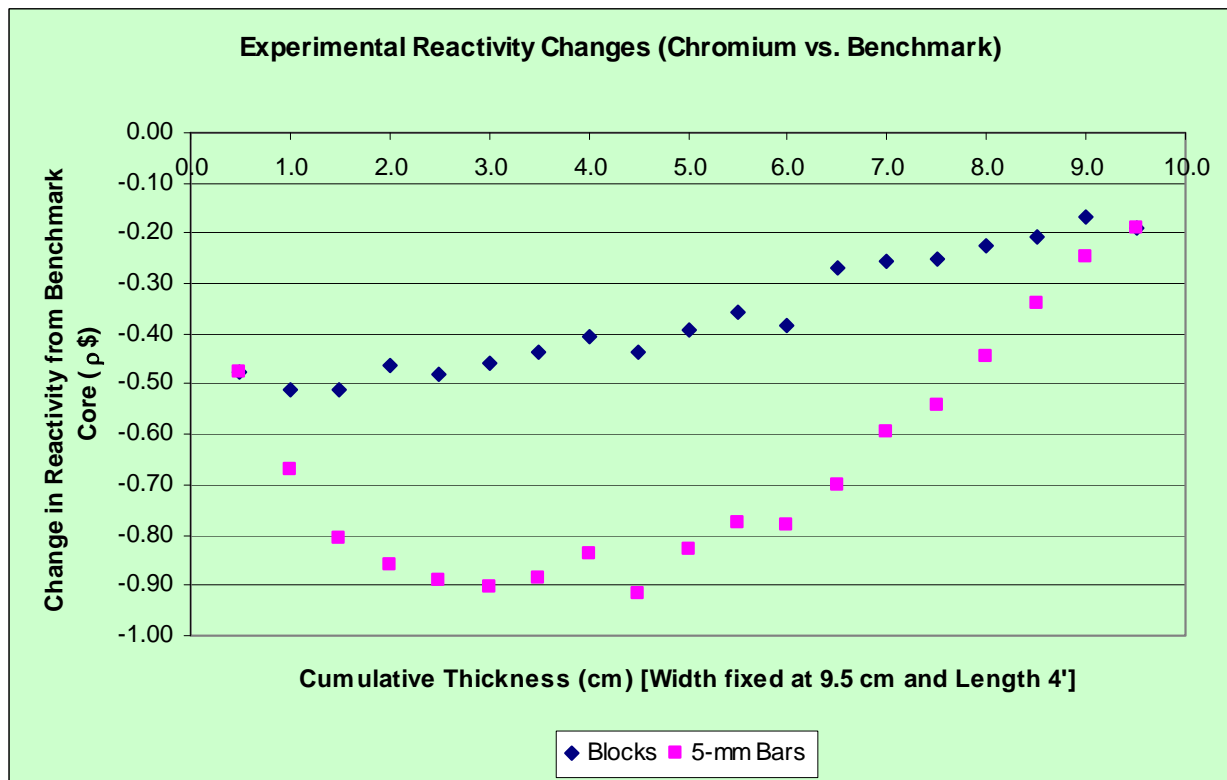
Figure A.3: Effective Reactivity of Chromium for Varying Material Quantities.
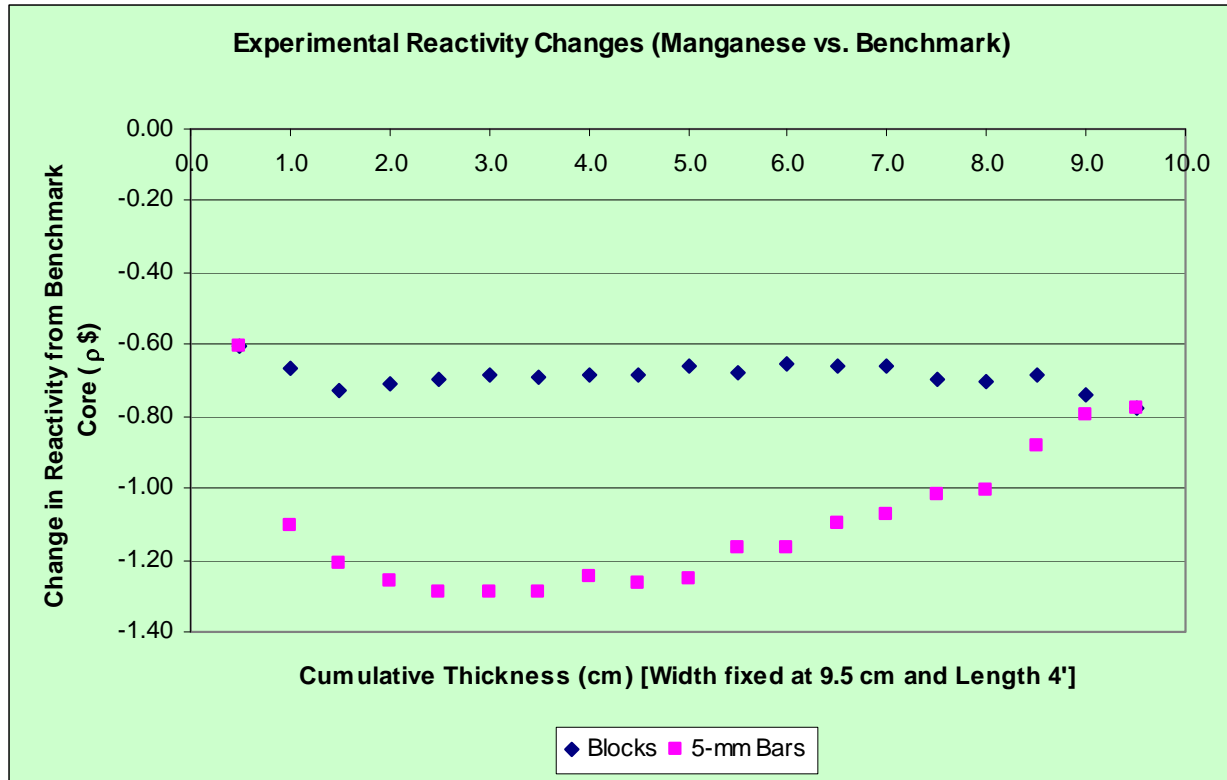
Figure A.4: Effective Reactivity of Manganese for Varying Material Quantities.
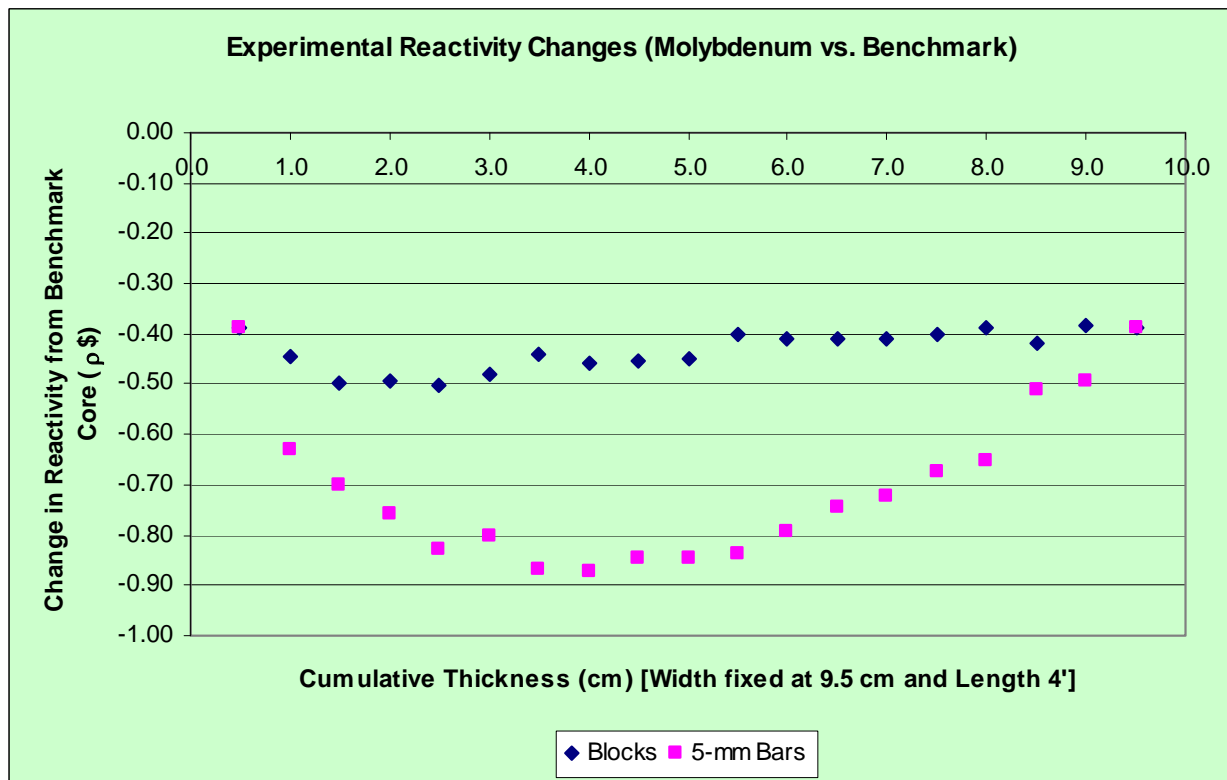
Figure A.5: Effective Reactivity of Molybdenum for Varying Material Quantities.
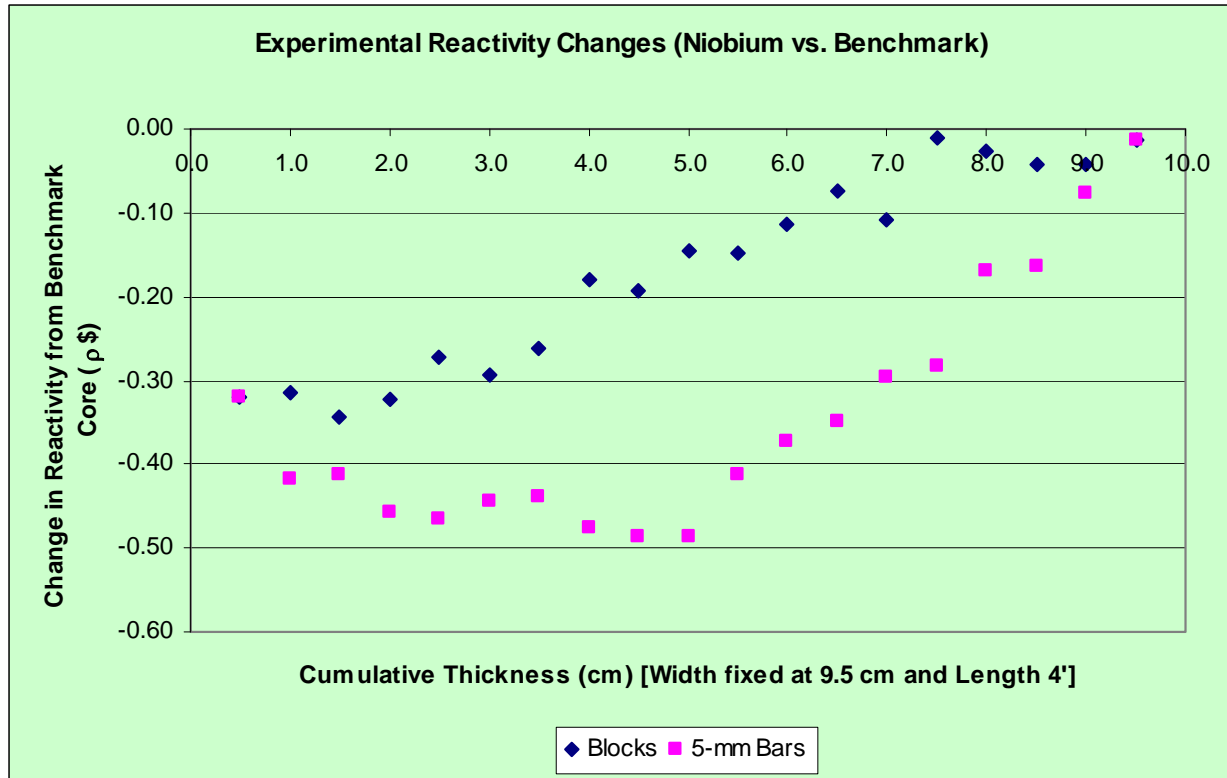
Figure A.6: Effective Reactivity of Niobium for Varying Material Quantities.
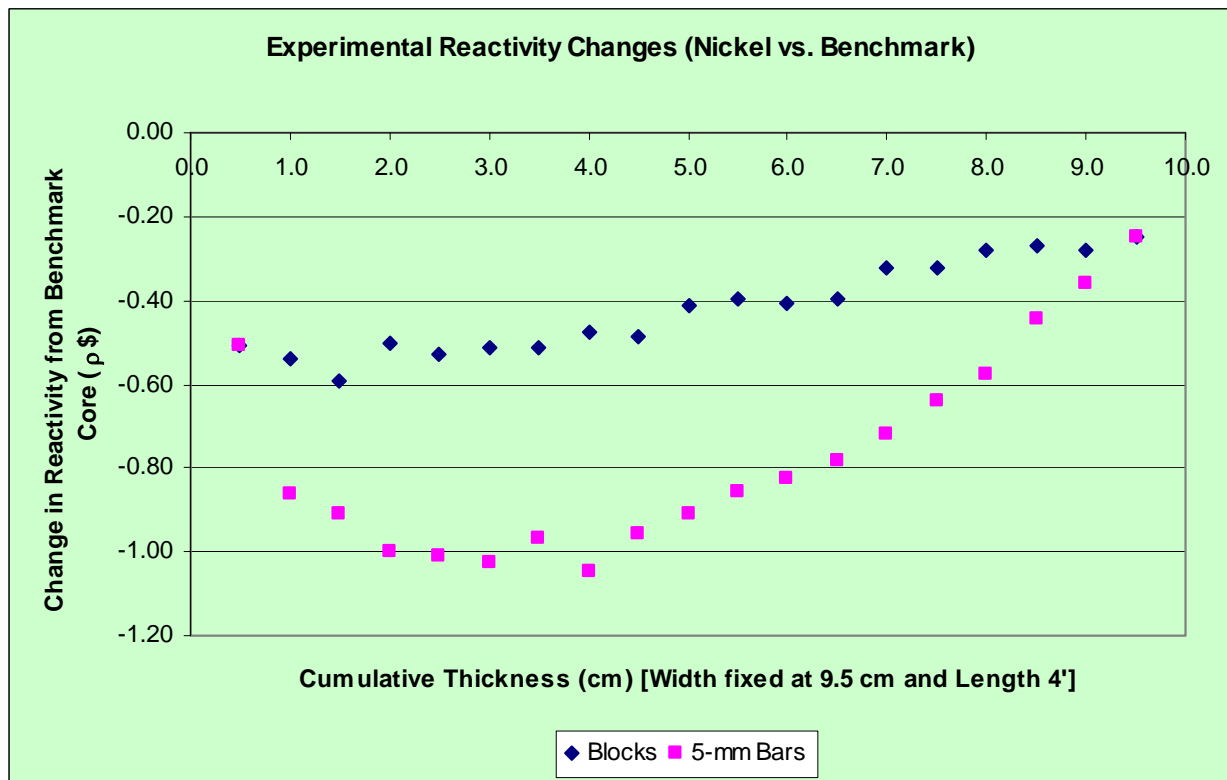
Figure A.7: Effective Reactivity of Nickel for Varying Material Quantities.

Experimental Reactivity Changes (Rhenium vs. Benchmark)
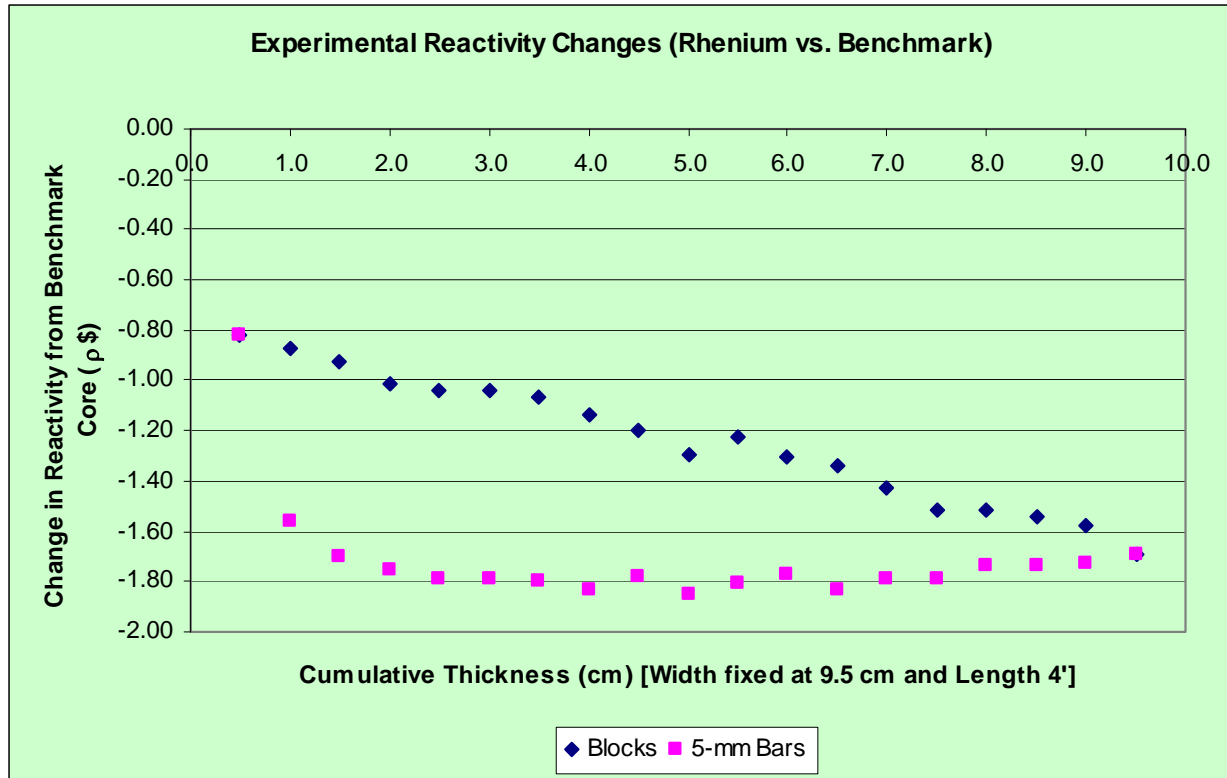
Figure A.8: Effective Reactivity of Rhenium for Varying Material Quantities.

Experimental Reactivity Changes (Titanium vs. Benchmark)
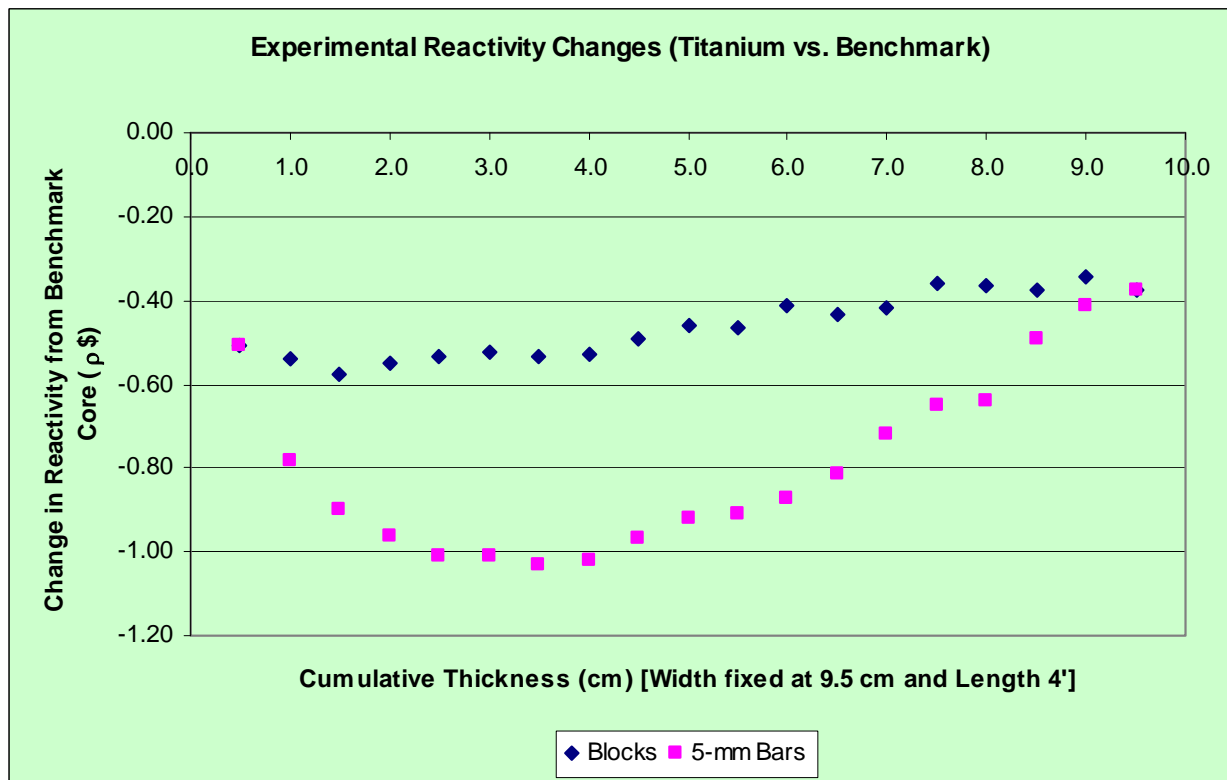
Figure A.9: Effective Reactivity of Titanium for Varying Material Quantities.
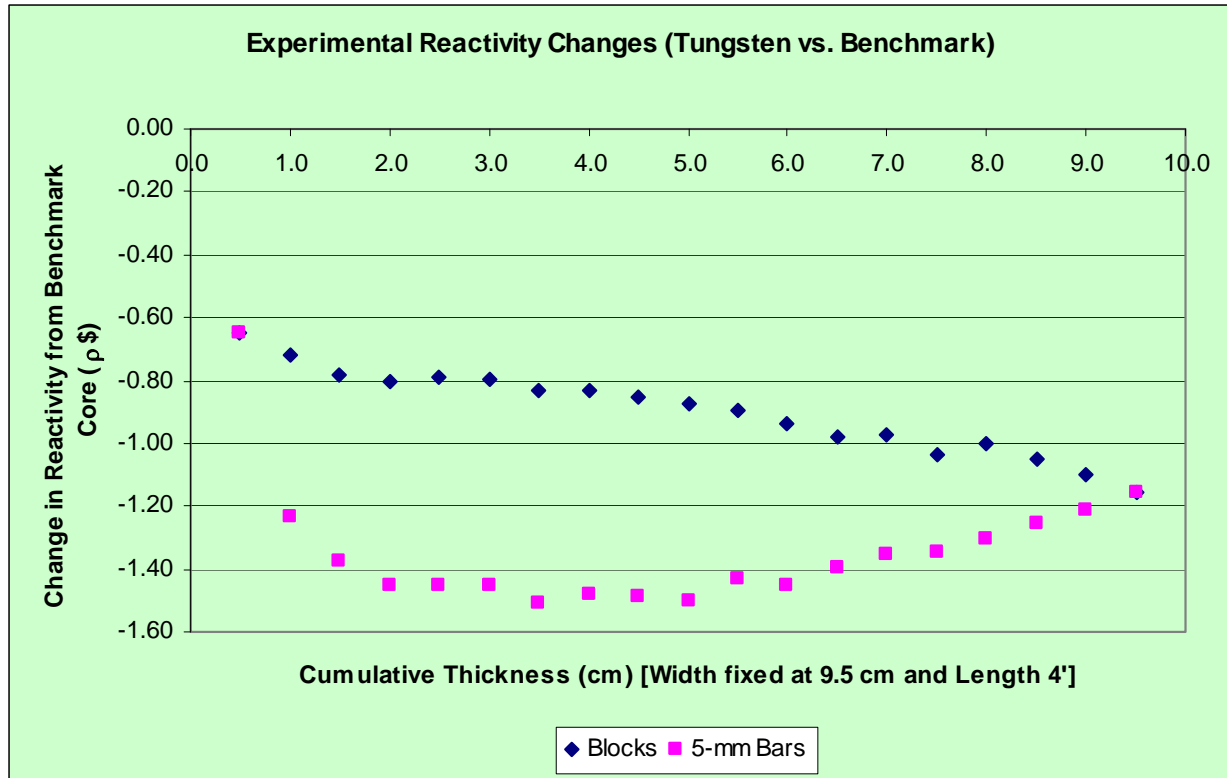
Figure A.10: Effective Reactivity of Tungsten for Varying Material Quantities.
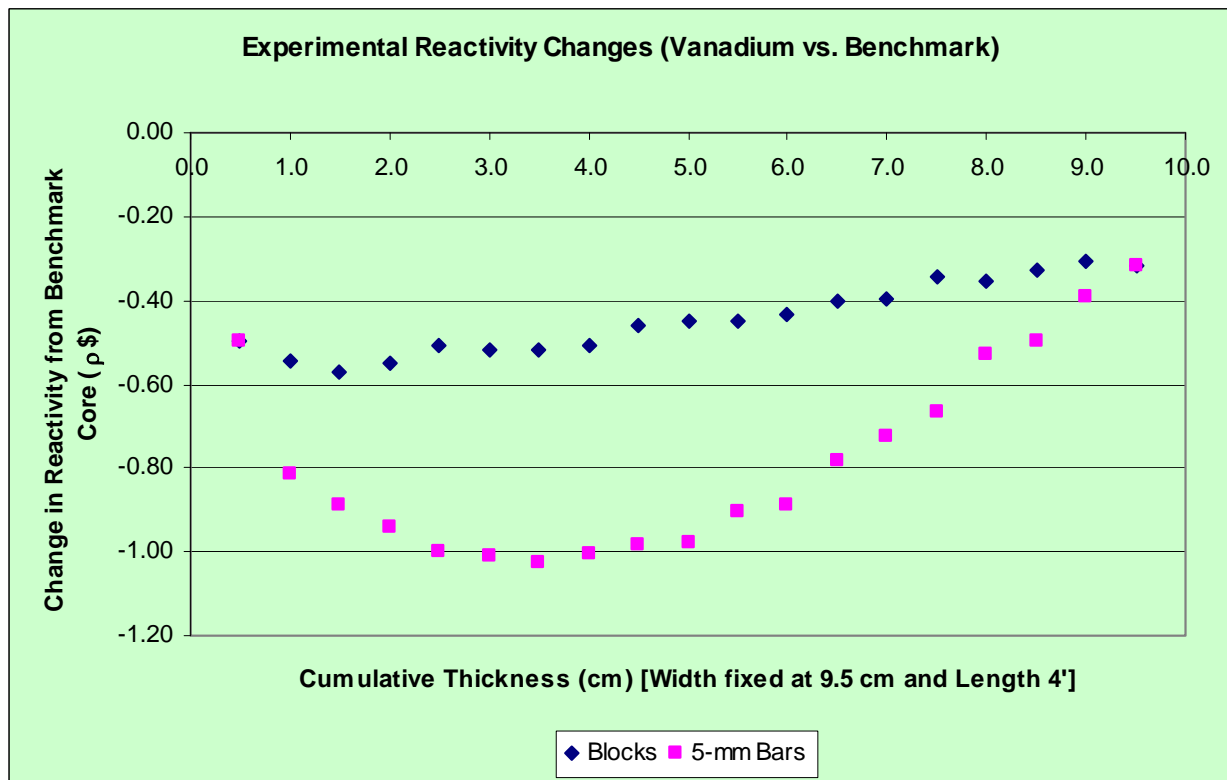
Figure A.11: Effective Reactivity of Vanadium for Varying Material Quantities.
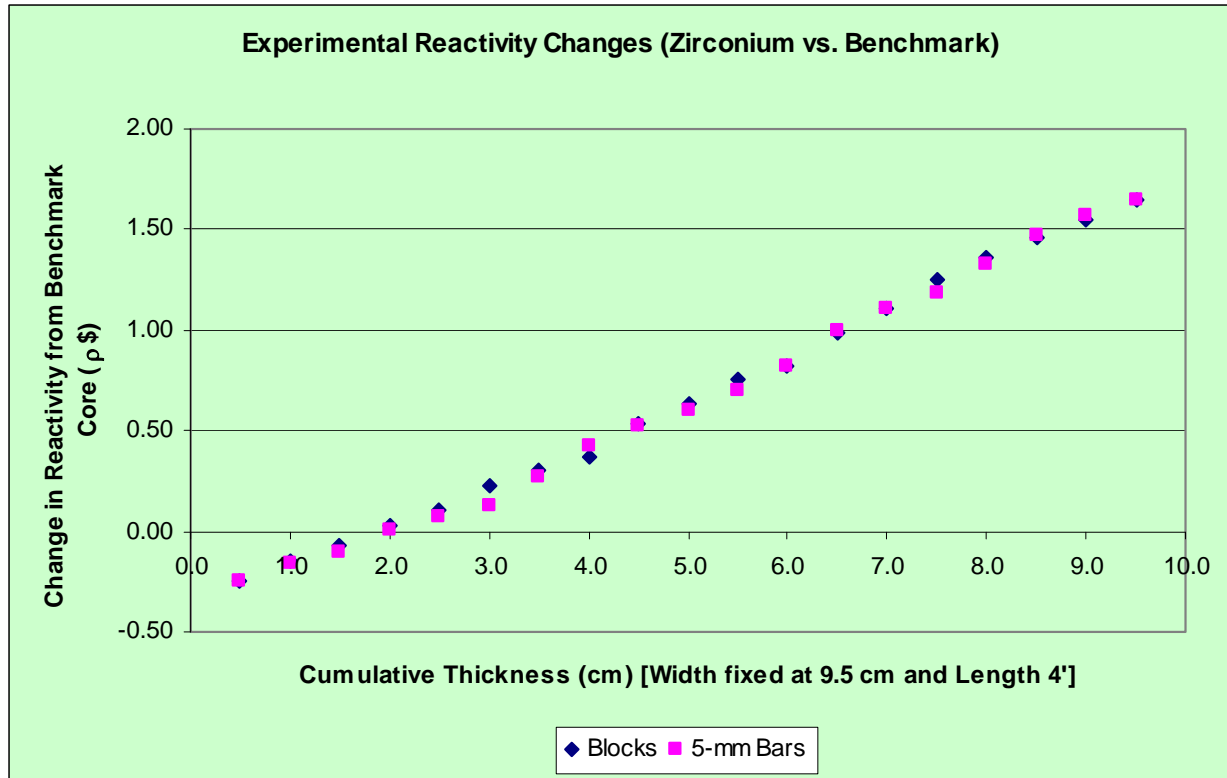
Figure A.12: Effective Reactivity of Zirconium for Varying Material Quantities.
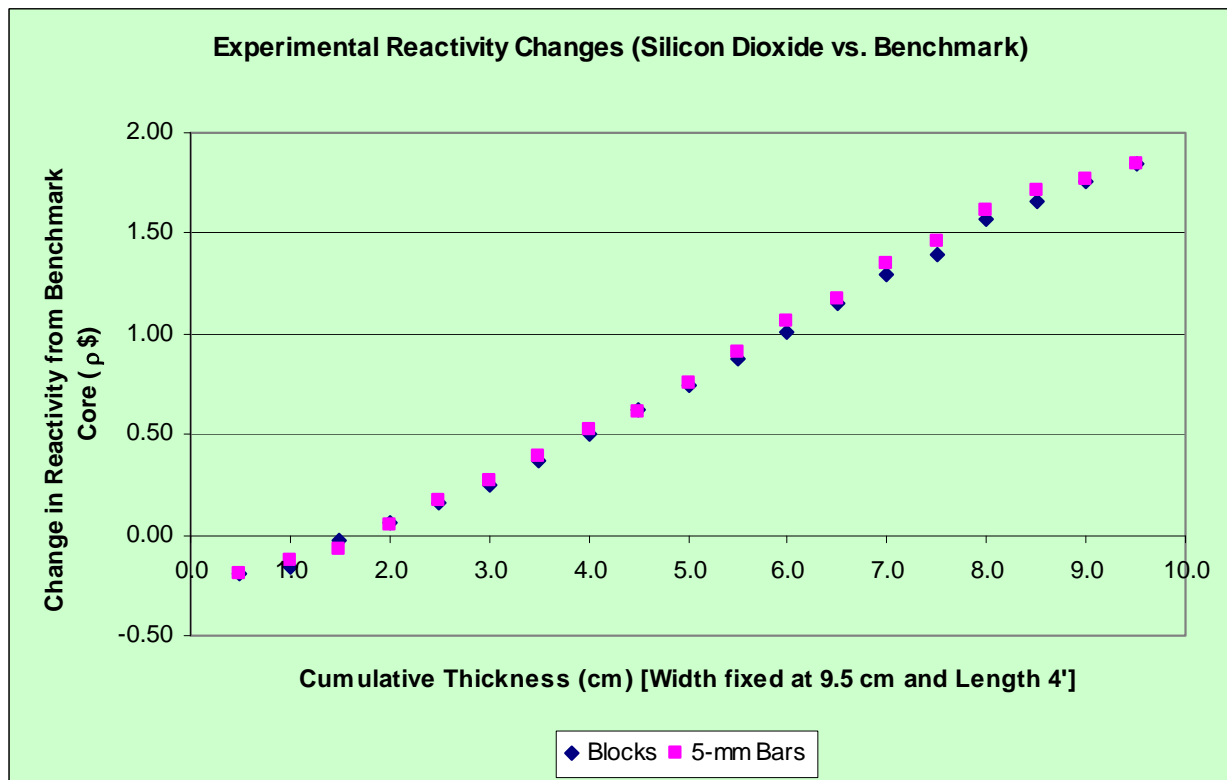
Figure A.13: Effective Reactivity of Silicon Dioxide for Varying Material Quantities.

APPENDIX B – Reactivity Effects Compared to Water-Filled Flux Trap

Experimental reactivity changes due to the insertion of materials into the ATR benchmark model compared against a water-filled flux-trap configuration.
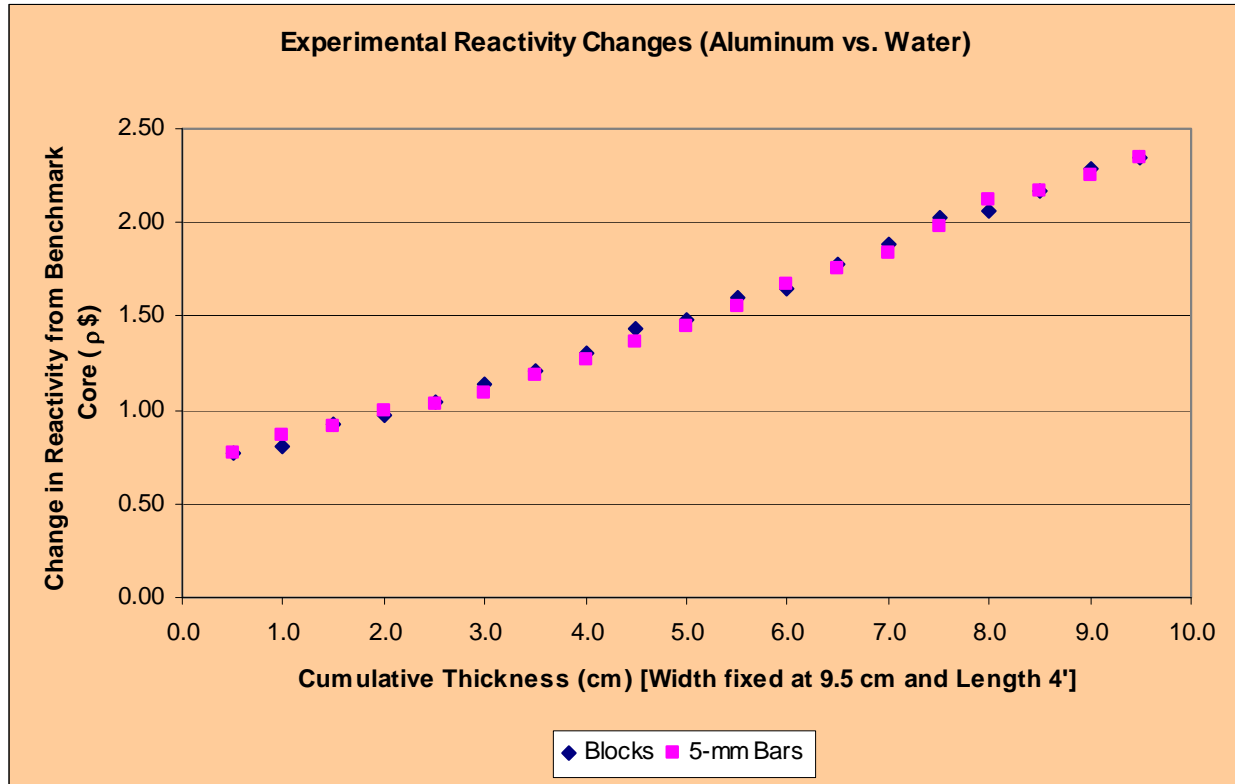
Figure B.1: Effective Reactivity of Aluminum Compared to Water in Flux Trap.
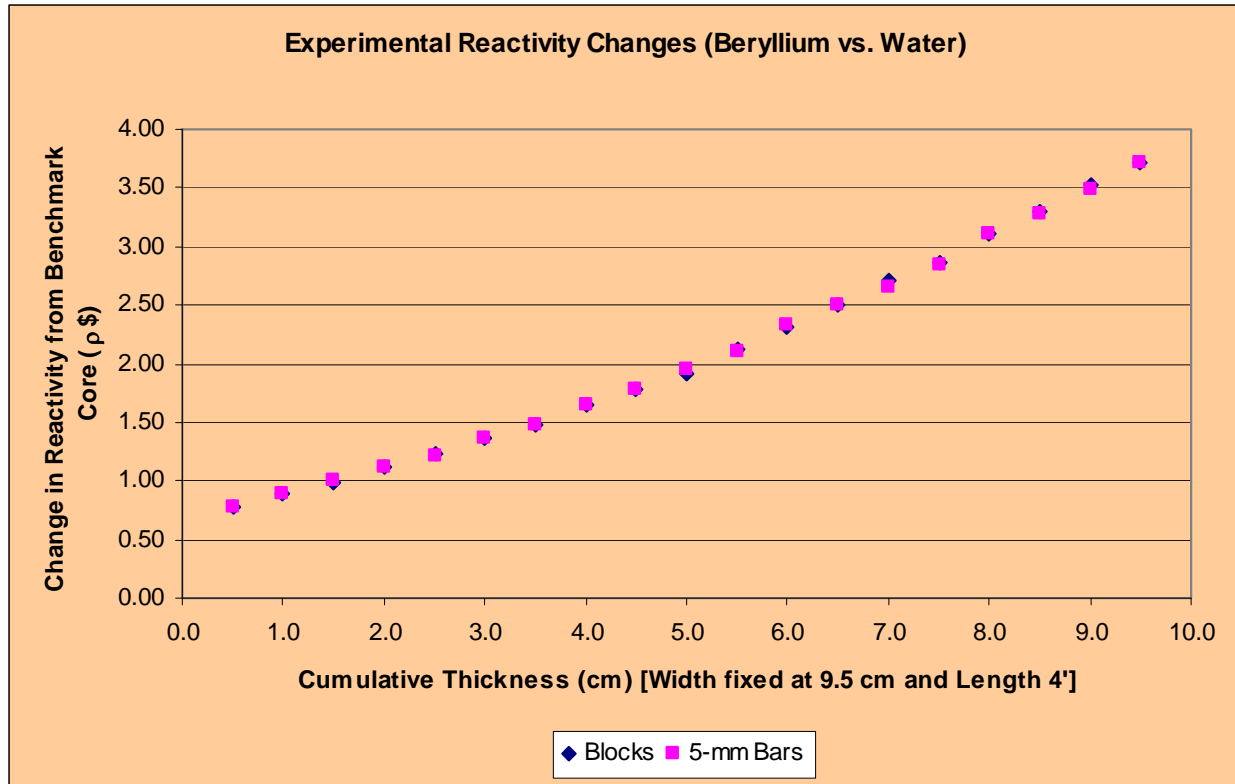
Figure B.2: Effective Reactivity of Beryllium Compared to Water in Flux Trap.
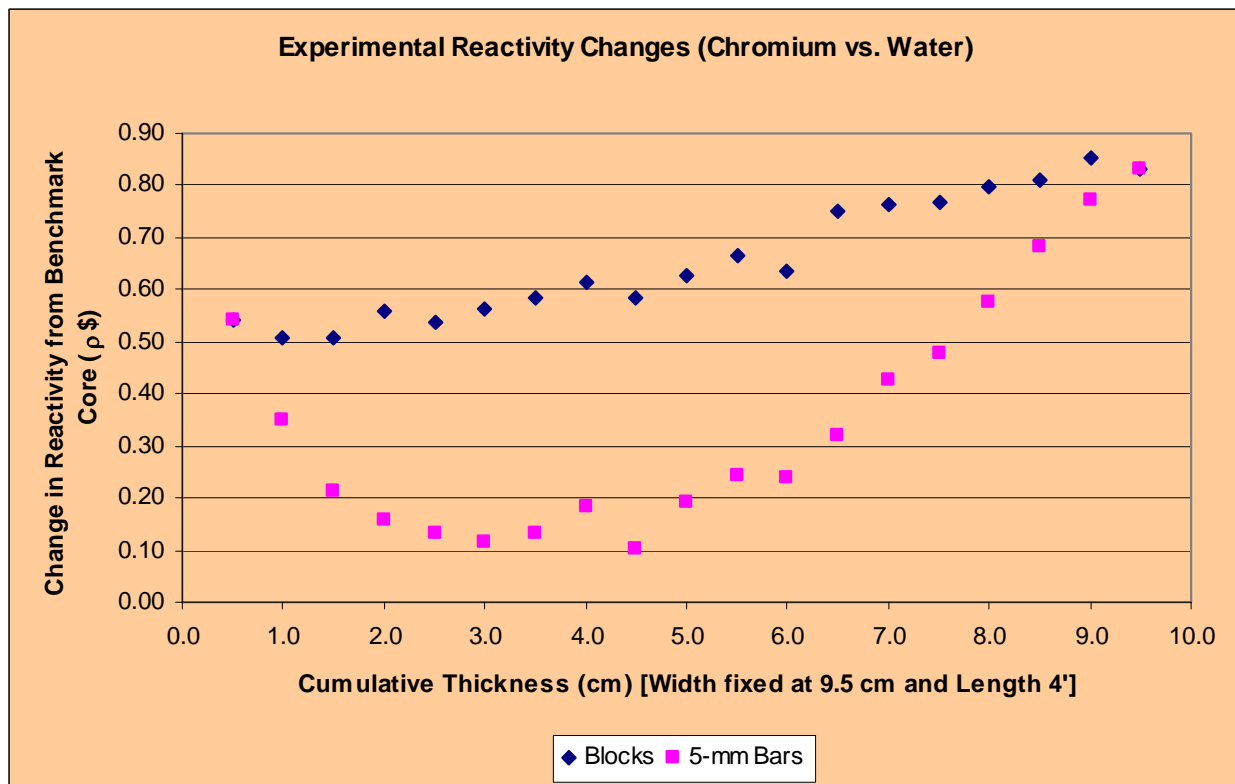
Figure B.3: Effective Reactivity of Chromium Compared to Water in Flux Trap.
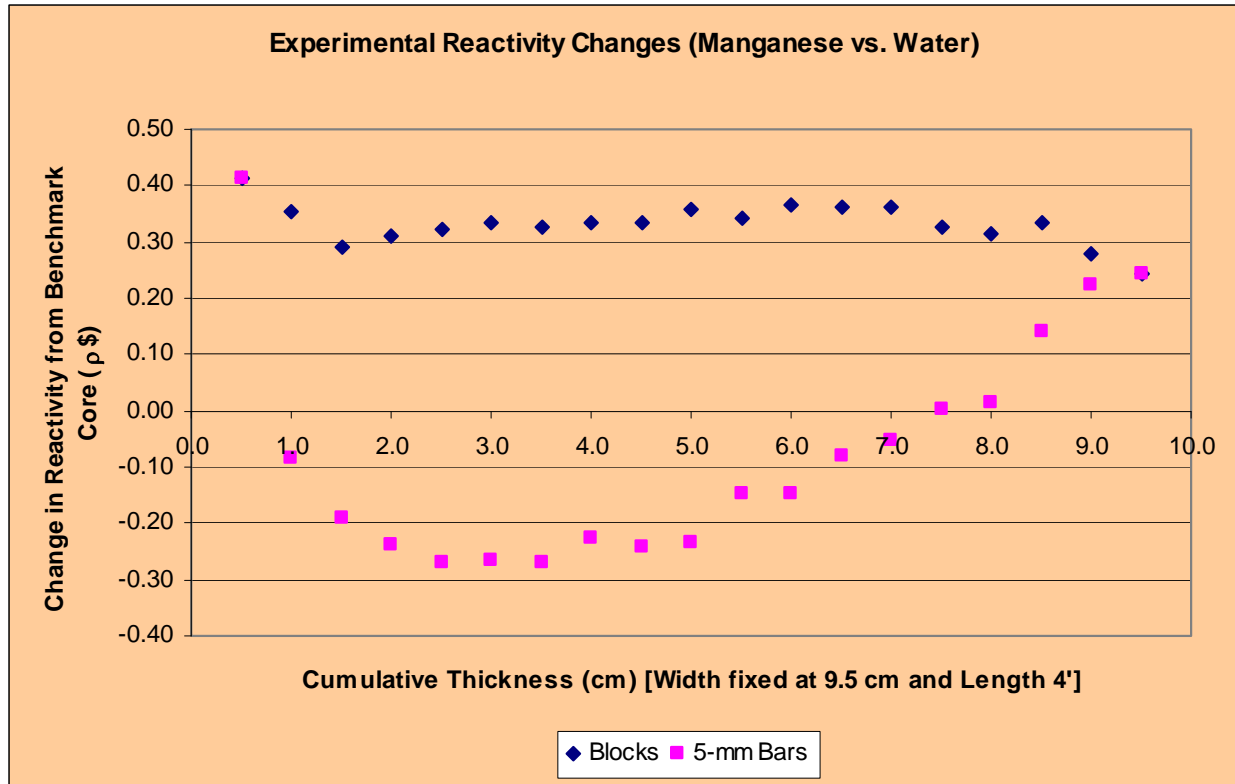
Figure B.4: Effective Reactivity of Manganese Compared to Water in Flux Trap.
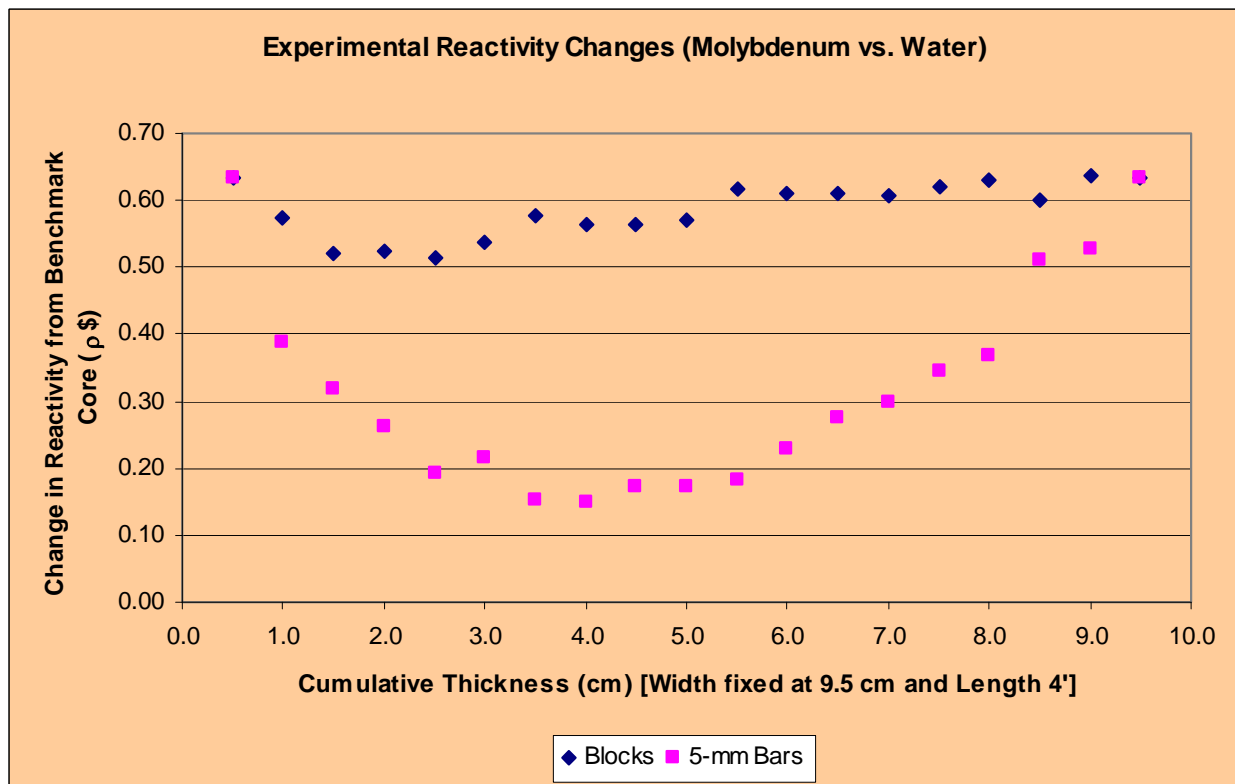
Figure B.5: Effective Reactivity of Molybdenum Compared to Water in Flux Trap.
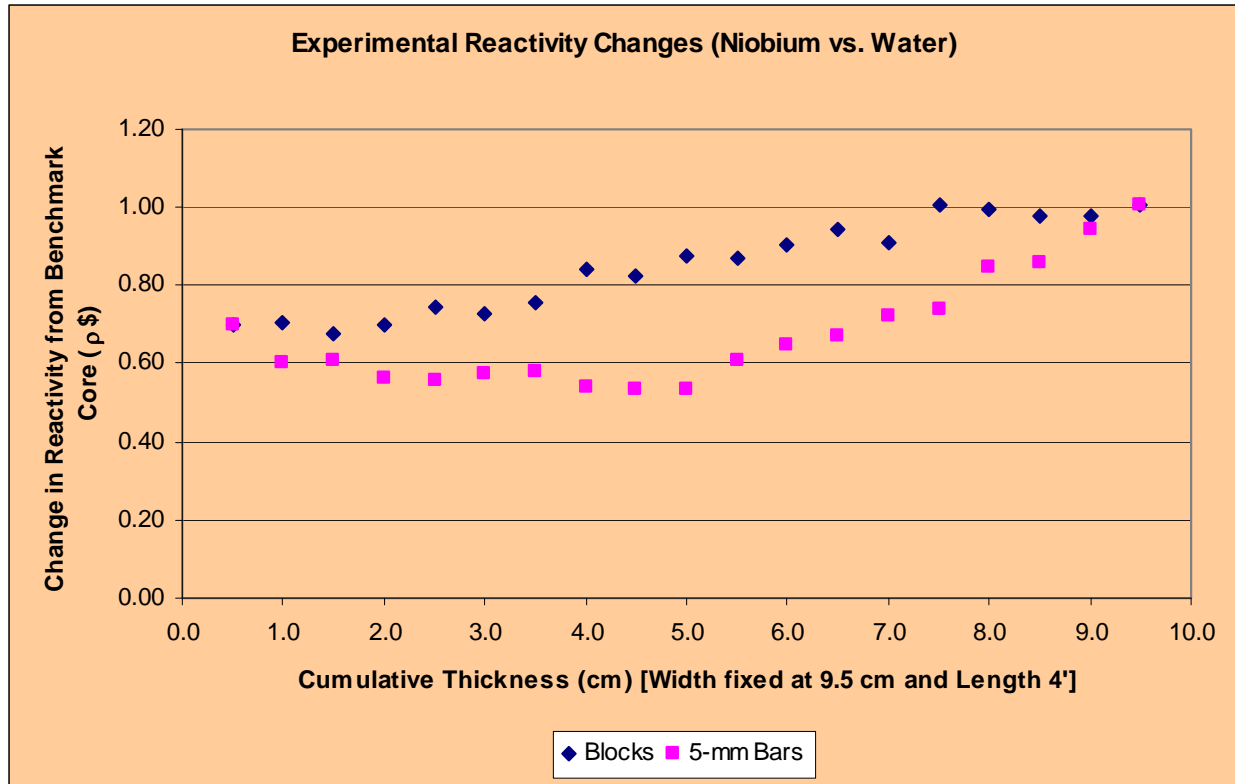
Figure B.6: Effective Reactivity of Niobium Compared to Water in Flux Trap.
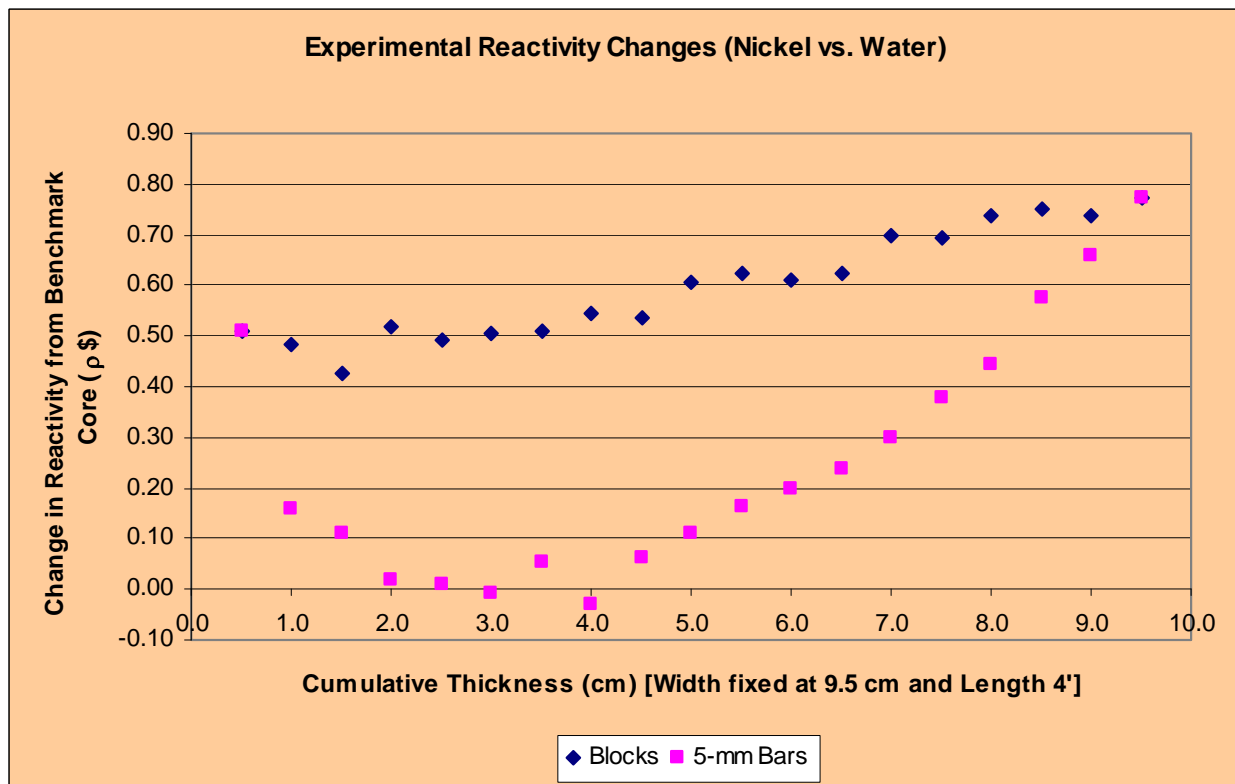
Figure B.7: Effective Reactivity of Nickel Compared to Water in Flux Trap.
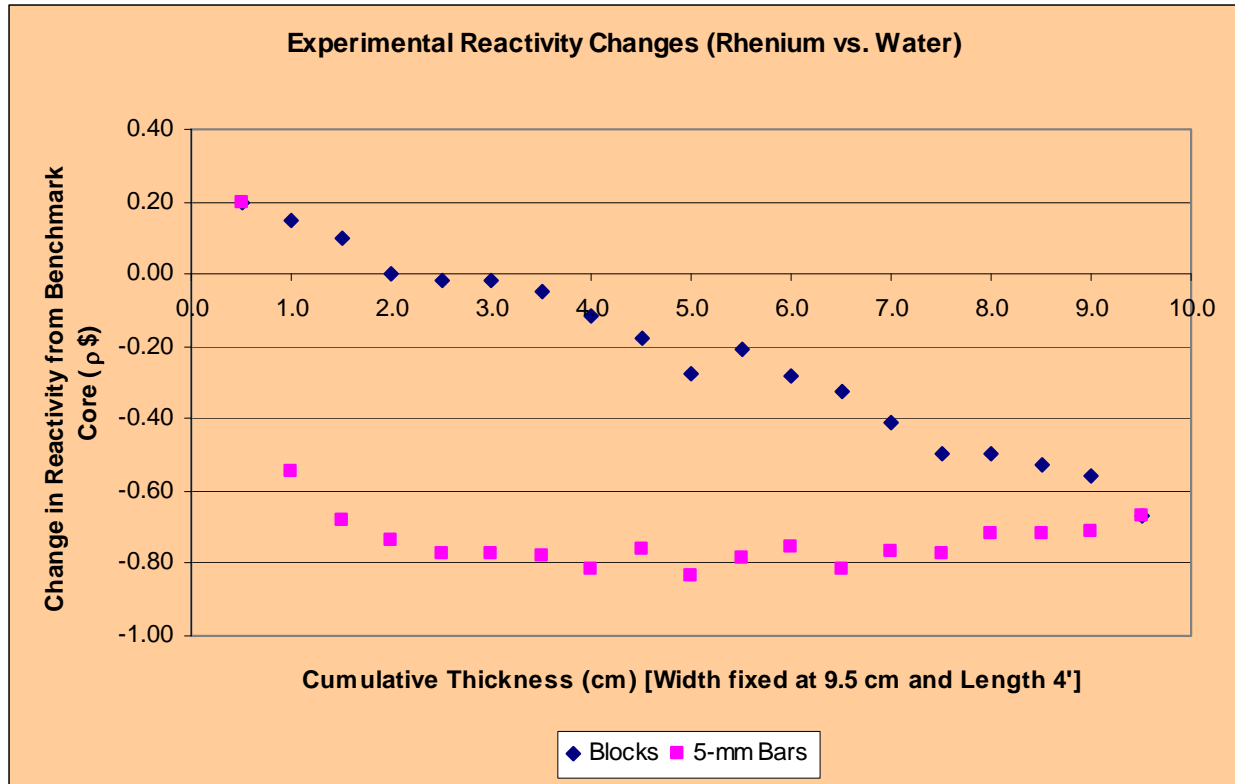
Figure B.8: Effective Reactivity of Rhenium Compared to Water in Flux Trap.
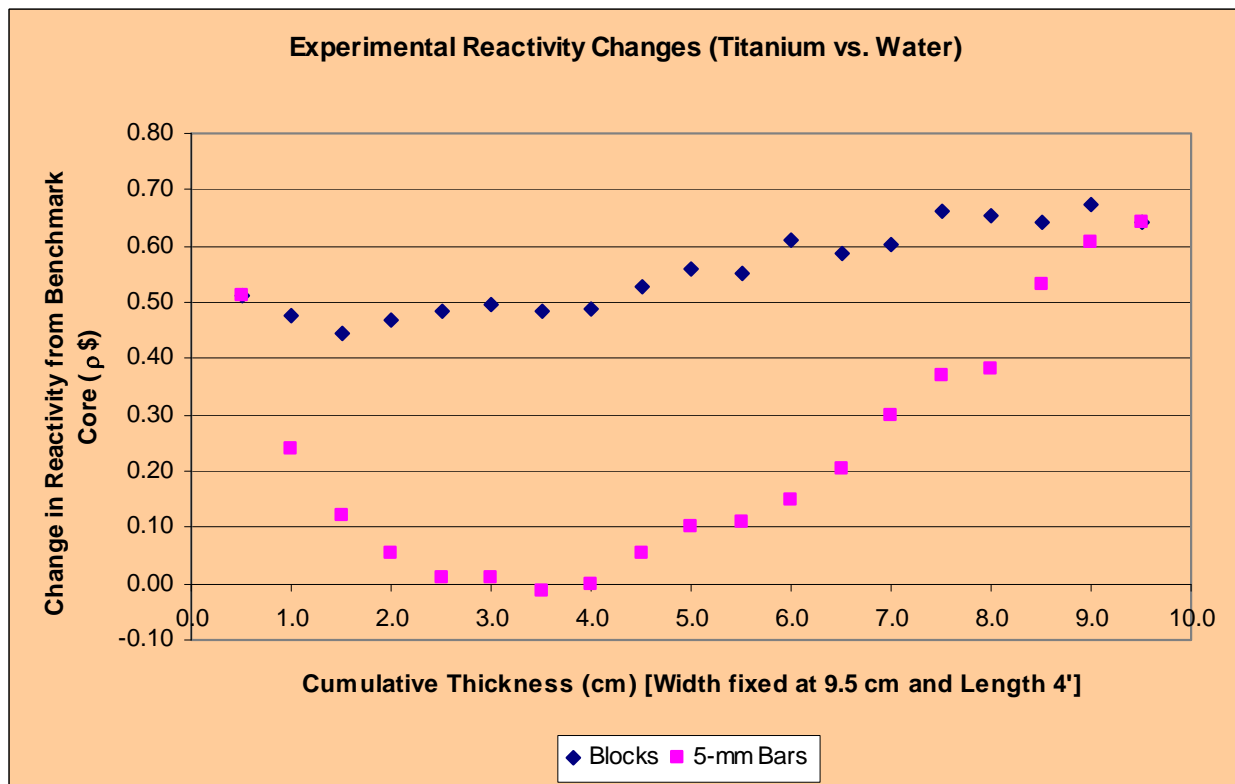
Figure B.9: Effective Reactivity of Titanium Compared to Water in Flux Trap.
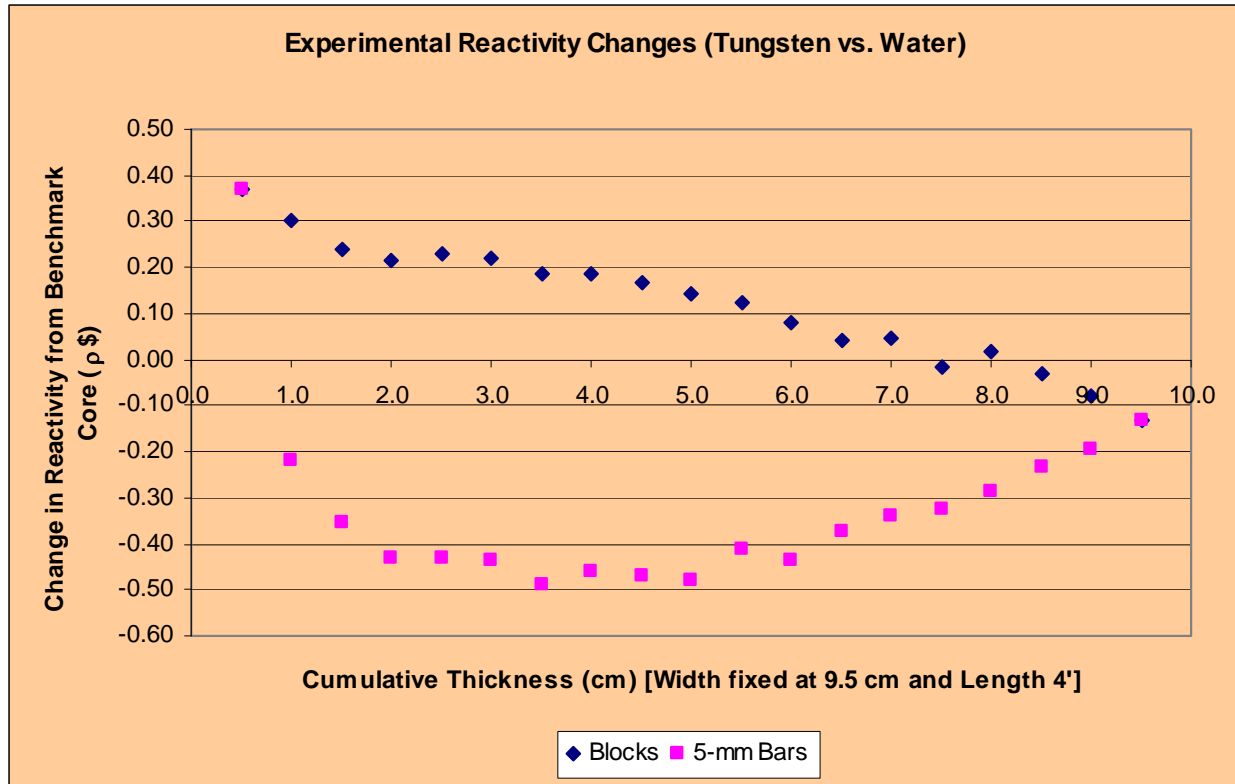
Figure B.10: Effective Reactivity of Tungsten Compared to Water in Flux Trap.
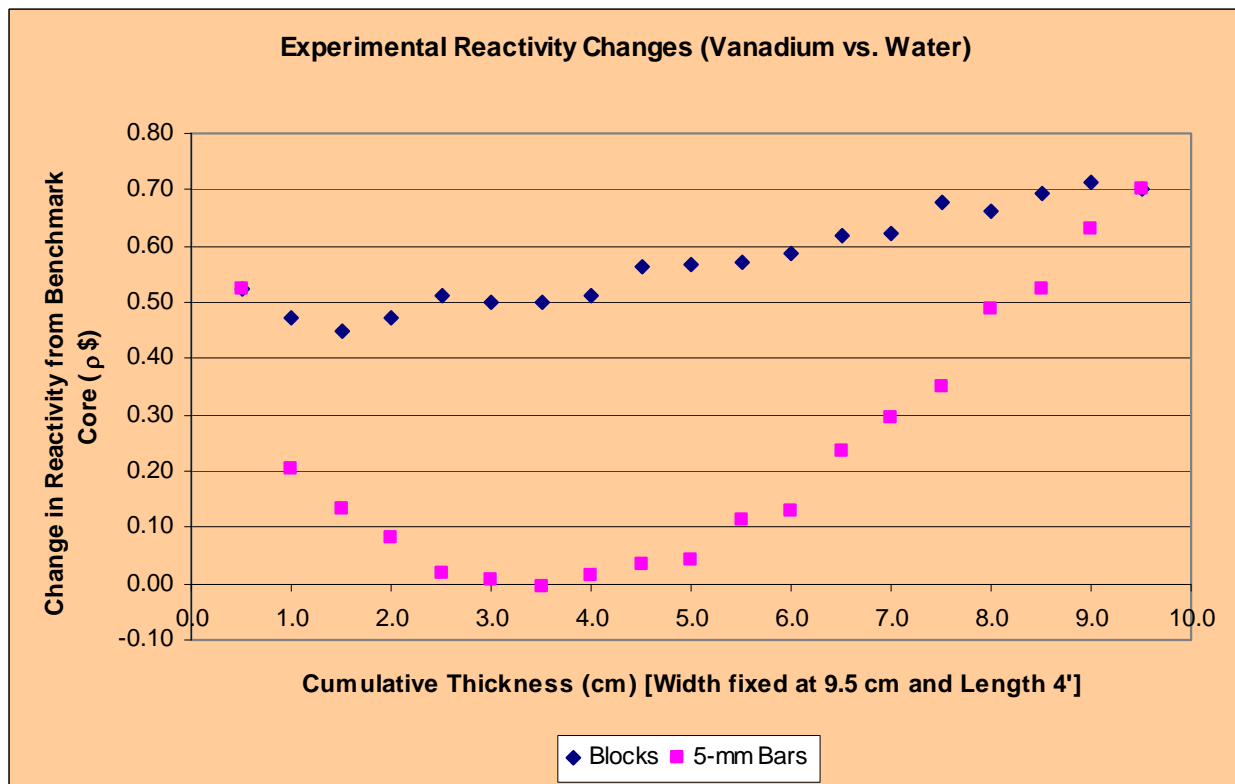
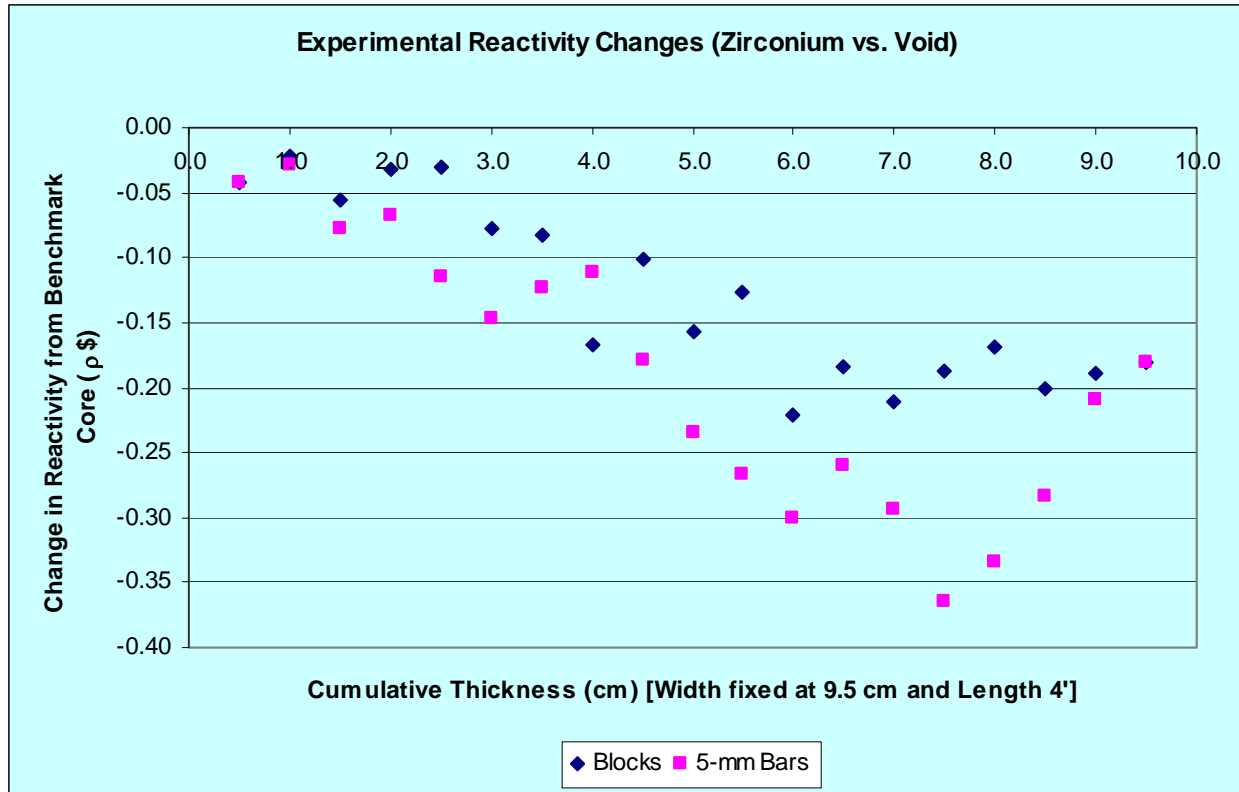Figure B.11: Effective Reactivity of Vanadium Compared to Water in Flux Trap.
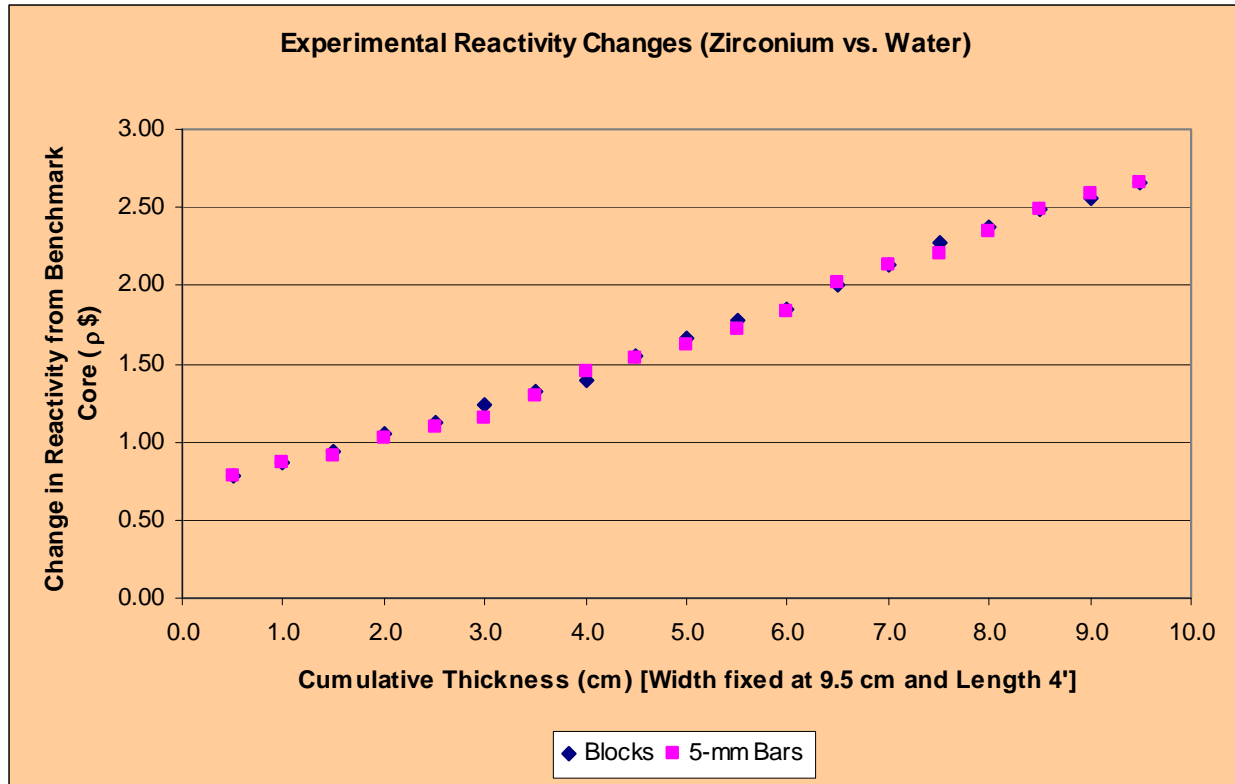
Figure B.12: Effective Reactivity of Zirconium Compared to Water in Flux Trap.
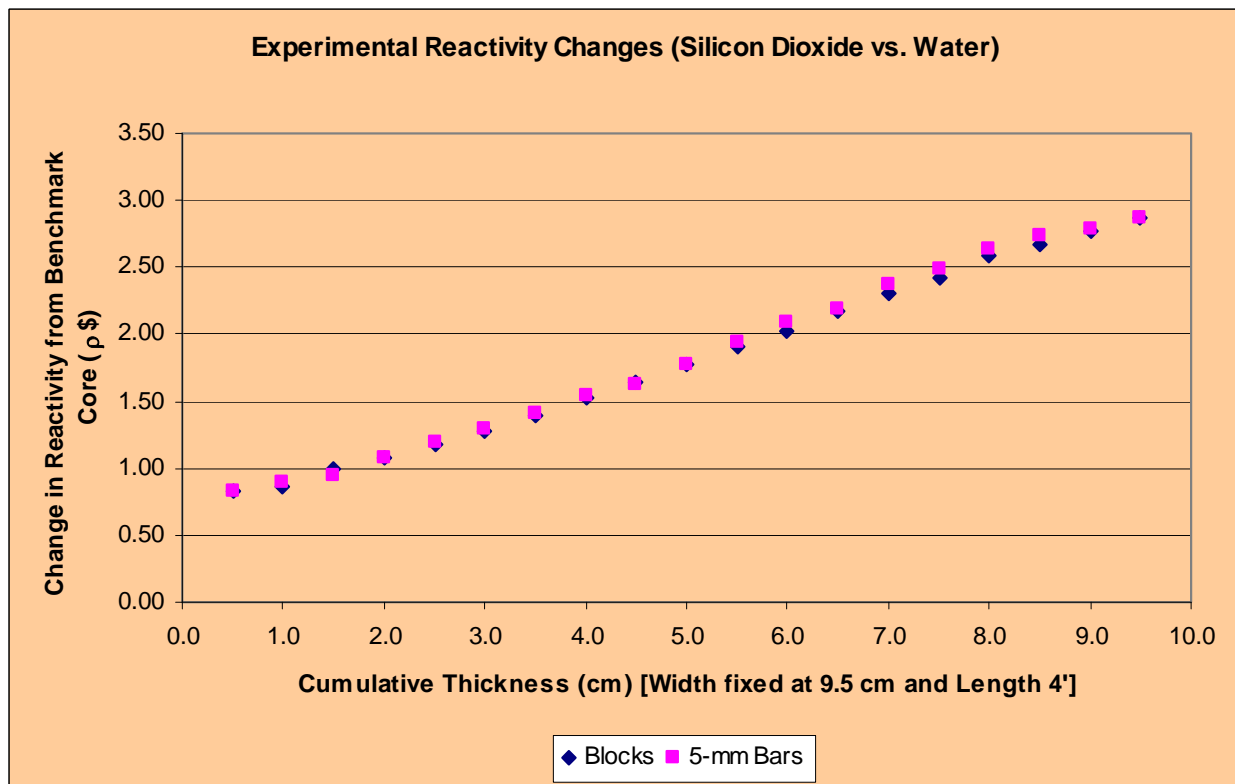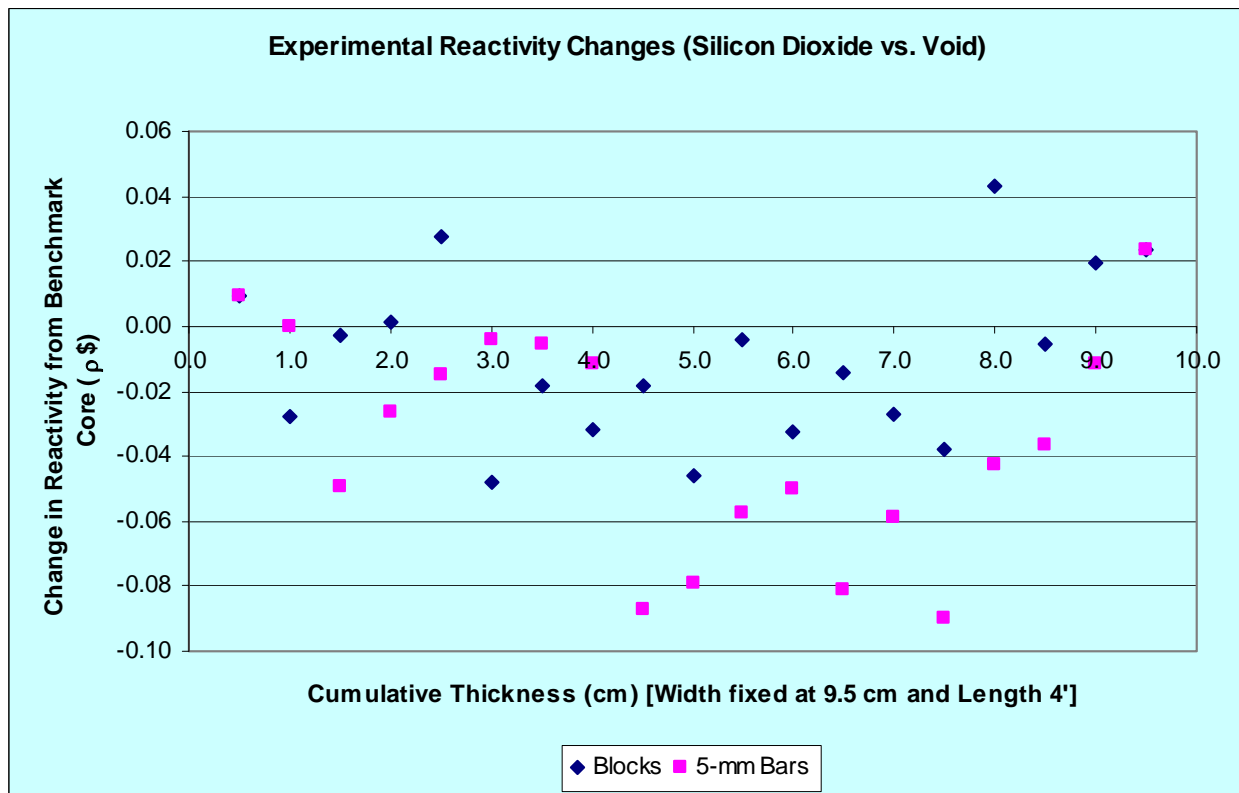

Figure B.13: Effective Reactivity of Silicon Dioxide Compared to Water in Flux Trap.

APPENDIX C – Reactivity Effects Due to Voiding of Water in Flux Trap

Experimental reactivity changes due to the insertion of materials into the ATR benchmark model compared against voided geometries of the same configuration.
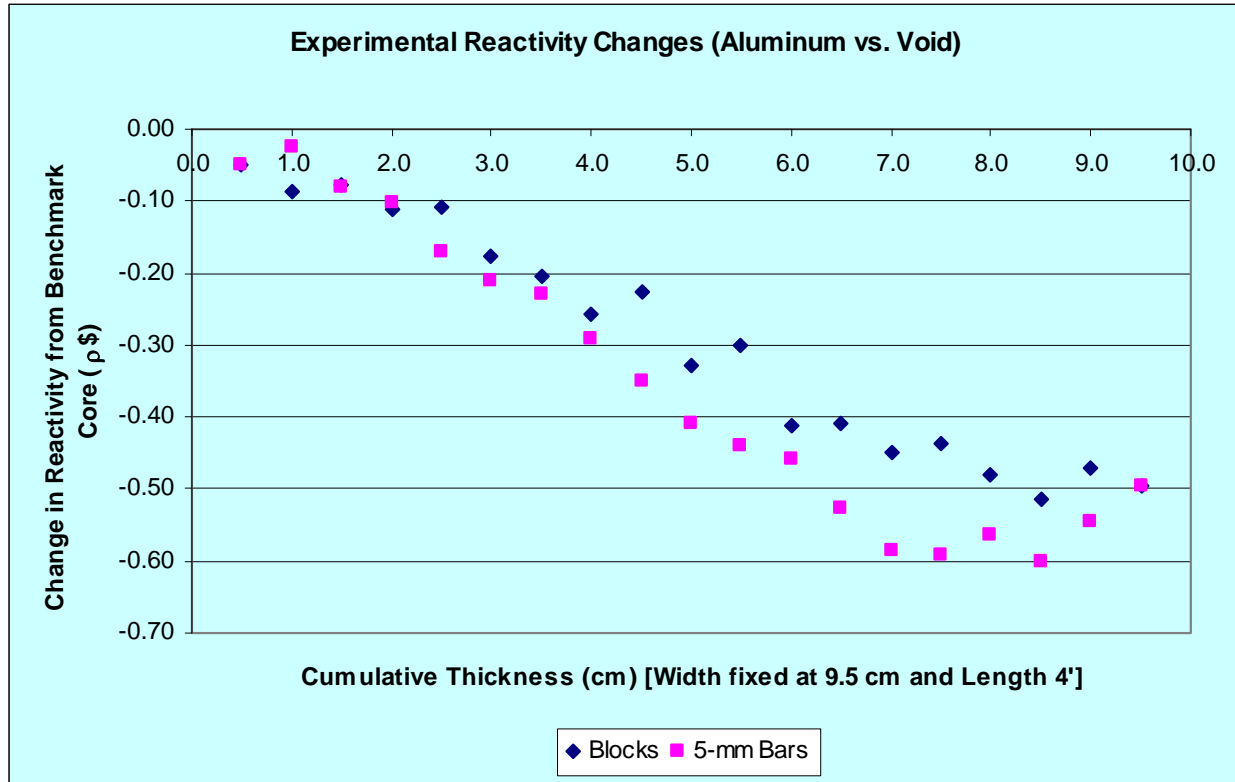
Figure C.1: Effective Reactivity of Aluminum Compared to Void Material.
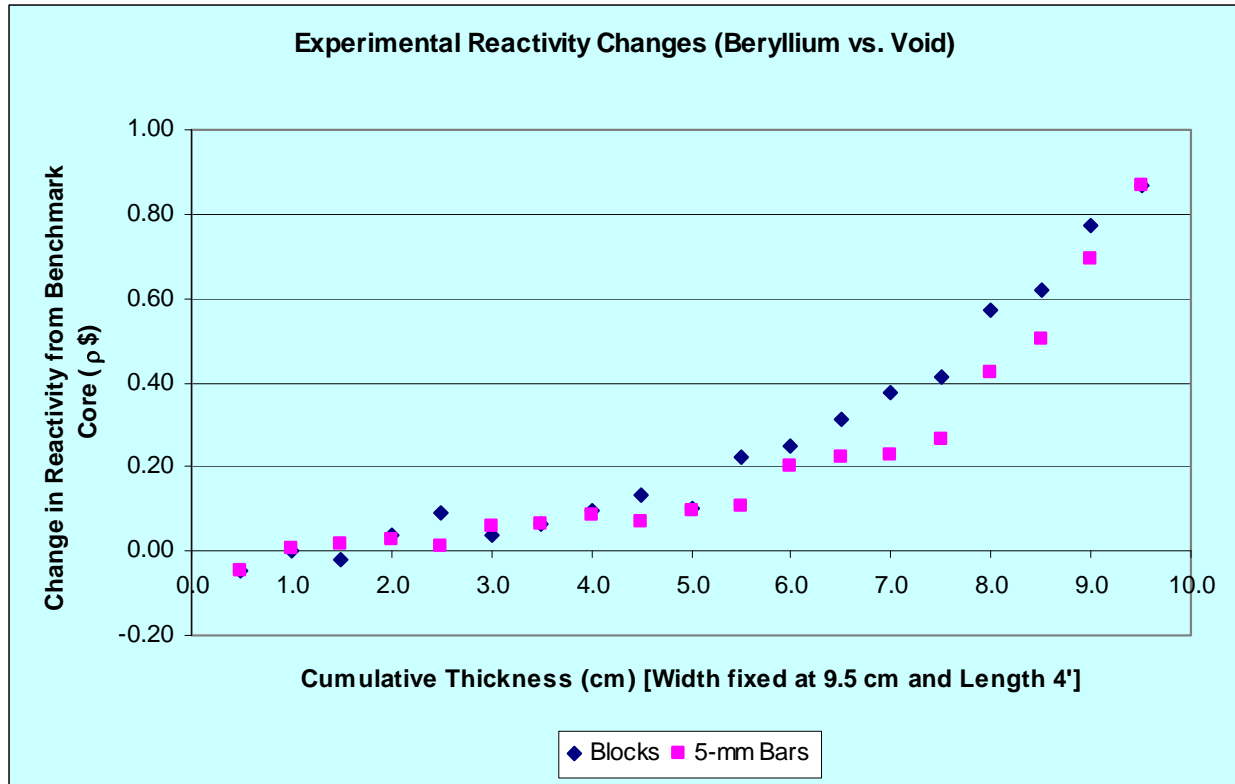
Figure C.2: Effective Reactivity of Beryllium Compared to Void Material.
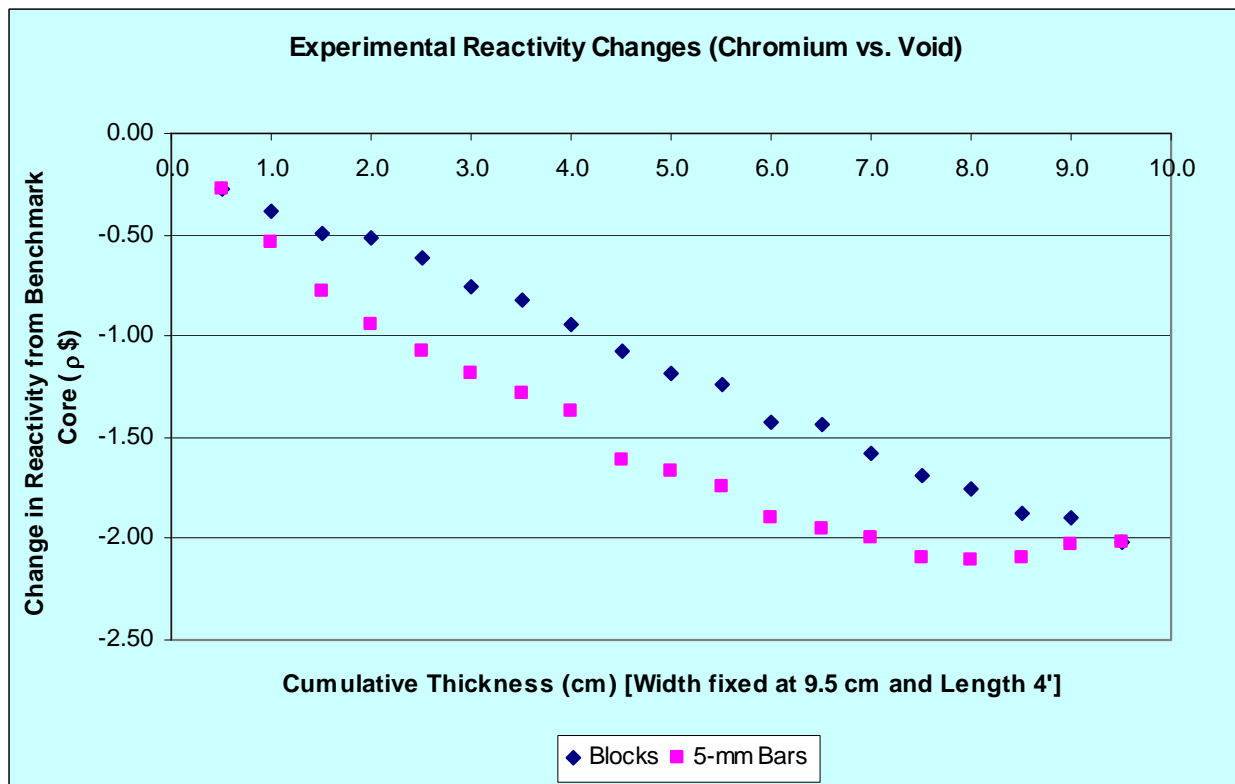
Figure C.3: Effective Reactivity of Chromium Compared to Void Material.
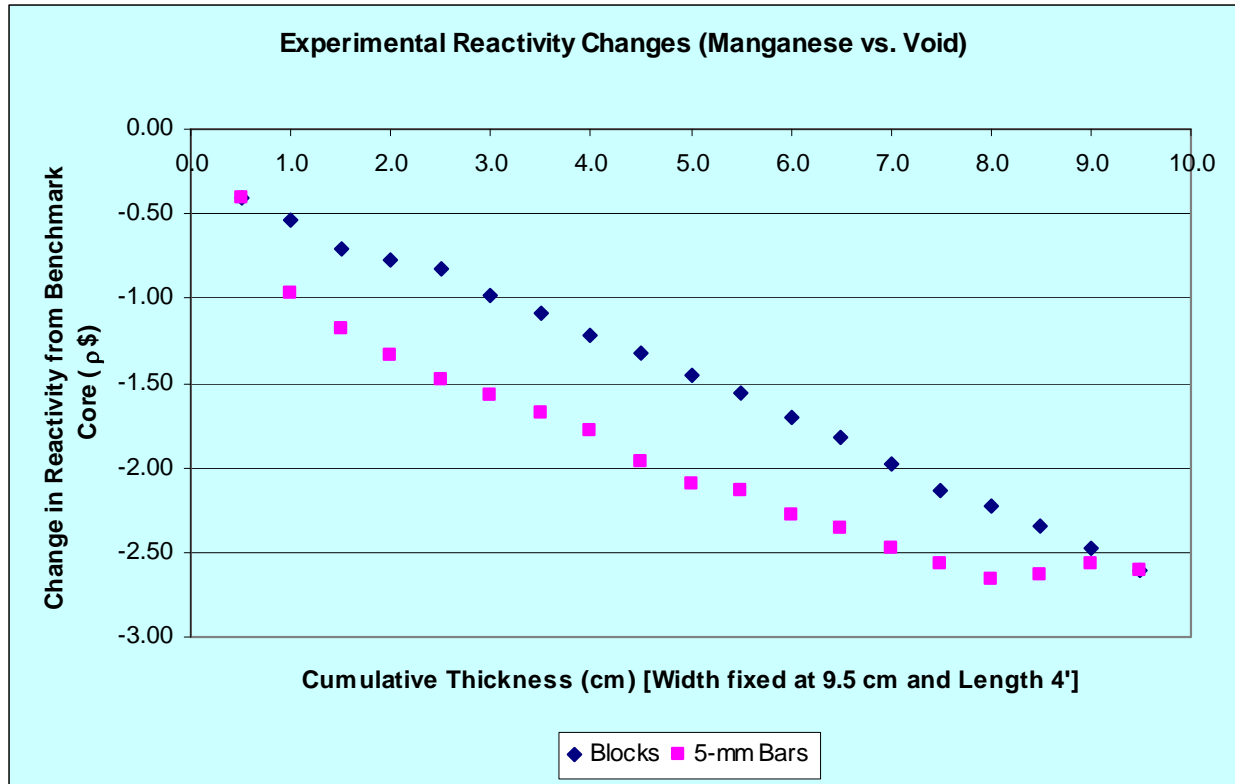
Figure C.4: Effective Reactivity of Manganese Compared to Void Material.
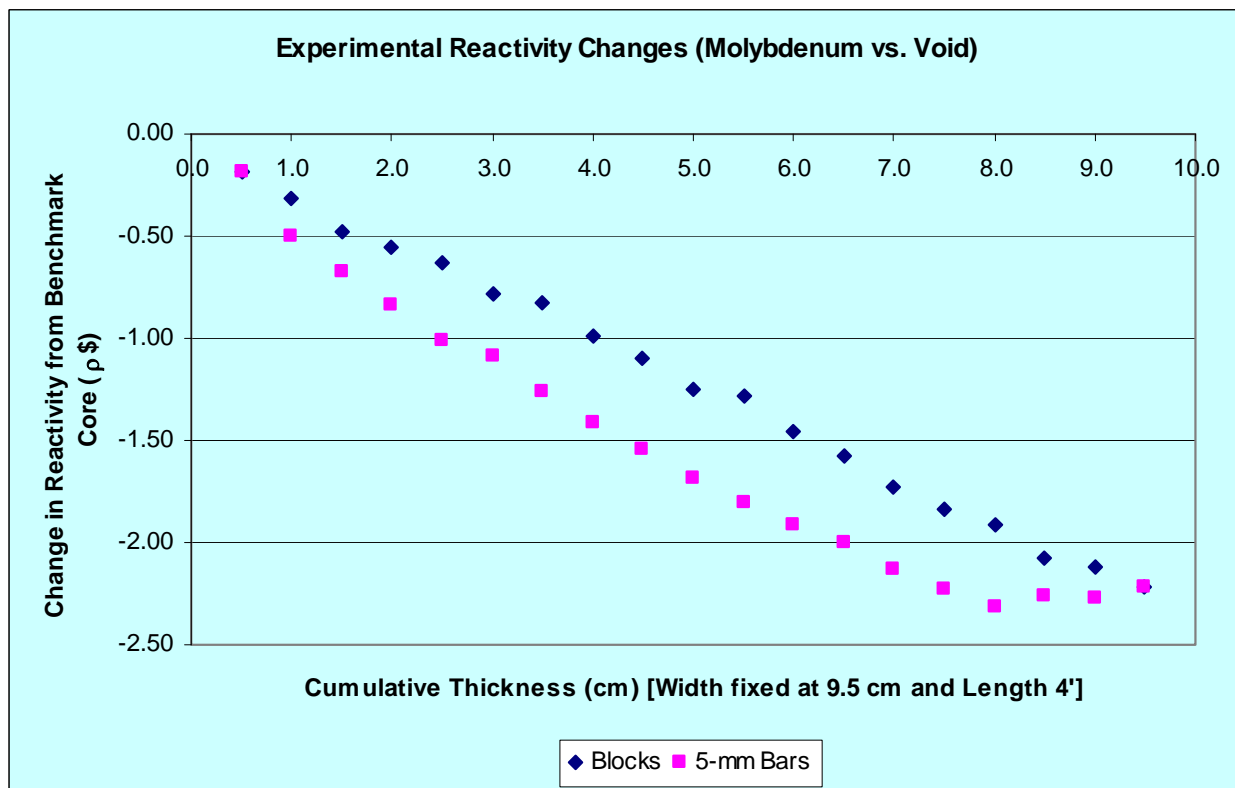
Figure C.5: Effective Reactivity of Molybdenum Compared to Void Material.
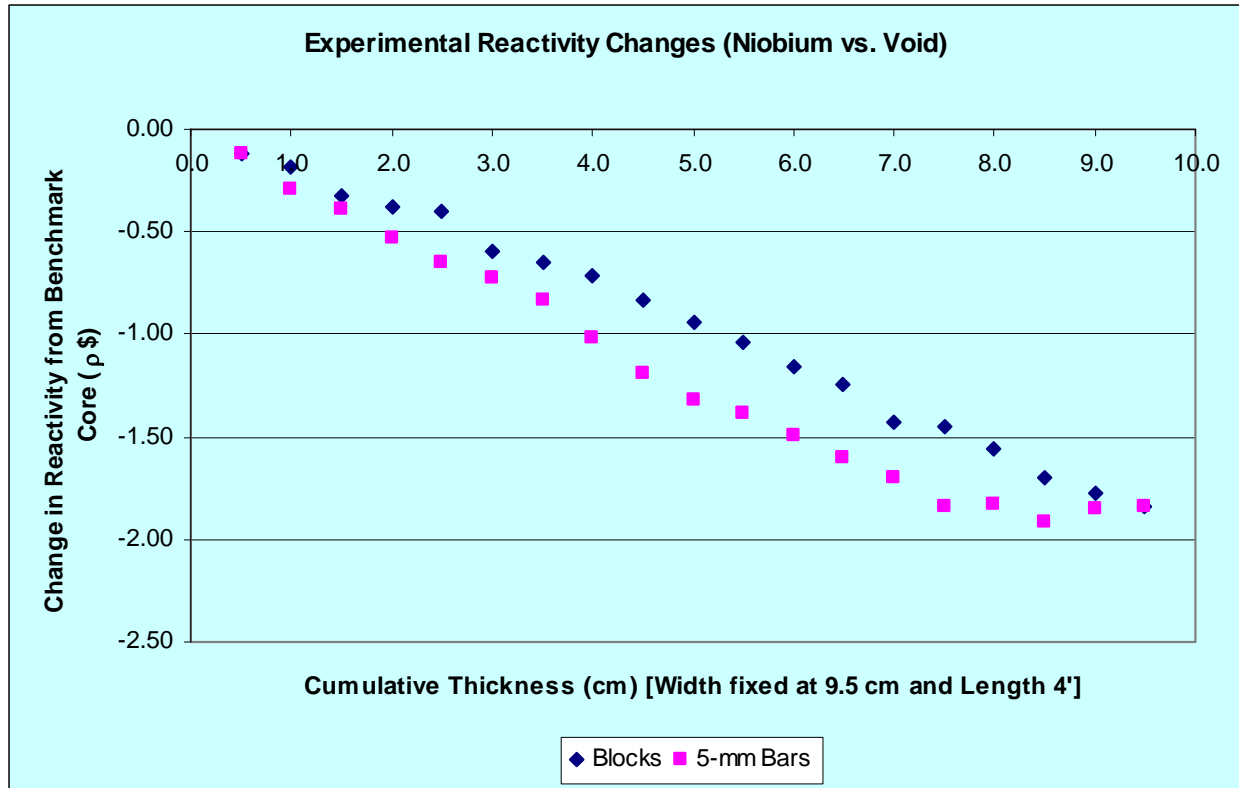
Figure C.6: Effective Reactivity of Niobium Compared to Void Material.
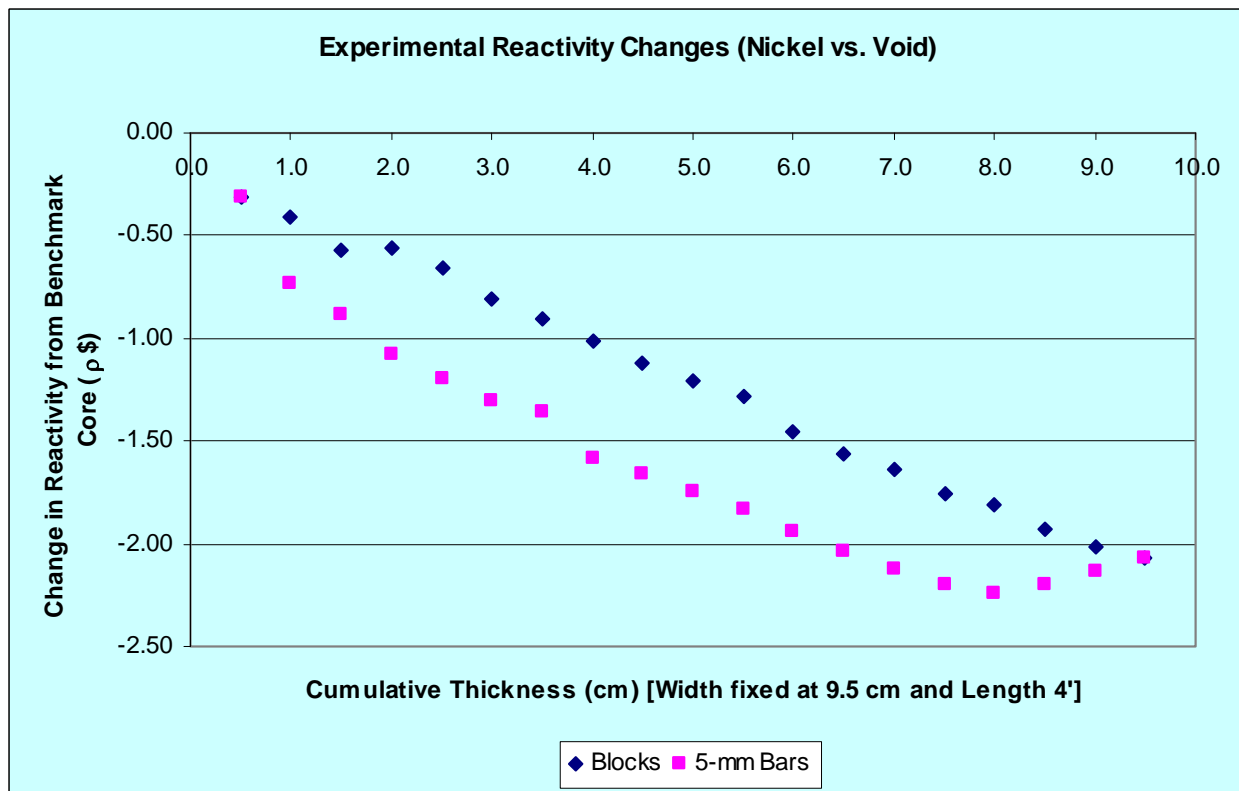
Figure C.7: Effective Reactivity of Nickel Compared to Void Material.
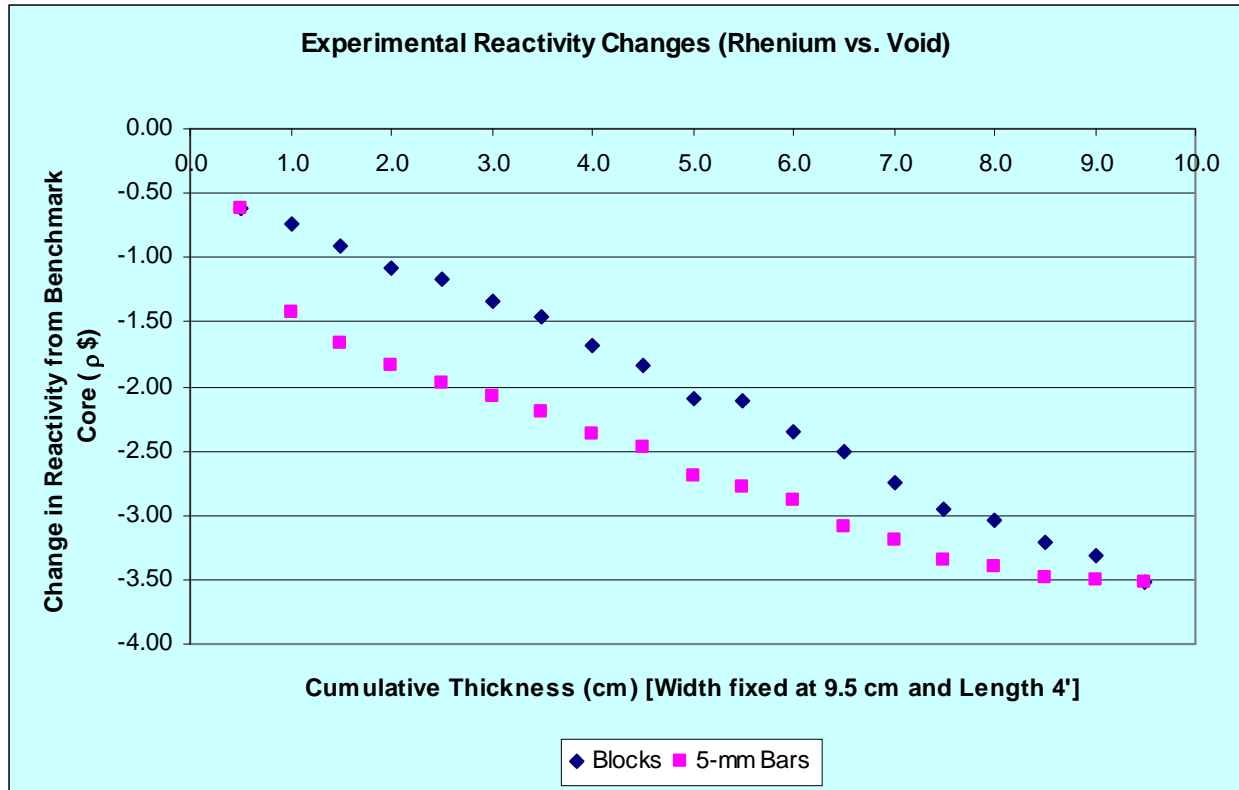
Figure C.8: Effective Reactivity of Rhenium Compared to Void Material.
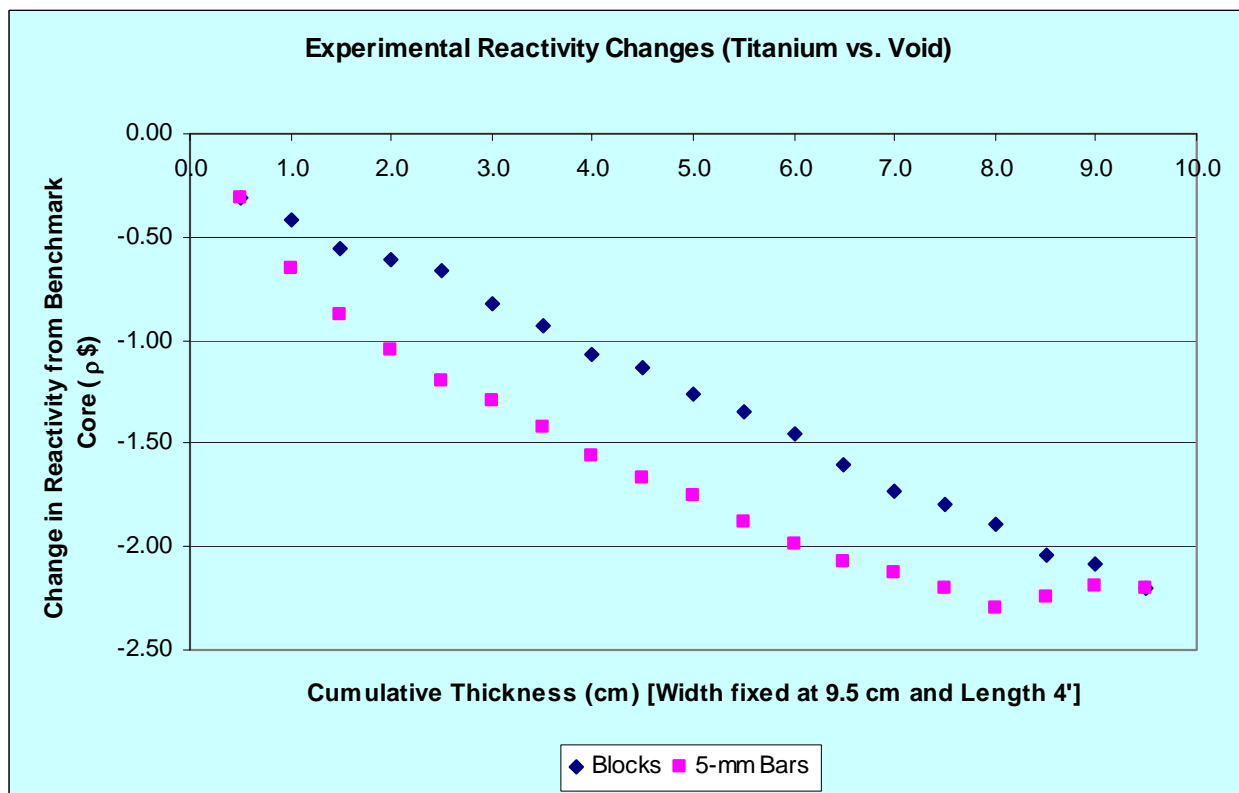
Figure C.9: Effective Reactivity of Titanium Compared to Void Material.
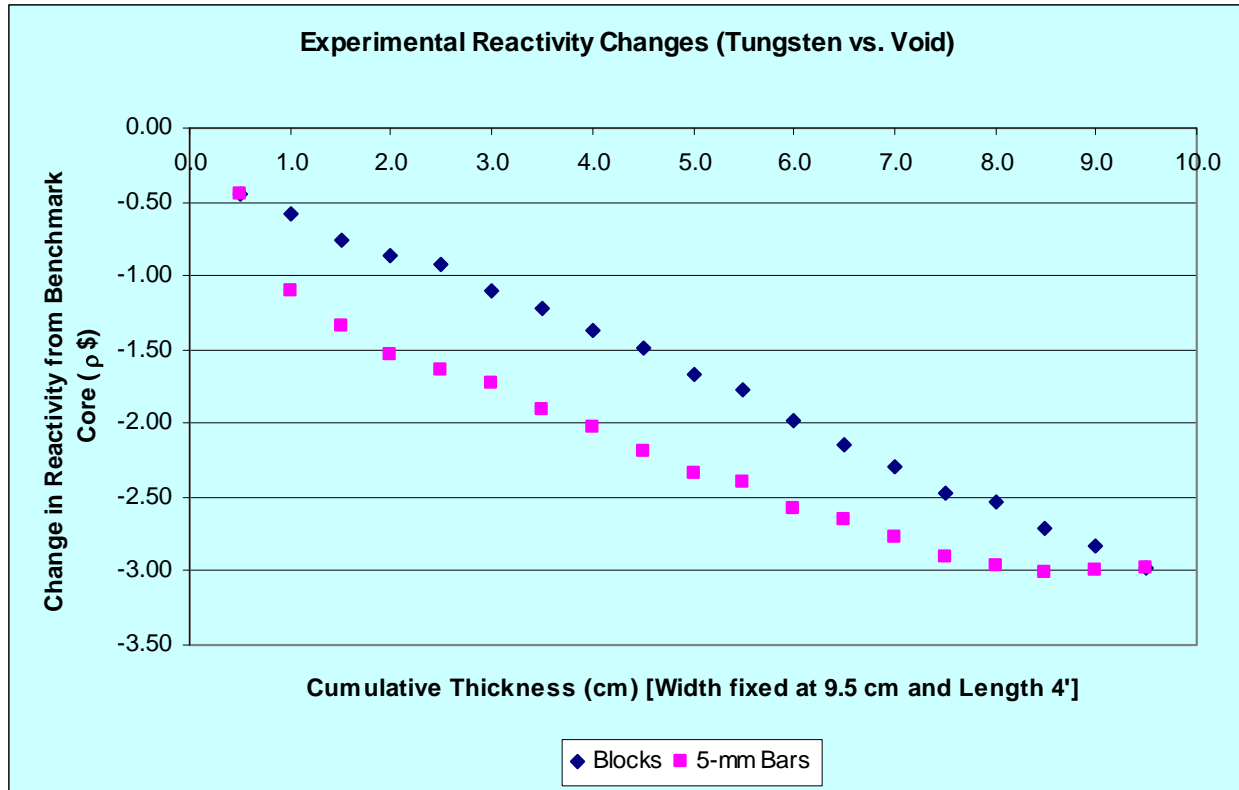
Figure C.10: Effective Reactivity of Tungsten Compared to Void Material.
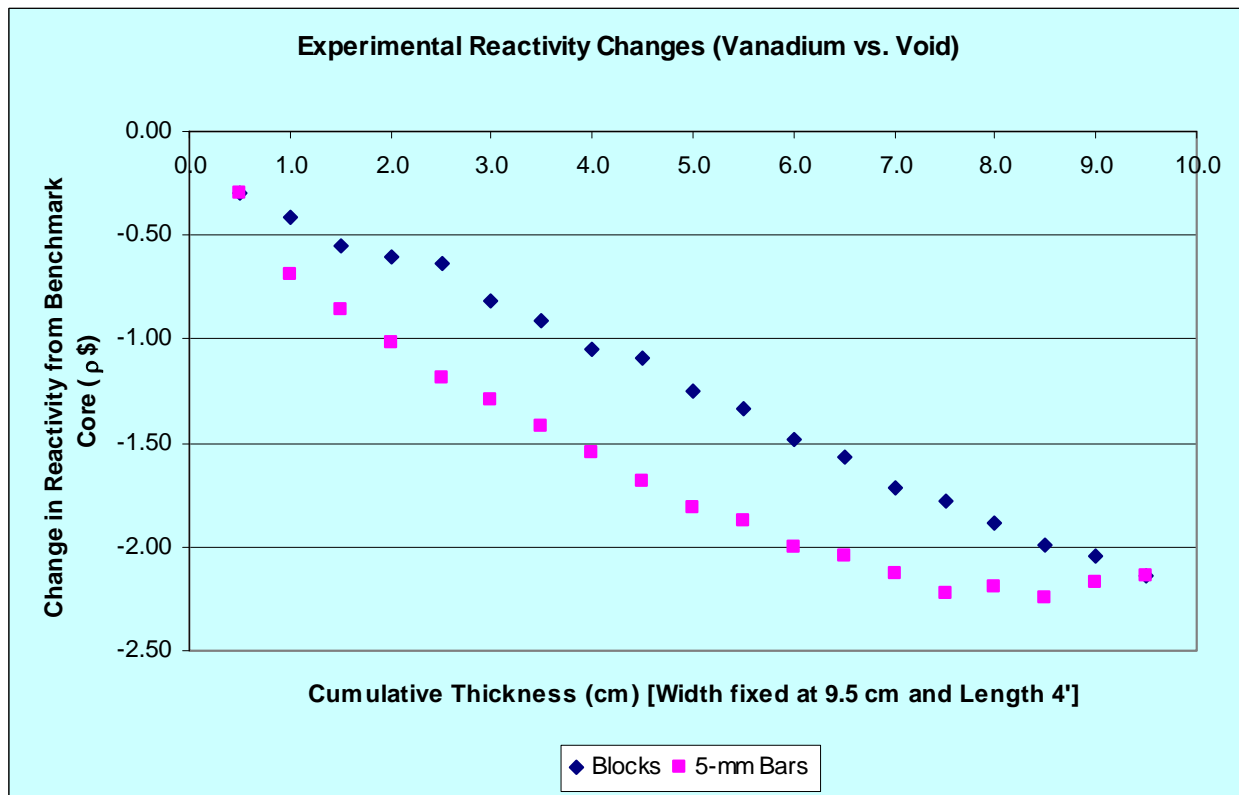
Figure C.11: Effective Reactivity of Vanadium Compared to Void Material.

Figure C.12: Effective Reactivity of Zirconium Compared to Void Material.

Figure C.13: Effective Reactivity of Silicon Dioxide Compared to Void Material.

APPENDIX D – Reactivity Effects Compared Against Aluminum Material

Experimental reactivity changes due to the insertion of materials into the ATR benchmark model compared against equivalent geometric configurations containing aluminum.
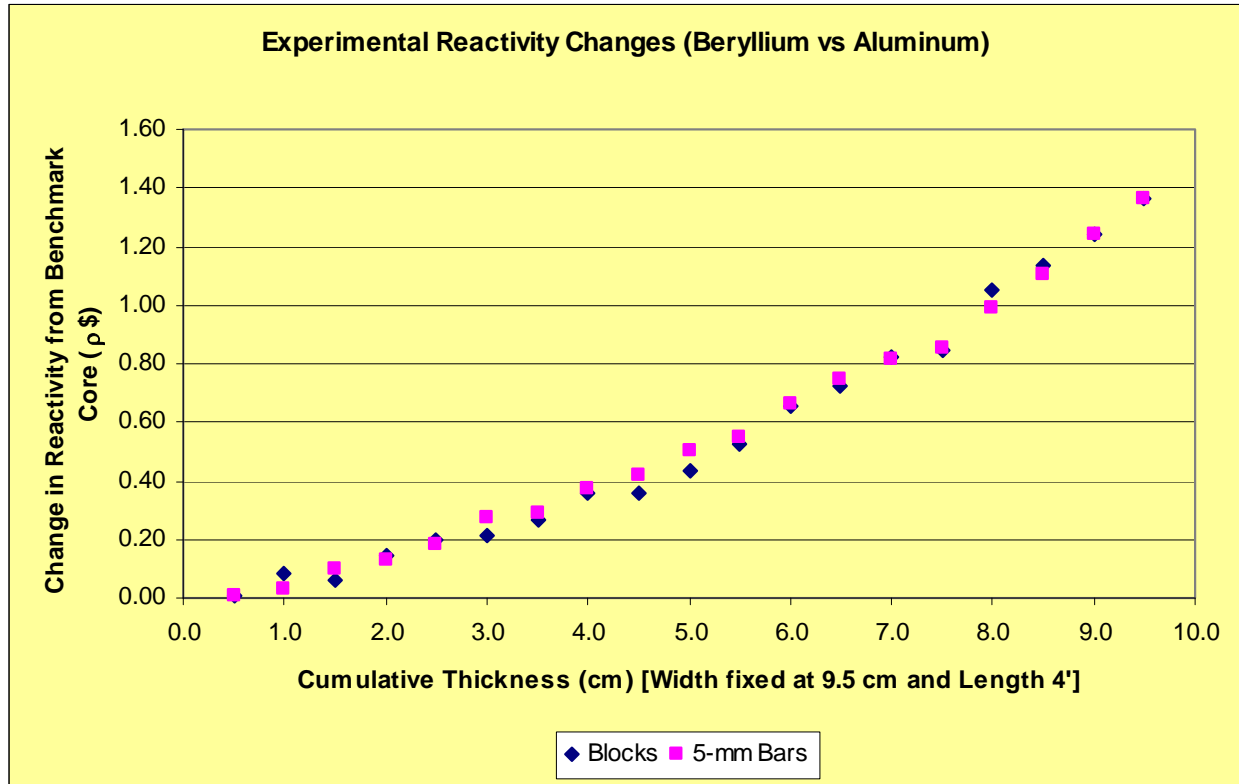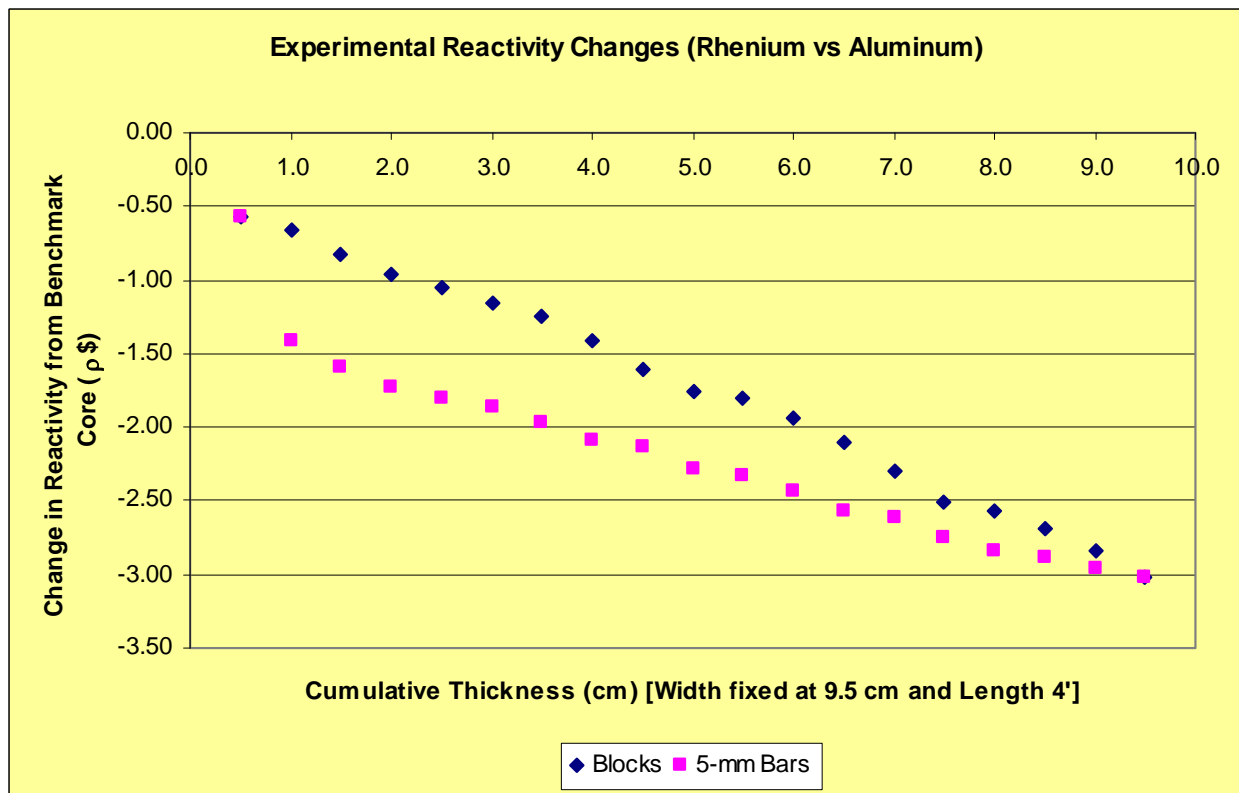

Figure D.1: Effective Reactivity of Beryllium Compared to Aluminum.
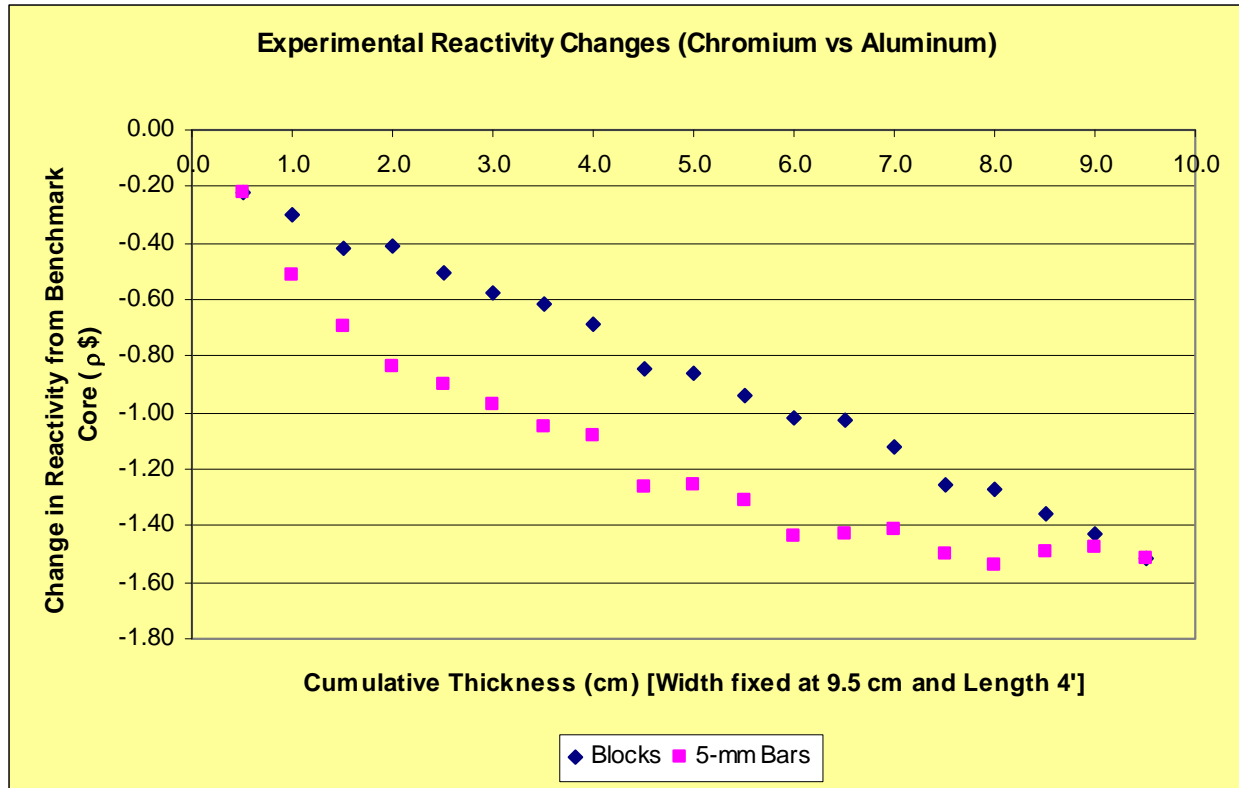
Figure D.2: Effective Reactivity of Chromium Compared to Aluminum.
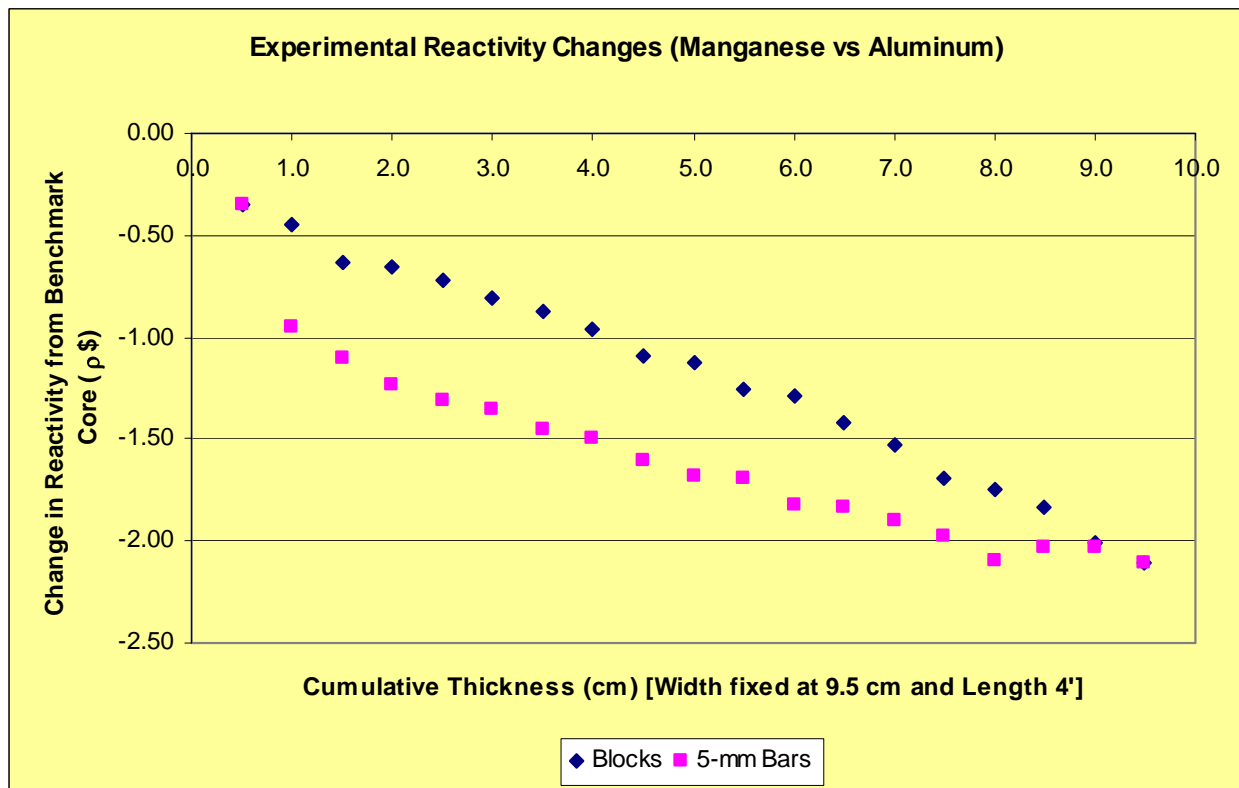
Figure D.3: Effective Reactivity of Manganese Compared to Aluminum.
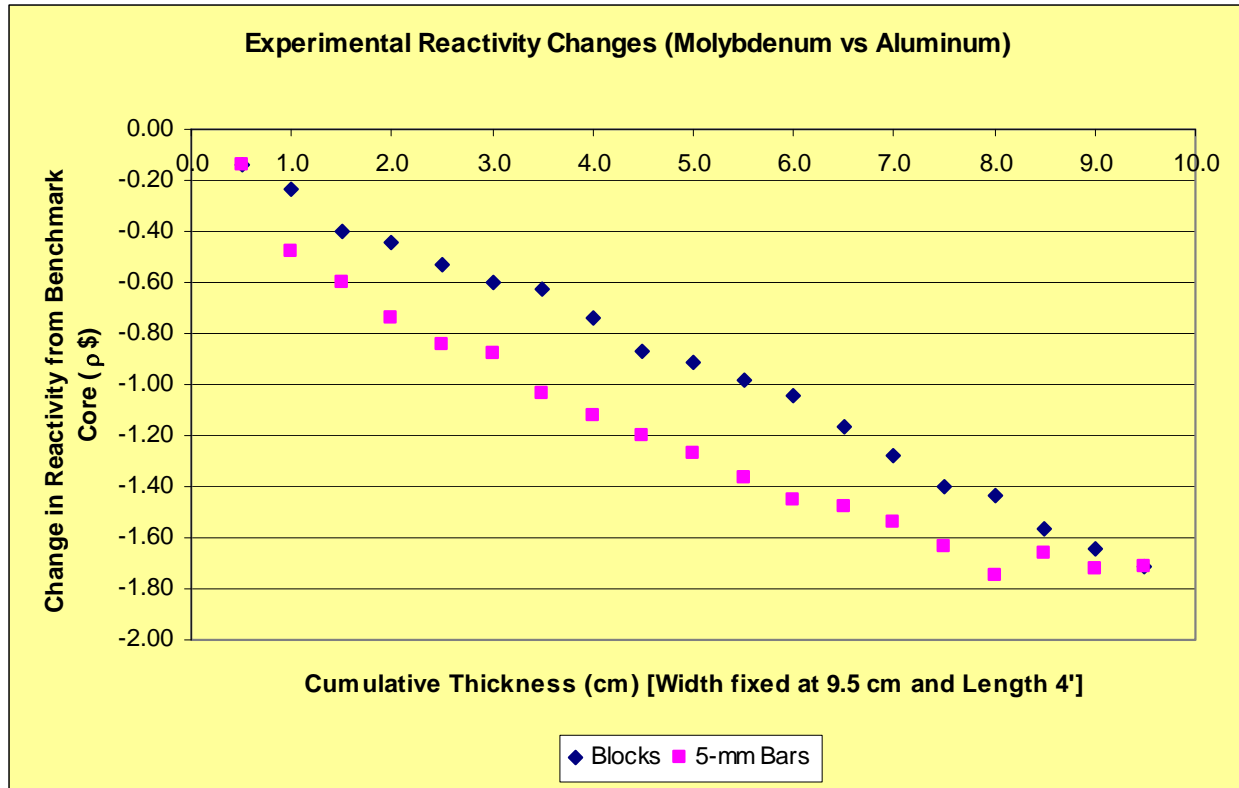
Figure D.4: Effective Reactivity of Molybdenum Compared to Aluminum.
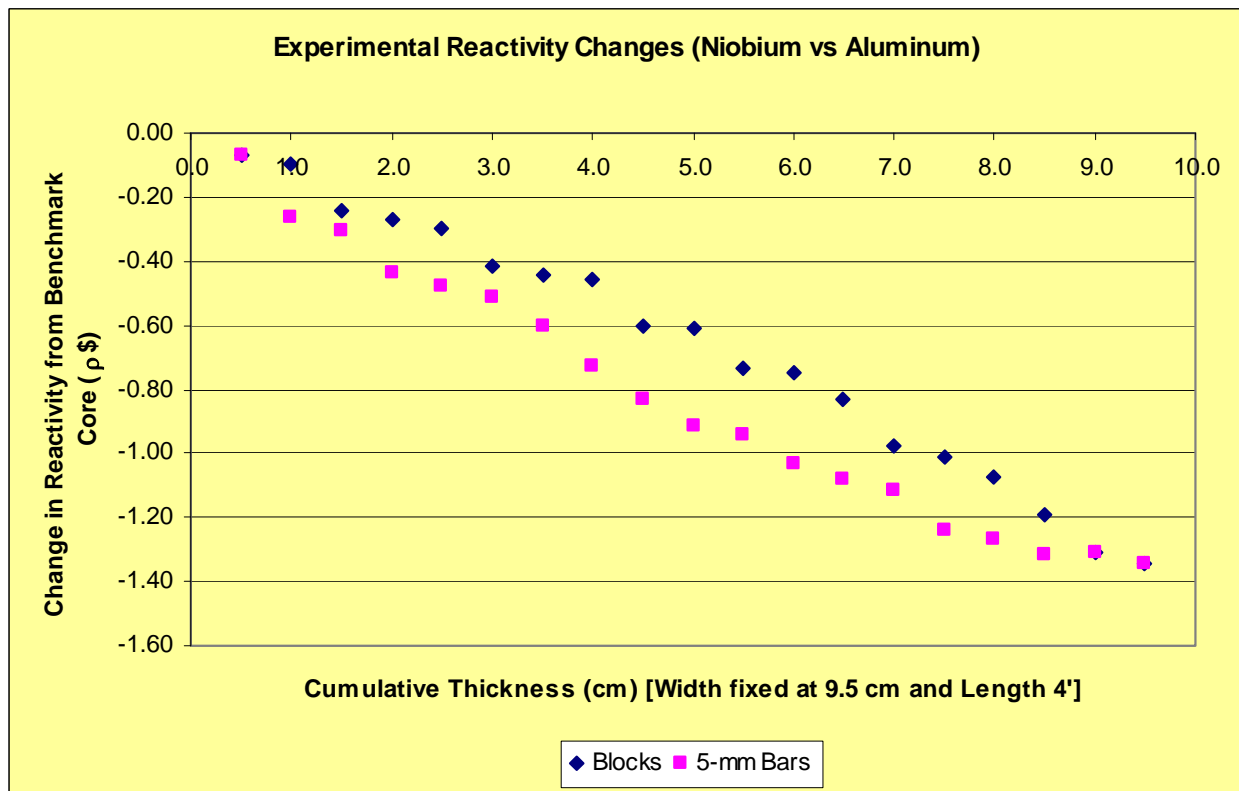
Figure D.5: Effective Reactivity of Niobium Compared to Aluminum.
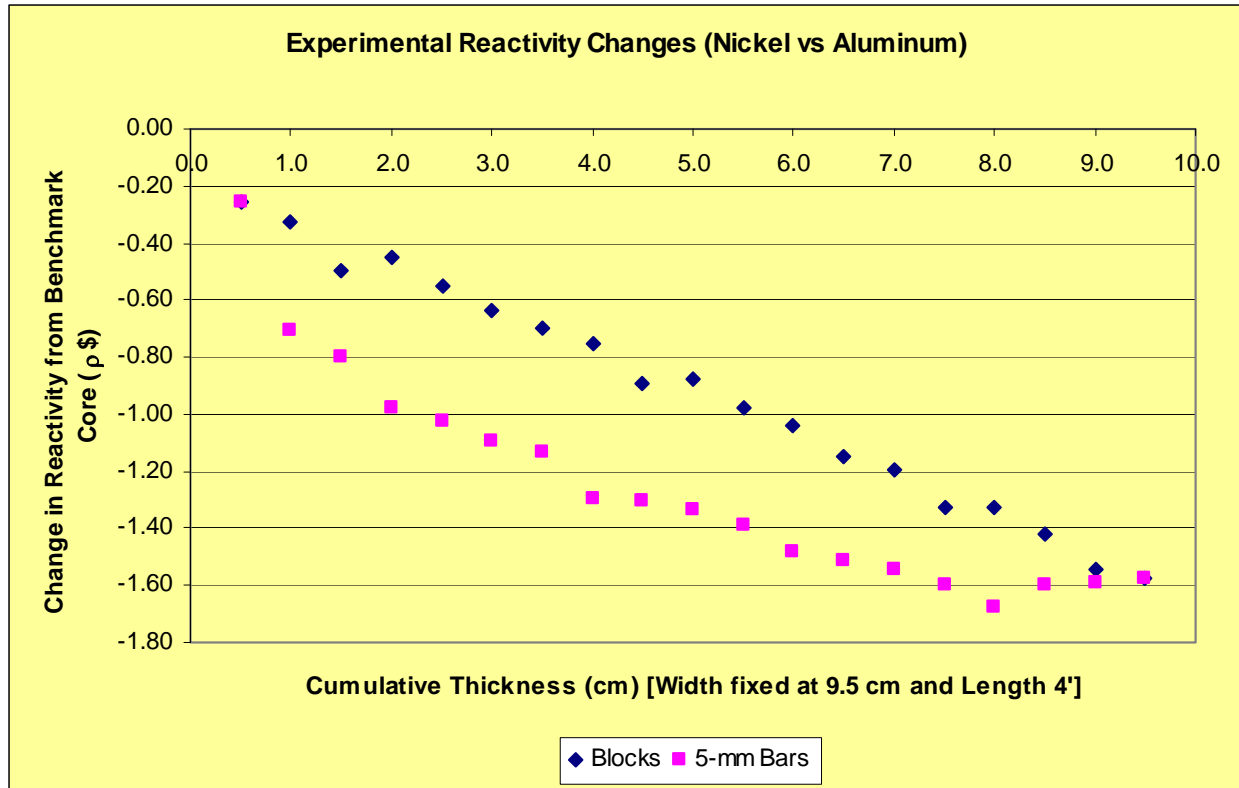
Figure D.6: Effective Reactivity of Nickel Compared to Aluminum.

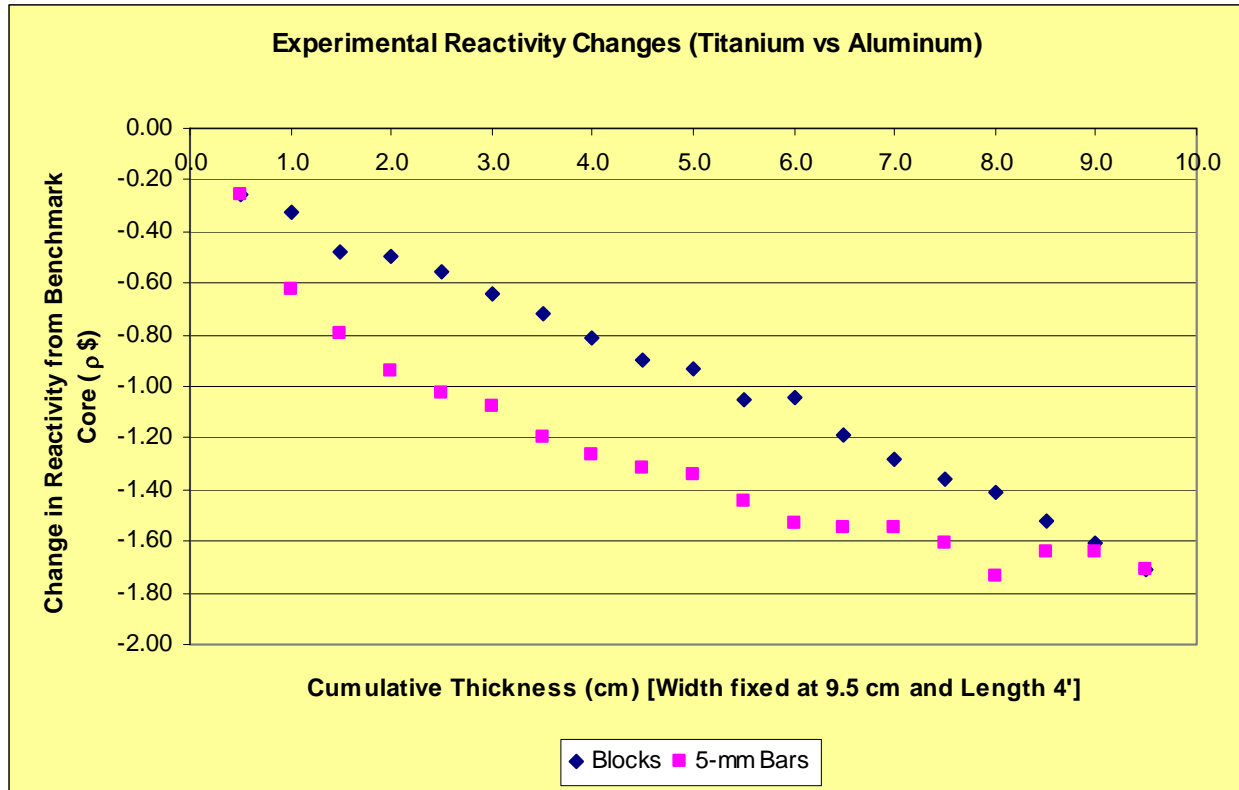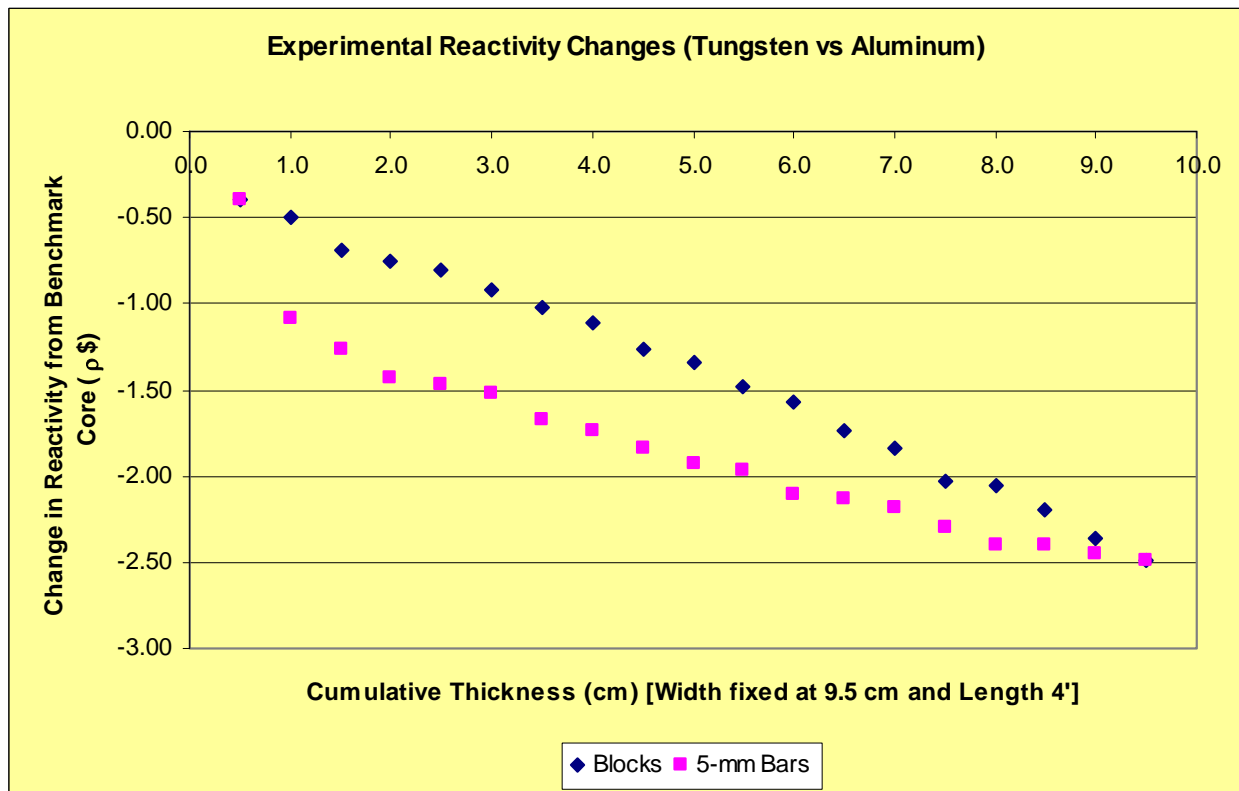Figure D.7: Effective Reactivity of Rhenium Compared to Aluminum.

Figure D.8: Effective Reactivity of Titanium Compared to Aluminum.

Figure D.9: Effective Reactivity of Tungsten Compared to Aluminum.
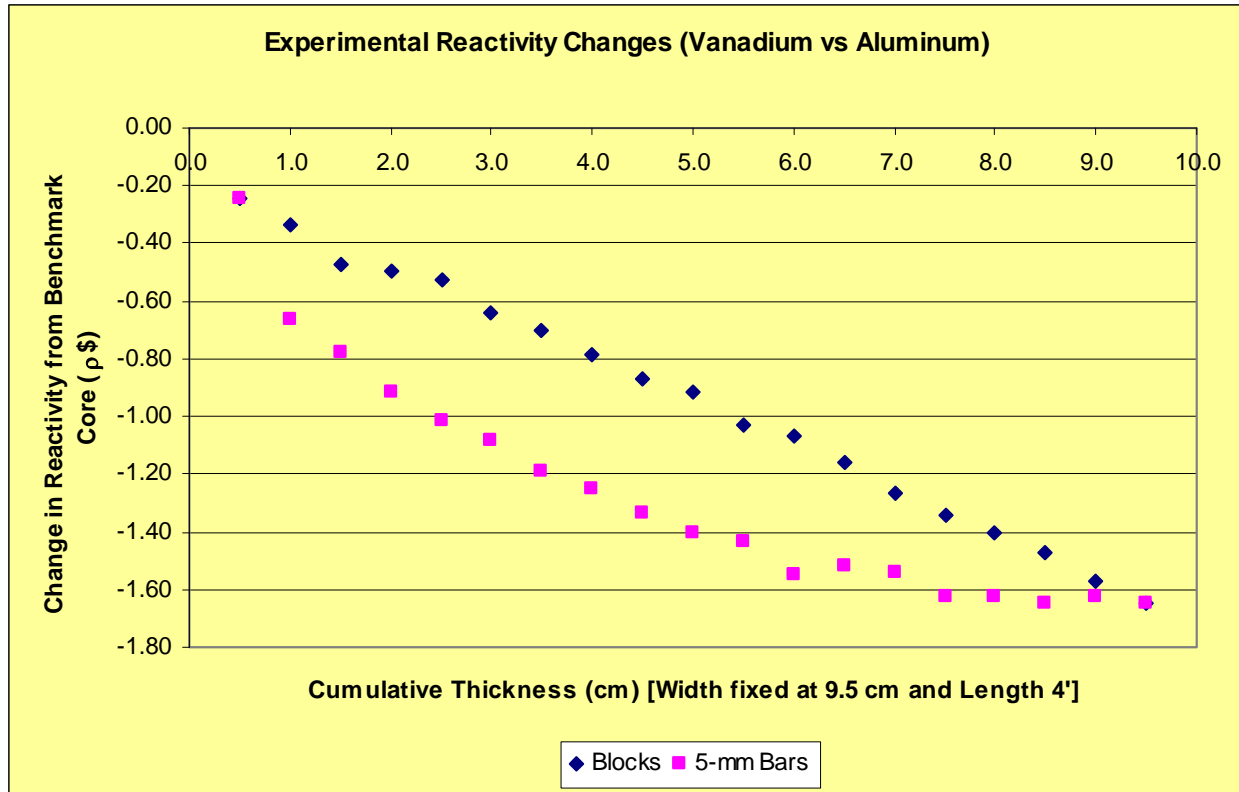
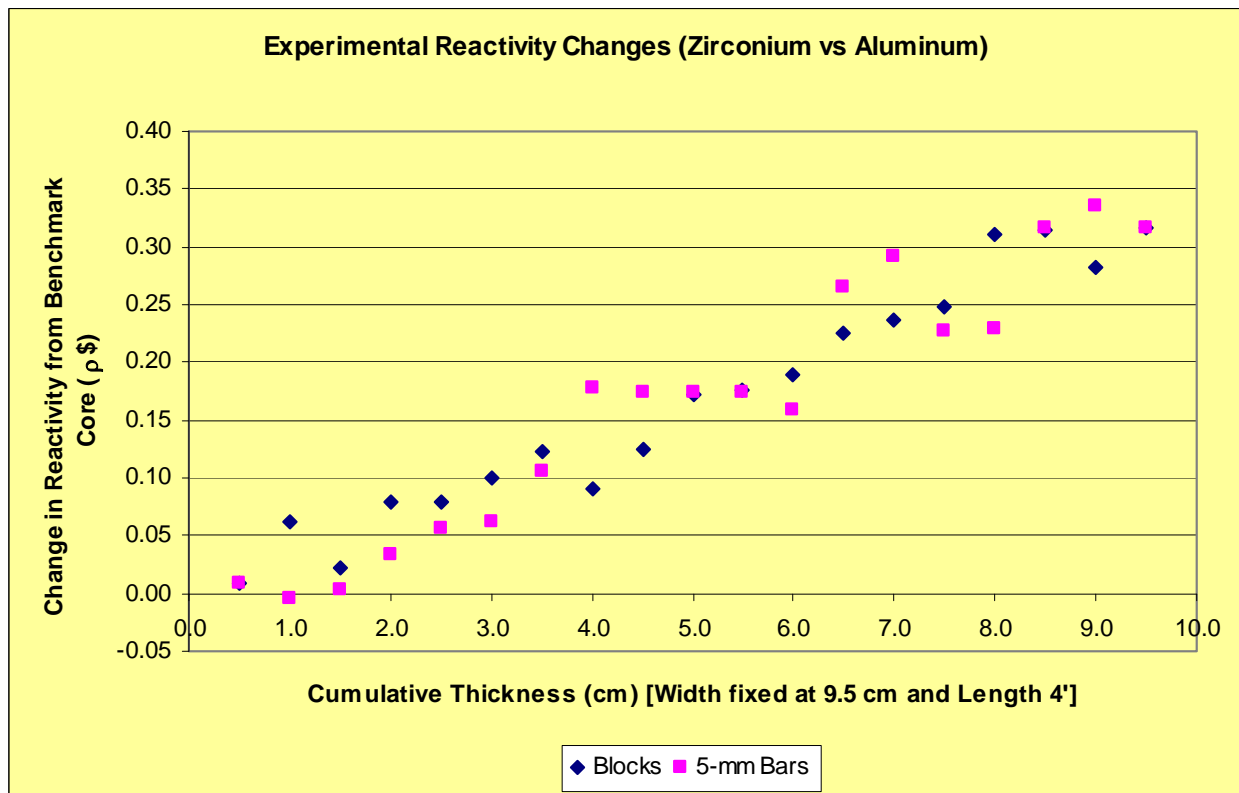Figure D.10: Effective Reactivity of Vanadium Compared to Aluminum.

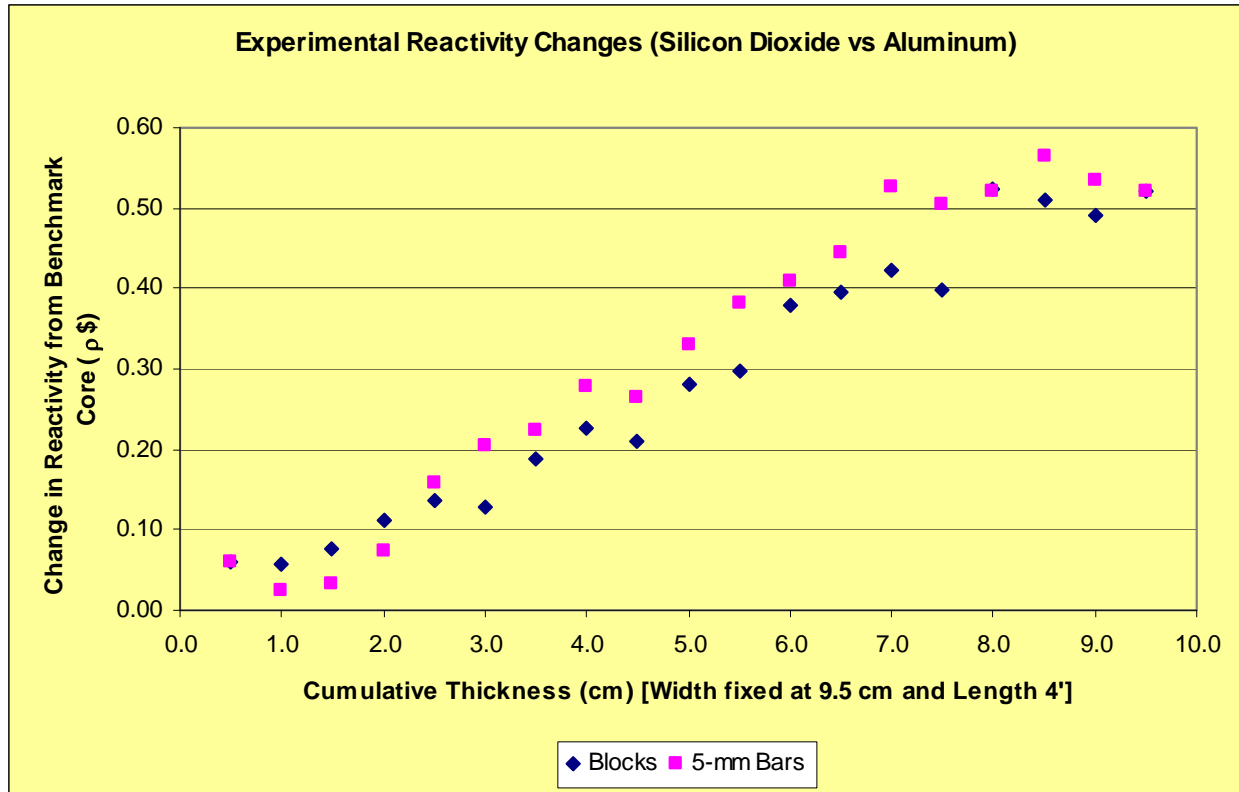Figure D.11: Effective Reactivity of Zirconium Compared to Aluminum.

Figure D.12: Effective Reactivity of Silicon Dioxide Compared to Aluminum.